AD NUMBER
AD418399
LIMITATION CHANGES
TO: **Approved for public release; distribution is unlimited.**
FROM: **Distribution authorized to U.S. Gov't. agencies and their contractors; Administrative/Operational Use; JUL 1963. Other requests shall be referred to Office of Naval Research, Washington, DC 20350.**
AUTHORITY
onr, ltr, 4 may 1977

Measurement of Fluid Properties for Magnetoplasmadynamic Power Generators

First Quarterly Technical Summary Report
(1 May—31 July 1963)

Contract No. Nonr-410(00)

Order No.: ARPA 420 Project Code No. 3980

Engineering Department Report No. 3511

Allison Division
General Motors Corporation
Indianapolis, Indiana

Measurement of Fluid Properties for Magnetoplasmadynamic Power Generators

First Quarterly Technical Summary Report

(1 May — 31 July 1963)

Contract No. Nonr-410(00)

Order No.: ARPA 420 Project Code No. 3980

Engineering Department Report No. 3511

20 August 1963

By: R. T. Schneider
H. E. Wilhelm
D. L. Tipton

Approved: [signature]
T. F. Nagey
Director of Research

FOREWORD

This technical summary report was prepared by the Research Department of the Allison Division of General Motors Corporation. The work reported was accomplished under Contract Nonr-4104(00).

The program was sponsored by the Advanced Research and Project Agency through the Power Branch of the Office of Naval Research under the direction of Dr. J. Huth of ARPA and Mr. J. A. Satkowski of ONR.

TABLE OF CONTENTS

LIST OF ILLUSTRATIONS

I. INTRODUCTION

The objective of this program is to obtain basic information on the plasma properties of working fluids for magnetoplasmadynamic (MPD) power generators. This information will be obtained through the use of diagnostic methods with emphasis on advanced spectroscopic techniques.

The experimental approach of the program concentrates on a plasma loop through which helium seeded with cesium circulates through the test section at a variable temperature range of 1000 to 2000°K. The flow rate of the atmospheric pressure helium is varied between 7 to 12 gm/sec to achieve a Mach number of 0.9 through an area of approximately 1.2 cm^2. Designed specifically for diagnostic investigation, the test section employs the basic features common to MPD generators. In preparation for the operation of the plasma loop, experimental effort has been applied to the development of new spectroscopic techniques and methods of evaluating observed spectra. Investigations will be made on the efficiency of various nonthermal ionization techniques.

The theoretical approach consists of developing a theoretical model to describe nonequilibrium plasmas and supplementary theoretical analyses to aid in design of improved MPD power generators. Instabilities occurring in the plasma flow will be investigated.

This report presents the technical review of progress during the period 1 May 1963 through 31 July 1963.

II. RESUME OF PROGRESS

Most of the components of the system have been manufactured. The final assembly of the test section will be completed during August 1963. Based on the experience of other closed loop experiments, unusual care has been taken in the design of the system. The final assembly of the diagnostic MPD system is planned for the next reporting period.

Further development of diagnostic methods was accomplished. A part of this work was the subject of a presentation, "A Spectroscopic Method Allowing Spatial Resolution," by Dr. R. T. Schneider at the VIth International Conference on Ionization Phenomena in Gases, in Paris, France, 8—13 July 1963.

Work on a theoretical model has been started. A portion of this work was devoted to plasma instabilities in a magnetoplasmadynamic generator. This effort was the subject of a presentation, "Convective Instability of Plasma Flow Across a Magnetic Field," by Dr. H. E. Wilhelm at the VIth International Conference on Ionization Phenomena in Gases, in Paris, France, 8—13 July 1963.

CLOSED LOOP DIAGNOSTIC DEVICE

The test section includes the electrodes and the windows for spectroscopic measurements. This section is made of tantalum and is housed in a stainless steel compartment. Successful welding of the tantalum components was done by Allison. Final assembly of this section is awaiting a few ceramic parts scheduled to be shipped in early August.

An uncooled magnet, for a 20% duty cycle, of Allison design was manufactured by a vendor. The vendor's test results indicated that on the third duty cycle (10 minutes on, 50 minutes off), the temperature rise became constant and was 115°C. This value is well within the protection limit given by the insulation. The vendor's test results also showed a flux density of 13, 800 gauss at 60 amp with a limited power supply. The performance curve shows that saturation is not reached at 60 amp; therefore, it appears probable that a flux density of 15, 000 gauss may be reached with the Allison power supply.

Difficulties were encountered in winding the tungsten coils for the heater. However, the manufacturing procedure has now been established and fabrication of the heater is progressing.

Status of other components is as follows:

- Received
  - Helium compressor (Miehle-Dexter)
  - 50-cfm vacuum pump (Welsh)
  - Pipes, valves, fittings, helium supply manifold
  - Helium and water flow measuring devices
  - Pressure gages and temperature measuring devices (also calibrated)
- Fabricated
  - Cesium supply tank
  - Cesium collection tank
  - Two-stage filter (charcoal and absolute) compressor inlet
  - Primary condenser
  - Concrete pad for compressor and cooler
- Fabrication in progress
  - Two-stage filter (charcoal and absolute) compressor discharge
  - Secondary condenser
  - First stage cooler
  - Second stage cooler
  - Helium cooler
  - He-Cs separator
  - Control panel
  - Cs flow meter
  - Compressor aftercooler

Final assembly and shakedown of the system are planned for the next reporting period.

DEVELOPMENT AND ADAPTATION OF DIAGNOSTIC METHODS

A theoretical study was made to calculate the absolute line intensities for cesium as a seeding substance in helium. That portion of the study which is now completed deals with the equilibrium values by thermal excitation. Results are based on an extensive parametric study using the IBM 7090.

In the experimental part of the program, a new spectroscopic technique was developed which allows a spatial resolution of the plasma properties. This technique makes it possible to segregate and photograph one component of an entirely mixed gas. The same photograph will show the sheaths on electrodes of the segregated component. Further, this method is a valuable adjustment aid for line broadening measurements.

For the investigations in the MPD-device, this new method is expected to give the spatial distribution of electron temperature and electron density. Composition of the sheaths on the electrodes, it is hoped, may be determined through use of this technique.

THEORETICAL INVESTIGATIONS

The theoretical investigations have been concerned with the stability of the plasma flow in MPD energy converters. Preliminary studies of the ionization degree of plasmas which deviate from thermodynamic equilibrium have been started.

Two convective processes which lead to instability have been investigated. A one-fluid approach has shown that the inertia forces of the flow cause a convective instability with a growth rate proportional to the gradient of the mean plasma velocity in the flow direction. A two-fluid theory has been used to derive a convective instability with a growth rate proportional to the electron-drift velocity. This latter instability is conditioned by the electron and ion streams making up the plasma current.

The investigations indicate that anomalous or nonequilibrium fluctuations are to be expected in the plasma flow, independent of the critical Reynolds number above which the hydromagnetic instability of the viscous flow field arises.

The calculations will be extended to supersonic flows. Another investigation will be concerned with a possible electrostatic convective instability of the plasma flow.

III. THE ALLISON DIAGNOSTIC CLOSED LOOP MPD DEVICE

The test apparatus utilized in this program is a diagnostic device with features of a medium scaled, closed loop, MPD power generator. To examine the basic properties of the plasma, the system has been designed to permit application of extensive diagnostic methods. This section presents pertinent design detail and operational features of the system, heater, test section, and diagnostic equipment.

THE SYSTEM

A schematic of the Allison MPD Diagnostic Facility is shown in Figure 1. The vacuum pump, used to remove all of the air within the system, is a 23.5-liter/sec (50 cfm) Welsh pump which has an ultimate vacuum capability of 0.01 micron. The piping is arranged so that vacuum can be achieved within three different areas of the loop at the same time by proper valve selection. The system will be evacuated to less than 10 microns at least twice and on each occasion refilled with purified helium from the purified helium source. A manifold of 10 bottles of helium (two banks of five bottles each) installed on the outside of the buidling is separately regulated so that one bank of bottles serves as the active bank, the other as a reserve bank. The helium enters a purification system consisting of two NaK bubblers (Figure 2). The first bubbler is heated electrically to approximately 480°K. The second bubbler is allowed to remain at approximately room temperature.

The two bubblers in combination have demonstrated the capability (in other Allison research activities) to remove oxygen to less than one part per million. However, the bubbler system is relatively small and would not purify the entire flow of helium that will pass through the MPD device. Consequently, this bubbler system is used only to purify the gas being admitted to fill the system. A separate purification system of a higher flow capability is used to purify the flow circulating within the loop. The discharge of the gas through the NaK bubbler is directed into various parts of the system through four different pressure regulators. One pressure regulator supplies helium to both sides of the diaphragm disk of the back pressure regulating control valve. If air were used for valve control, there would be the danger of air diffusing through the diaphragm into the system.

A second regulator is used to maintain a positive pressure on the compressor suction at all times. This pressure will vary slightly (in the order of a few millimeters of mercury). The other regulators, No. 3 and 4, are used to supply the helium necessary to transport the cesium from one cesium container to the other.

The helium compressor is a Miehle-Dexter lobe type (Figure 3). The compressor bearings are mounted outboard to the actual helium path, and there are carbon-face seals between the bearing cavity, which is oil lubricated, and the compressor cavity, which the vendor claims to be entirely free of oil. This type of compressor has been used successfully by various manufacturers of gas purification systems for dry boxes and other purposes where high purity gases are required. This type of compressor has a rather low compression ratio in order to operate in a nonlubricated condition; therefore, the compressor used requires two stages to provide a 1.36-atm (gage) output pressure. The high pressure helium then is fed through an aftercooler. The compressor discharge temperature is approximately 420°K. The aftercooler is a specially designed heat exchanger in which care was taken to prevent the admission of water from the cooling side of the heat exchanger into the pipe where the helium flows. The stainless steel pipe used to carry the helium through this heat exchanger has been hydrostatically pressure tested and ultrasonically inspected to rigid requirements. The helium leaves the aftercooler at approximately 310°K and proceeds through an activated charcoal filter. The filter is possibly not necessary; however, in the interest of complete safety, the filter was placed in the circuit in the event that the compressor should permit slight traces of oil vapor to enter the helium stream. As the charcoal used is made from coconut shell, the problem of releasing ammonia found by other investigators where animal charcoal was used should not exist. The charcoal filter also includes an absolute filter to prevent any charcoal dust from being carried into the helium stream. This type of filter combination has been used successfully at Allison for the removal of quite large quantities of oil vapor from helium and should work very well in the removal of traces of vapor.

Immediately after the charcoal filter is a tap for providing cool helium to the MPD device itself. Several small lines are fed to the device for the purpose of keeping various areas in the device cool. All the flow will be measured. These small flows enter the main helium downstream from the MPD device and do not alter the flow through the device which is separately measured. After passing through the main flowmeter, the helium enters the heater and the MPD device. The flowmeter is a standard-gas, ASME sharp-edged orifice utilizing a differential pressure gage and a Heise reference pressure gage. By the use of the aftercooler, the temperature entering the orifice run will be reasonably constant, and by the use of the backpressure regulating valve, the pressure entering the orifice meter run will be relatively constant. Therefore, only minor corrections will be required for the flow measurement. Downstream of the flow measurement device is a remote-operated throttling valve which will be used to adjust the flow through the heater and the MPD device. The adjustment of this valve will be by remote means at the control panel in the vicinity of the orifice differential pressure gage so that the flow can be observed at the same time the flow is being adjusted.

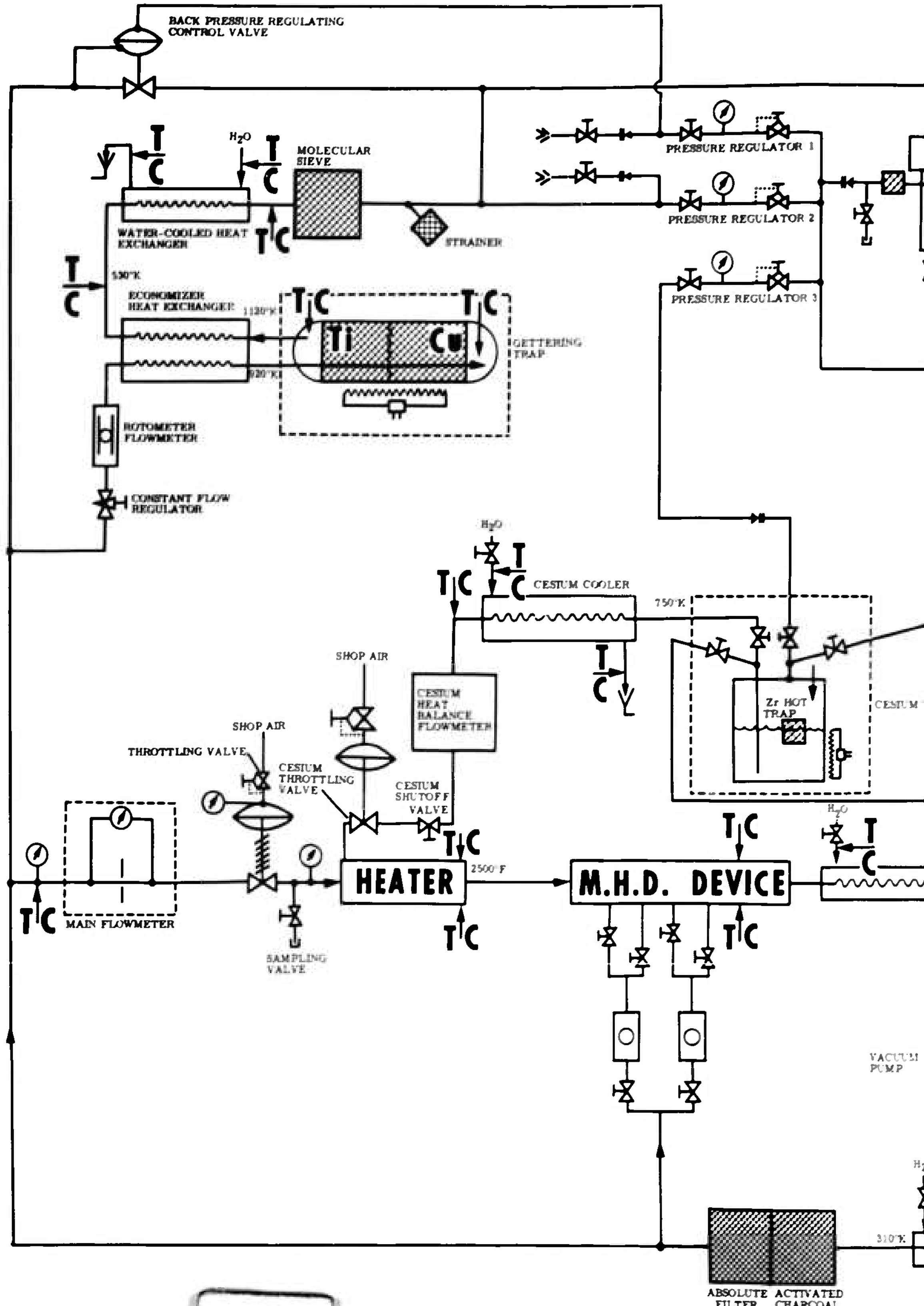
BACK PRESSURE REGULATING
CONTROL VALVE
MOLECULAR
SIEVE
WATER-COOLED HEAT
EXCHANGER
STRAINER
PRESSURE REGULATOR 1
PRESSURE REGULATOR 2
PRESSURE REGULATOR 3
530°K
ECONOMIZER
HEAT EXCHANGER
1120°K
920°K
Ti
Cu
GETTERING
TRAP
ROTOMETER
FLOWMETER
CONSTANT FLOW
REGULATOR
CESIUM COOLER
750°K
Zr HOT
TRAP
CESIUM
SHOP AIR
SHOP AIR
THROTTLING VALVE
CESIUM
THROTTLING
VALVE
CESIUM
HEAT
BALANCE
FLOWMETER
CESIUM
SHUTOFF
VALVE
HEATER
2500°F
M.H.D. DEVICE
MAIN FLOWMETER
SAMPLING
VALVE
VACUUM
PUMP
310°K
ABSOLUTE
FILTER
ACTIVATED
CHARCOAL

1

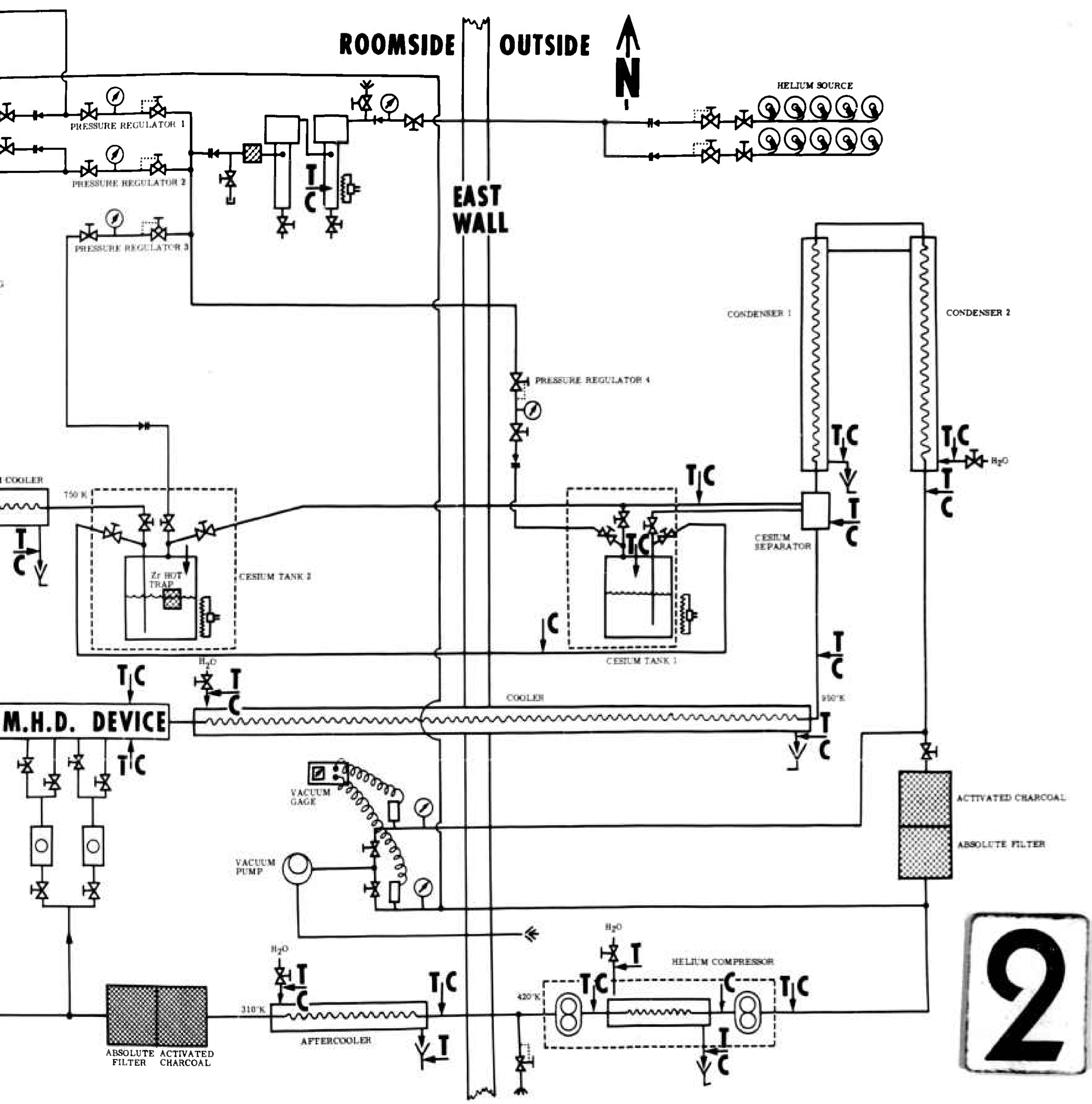

Figure 1. Magnetoplasmadynamic Facility Schematic

Figure 2. NaK Bubblers

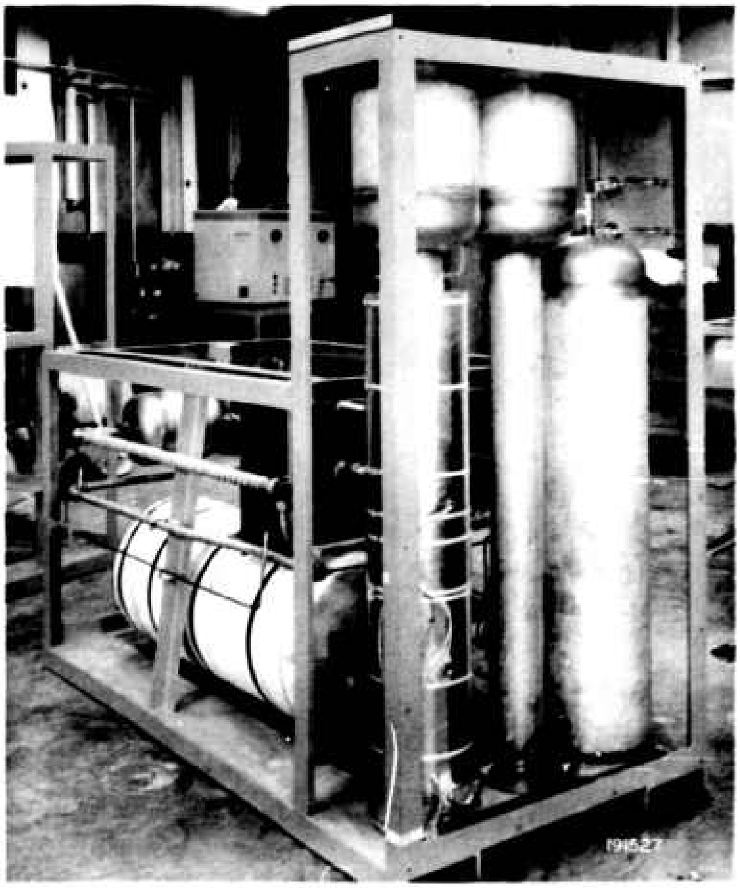

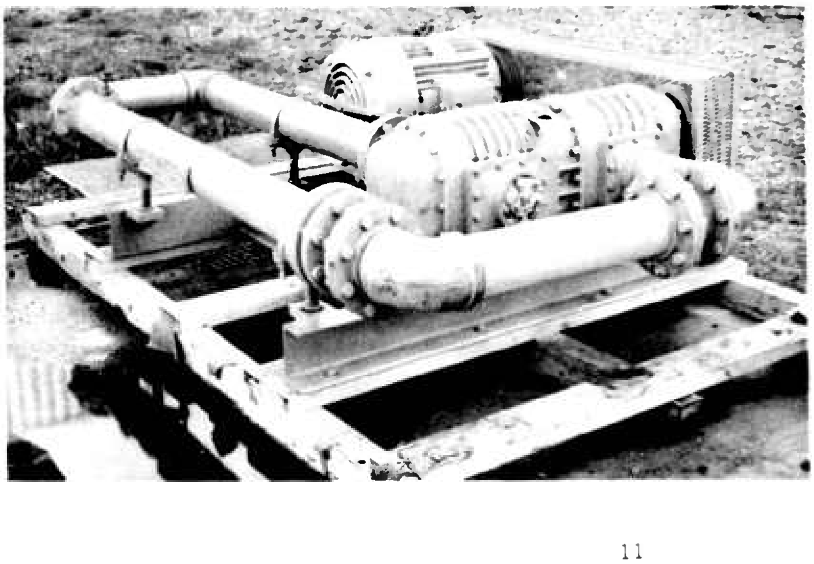

Figure 3. Helium Compressor

Immediately behind the throttling valve is a small sampling valve. The helium can be circulated in the loop at a low temperature until samples removed from the sampling valve indicate that oxygen, moisture, hydrocarbons, and various other impurities are removed to sufficiently low levels to permit heater operation. A common heater is used to heat both the helium and cesium to the required 2500°K for the MPD device. The heater, however, heats the cesium and the helium in separate channels utilizing the same heating element. The heating is accomplished with wound tungsten elements which have a capacity in excess of 200 kw. The Allison power supply available for use with this heater has a rated capacity of approximately 175 kw. This power supply is a remotely operated motor generator set supplying a d-c voltage to the heater.

The helium and the cesium being heated separately are then mixed together at the exit of the heater. The schematic (Figure 1) shows a space between the heater and the MPD device, but, actually, these are closely coupled. The 2500°K helium-cesium mixture is then fed to the MPD device which is explained later in this report. The helium will exit from the device at at a temperature somewhat less than the 2500°K; however, the cooling system was designed to take care of the full helium and full cesium flow at a temperature of 2500°K. The first cooler was designed with a film coefficient sufficiently low that the actual pipe or tube wall would remain relatively cool even though the pipe contained a helium-cesium mixture at 2500°K.

The condenser is water cooled. The condenser (Figure 4) consists of a tube within a tube in which the helium-cesium mixture flows through the inner tube, and water, at a relatively high velocity, flows through the annular area between the two tubes. The first condenser (Figure 5) is approximately six meters long. The exit temperature of the helium-cesium mixture from this condenser is estimated to be approximately 450°K. Calculations of pipe wall temperature show that the maximum pipe wall temperature will be approximately 322°K. The cesium will start to condense at approximately 4.6 meters from entry of the heat exchanger condenser, and most of the condensation will be complete before the helium-cesium mixture exits from the end of the six-meter run. Pipe wall temperatures at the end of the run are estimated to be 305°K, which is still above the freeze point of the cesium that is rolling along the bottom of the pipe. The cesium, of course, will not fall immediately to the bottom of the pipe, but will remain suspended. To separate the suspended cesium, the mixture of helium gas and cesium liquid will then be ejected from the six-meter section into a helium-cesium separator of the centrifugal type. This separator will remove the bulk liquid that is suspended in the helium and allow it to drain to the first cesium tank. The remaining helium will still contain large quantities of cesium vapor, and additional cooling and condensing is required. This is accomplished in three additional cooler-condenser stages. All of the remaining cooler-condenser

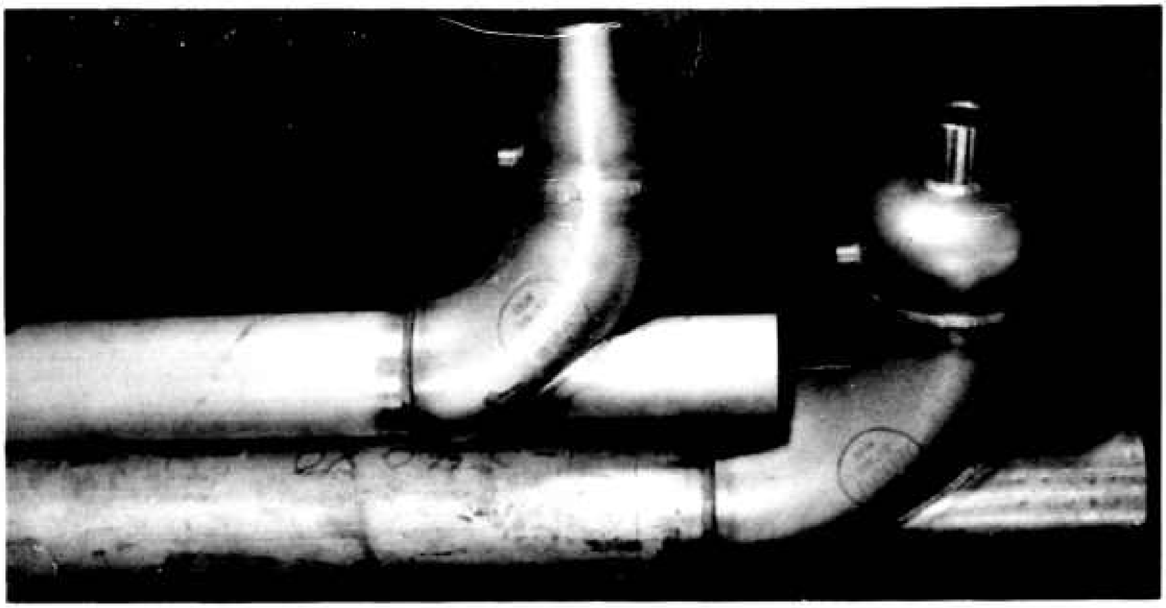

Figure 4. Heat Exchanger (Details)

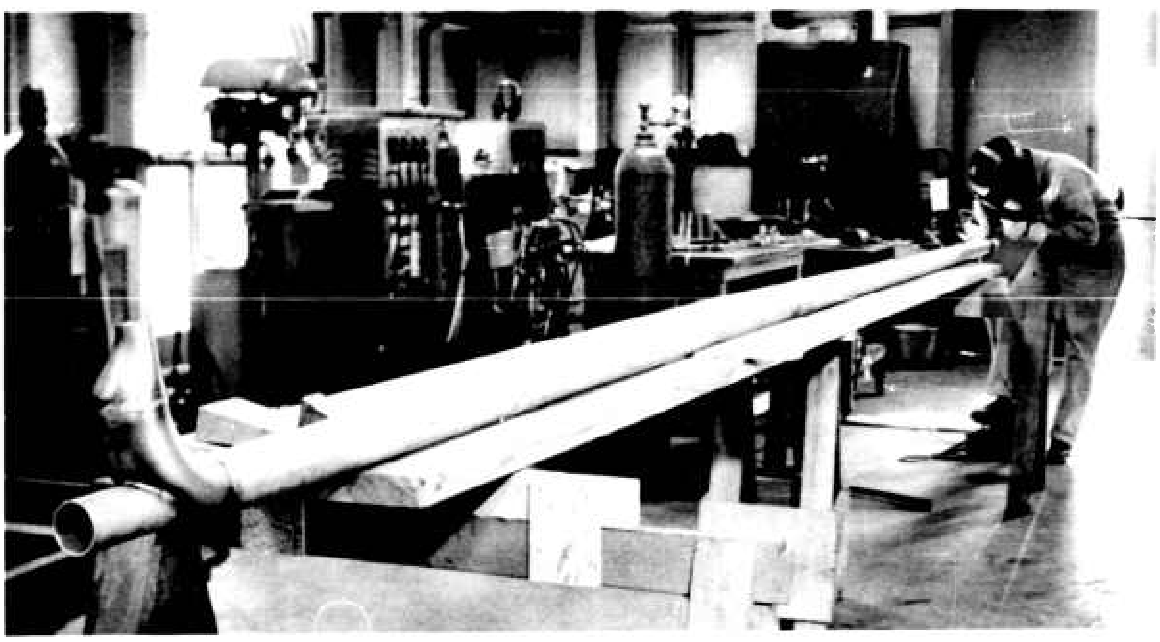

Figure 5. Heat Exchanger

stages are sloped in such a manner that as the cesium condenses it collects at the lower portion of the inner pipe of the double-tube heat exchanger and returns to the cesium separator and to the cesium tank. The second stage of heat exchangers has even lower pipe wall temperatures due to the high velocity of water and a relatively low film coefficient for the helium-cesium mixture. This means that some of the cesium which has collected in the tube will have a tendency to freeze as it rolls along the pipe length. Because the pipes are sloped toward the cesium separator, this cesium will be constantly rolling in the direction of higher temperature. It is believed that the slight amount of frozen cesium will not effect a blockage of the cooler for a considerable length of time.

Provision has been made to circulate hot water through the helium-cesium coolers so that, after an experiment is completed, any cesium that has been frozen out on these relatively cool pipe walls can be melted and returned to the separator and then to the cesium tank. At the end of approximately 12 m of this type of helium-cesium cooler travel, the estimated cesium vapor concentration in the helium has been reduced to one part per million. At the completion of approximately 18 m of this type of cooler travel, the concentration is less than five parts per billion. There are approximately 21 m of helium-cesium coolers in this circuit. At the end of the 21-m run, the helium should be at a temperature of less than 311°K. If for some reason the helium-cesium separation has not been complete, the helium is then passed through a second activated charcoal and absolute filter-type combination. Any cesium vapor remaining in the helium flow is then reacted with the charcoal and prevented from entering the helium compressor where the cesium might do damage to the carbon-face seals. This completes the main circuit of the main flow of helium through the loop.

The purification system, through which a part of the helium is continuously circulated, is connected to the loop at the main flowmeter. The total flow in the compressor is approximately 117 liters/sec (200 cfm). The MPD device will require up to 56.4 liters/sec of this total flow. Approximately 2.35 liters/sec (5 cfm) will flow continuously through the purification system regardless of the flow elsewhere in the circuit; the remaining 35.2 liters/sec (75 cfm) will flow through the back pressure regulating valve. The flow through the heater purification train is regulated by a constant flow regulator and is measured by a small rotometer-type flowmeter. The helium passes through an economizer heat exchanger (Figure 6) where it is preheated slightly before entering a gettering trap. The helium is admitted to the copper wool end of the trap and is heated to approximately 920°K. The helium then passes through the copper wool gettering trap and enters the titanium chips trap where it is further heated—to ap-

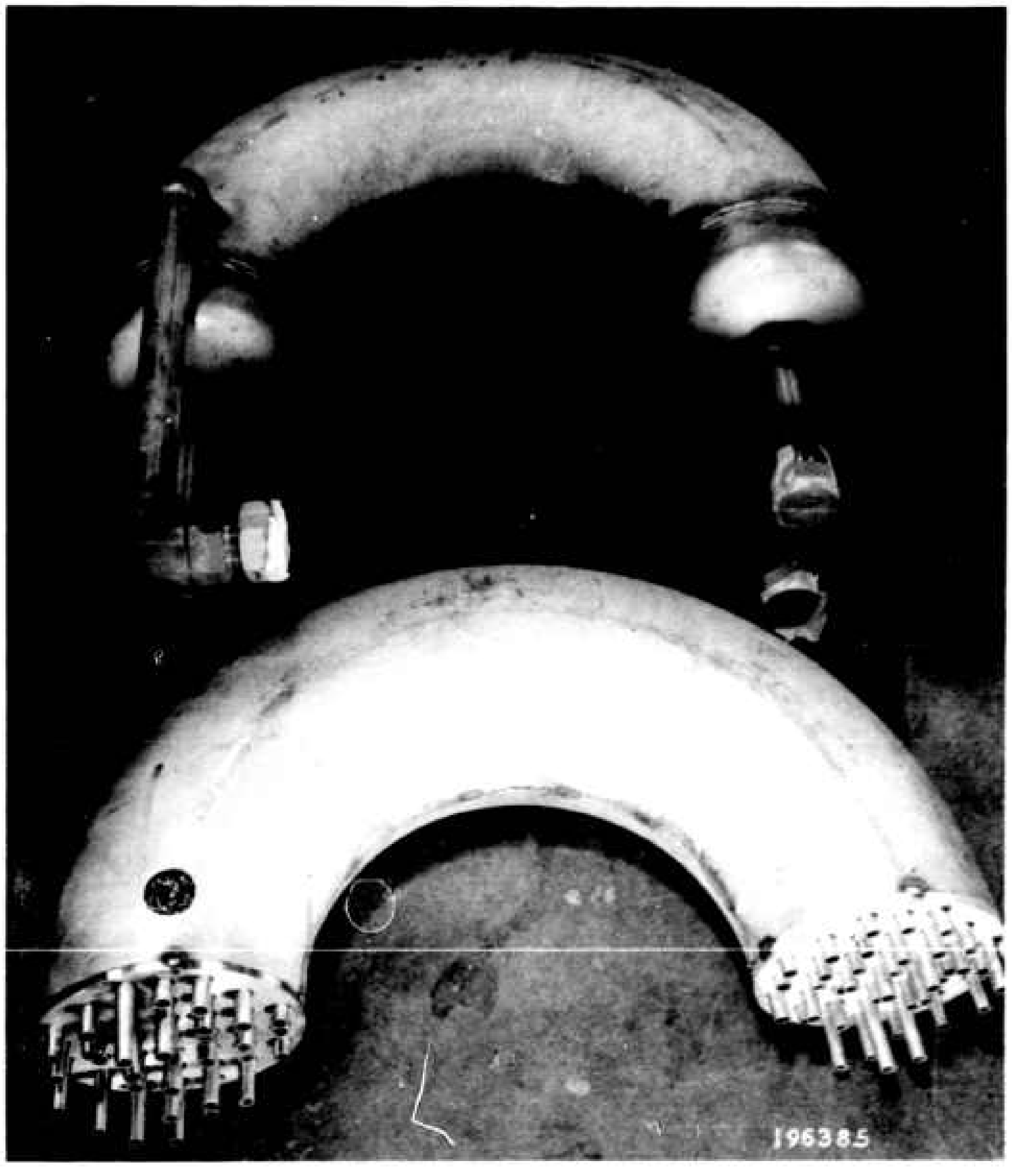

Figure 6. Economizer Heat Exchanger

proximately 1120°K; it is fed to the economizer heat exchanger where it gives up some of its heat to the incoming gas to the gettering trap. The gas then leaves the economizer heat exchanger at approximately 530°K and enters a water-cooled heat exchanger. This heat exchanger is also designed to prevent the water vapor from entering into the helium path. This type of heat exchanger has been used successfully—in fact, the entire purification train has been used on Allison glove box purification systems. All helium piping in contact with water has been ultrasonically inspected and hydrostatically pressure checked to eliminate the possibility of any flaws which might permit water vapor to enter the helium stream.

Downstream of the water cooler is a molecular sieve utilizing a Linde molecular sieve material. This sieve will remove water vapor in the stream which may have been introduced with the original filling, in addition to the water vapor which might be generated by the gettering trap. The crystalline absorbent sieve material has a chemical composition of $\left[0.83 \pm 0.05\ Na_2O\right] \cdot \left[1.00\ Al_2O_3\right] \cdot \left[2.48 \pm 0.03\ SiO_2\right] \cdot \left[x\ H_2O\right]$. It is chemically stable to above 600°C. In addition to removing water vapor, the sieve absorbs ammonia, should any appear within the system. Because the sieve and the charcoal do absorb gases, it is necessary to ensure a sufficient time in a vacuum for outgassing. The copper wool and titanium chip gettering trap may, under certain conditions, generate water vapor. If there is any hydrogen in the helium, the hydrogen will have a tendency to reduce the copper oxide and titanium oxide in the trap to water vapor.

A fine stainless steel wire mesh strainer is located downstream from the molecular sieve to prevent any molecular sieve material from flaking off and entering the helium stream. The purified helium is then admitted into the discharge side of the back pressure regulator valve and returned to the pressure suction line.

The cesium flow path begins with the cesium container No. 2. The cesium is contained in a Mine Safety Appliance shipping container which includes a zirconium hot trap and heating system. The cesium can be heated in this container for the time necessary to achieve the required purity. When cesium is required in the system, cesium can be forced through the dip leg to a heat exchanger by applying helium pressure to the shipping container. The cesium in the container will be at approximately 750°K for the purification process. Since the cesium should be cooled prior to entering the 200-kw heater to protect the heater power leads, the cesium will be cooled to approximately 360°K through a water-type heat exchanger. This heat exchanger is different from the heat exchanger used for cooling the helium-cesium mixture in that the cesium passes through a straight tube around which is wound a smaller-diameter water tube. Only if leaks occur in both pipes could the water ever contact the cesium. The cesium flow is measured with a heat balance flowmeter which uses a small Chromolox electric heating element to heat the cesium through a small temperature differential. A wattmeter will be provided to measure power supplied to the cesium. A precision differential temperature measuring device developed by Allison will be used to measure the temperature increase of the cesium. Then the cesium flow can be calculated.

Two valves are provided downstream of the flowmeter, one a cesium shutoff valve and the other a cesium throttling valve. The throttling valve is a remote-operated type actuated from the control panel. This valve will be air-operated since the underside of the diaphragm will be exposed to the atmosphere and the air on the diaphragm will not have an opportunity to diffuse into the system. The cesium leaving the helium flow channel at the cesium separator is directed to a second shipping container without hot trap and high temperature heating system. The low power heater for the cesium tank No. 1 is used only to prevent the cesium from freezing. This container is capable of storing the full quantity of cesium that is in the system. The cesium collected in container No. 1 may be either transferred back to the supply container or allowed to remain. The cesium inventory within the supply container will be monitored by an induction circuit which remotely locates the position of a floating permanent magnet. The continual monitoring of the cesium level provides a second method for measurement of cesium flow and indicates when cesium transfer is necessary.

Cesium in the supply container will be heated to the gettering temperature and allowed to undergo purification for 12 hours before a run is made. Further purification will be made as necessary to keep cesium impurities low. The initial charge of cesium in the loop will be approximately 9 kg. The cesium cooler is used to decrease the cesium temperature from gettering temperature low enough to enter the flowmeter. The cooler will be supplied with temperate water to prevent the cesium from freezing in the heat exchanger. Valves are supplied in the loop so that maintenance can be done on the MPD device or on the heater without exposing the entire loop up to the atmosphere. The throttling valve upstream of the heater is a Grinnell-Saunders diaphragm valve which is a totally enclosed, mass spectrometer leak-tight valve. The valve at the upstream side of the activated charcoal and absolute filter combination in the compressor suction line is of the vacuum type. These two valves can be closed to isolate the heater MPD device and heat exchangers from the balance of the loop. The vacuum piping is arranged so that this isolated section can be evacuated and refilled without evacuating and refilling the remainder of the loop at the same time. This will permit a savings in helium and prevent air from entering large areas of the loop when work is required on the device or on the heater. The full capacity of the 23.5-liter/sec pump can then be used to outgas a smaller volume of the loop.

HIGH TEMPERATURE HEATER

Figure 7 is a cross section of the heater. The tungsten rod in the center of the heater is bored to provide a heating duct for the cesium flow. At the end of the tungsten rod is one end of a tungsten filament which is wound in an annular area between the large tungsten rod and the outer shell of the heater. The tungsten filament is attached to an electrode at the position where cool helium (310°K) is admitted, thus providing cool electrodes for attachment of the power leads. The cesium also enters this cool end of the heater and is at a temperature of about 360°K.

The tungsten filament in the heater is supported by stand-off types of insulators which are mounted in grooved slots on the large tungsten rod extending down through the middle of the heater.

The tungsten filament is designed to operate at power levels to 200 kw. It is not anticipated that full capacity of the heater will be required. A manufacturing process to wind the heater coil has been established. Fabricated parts are shown in Figure 8.

TEST SECTION

The MPD test section has been designed specifically for diagnostic investigation of plasma properties. Emphasis has been placed on versatility, ease of maintenance, and simplicity. As shown in Figure 9, the test section consists of a flow channel, electrode blocks, observation ports, and electromagnet assembly.

As the helium-seeded plasma enters the test section, it is expanded through a replaceable tungsten nozzle. By varying the size of the nozzle, a wide variation of flow rate may be achieved for any given fluid velocity. The tantalum channel is lined with high purity alumina panels to provide electrical insulation with respect to currents induced in the $\vec{V} \times \vec{B}$ interaction. The flow stream from the nozzle is in the form of a free jet and does not contact the channel

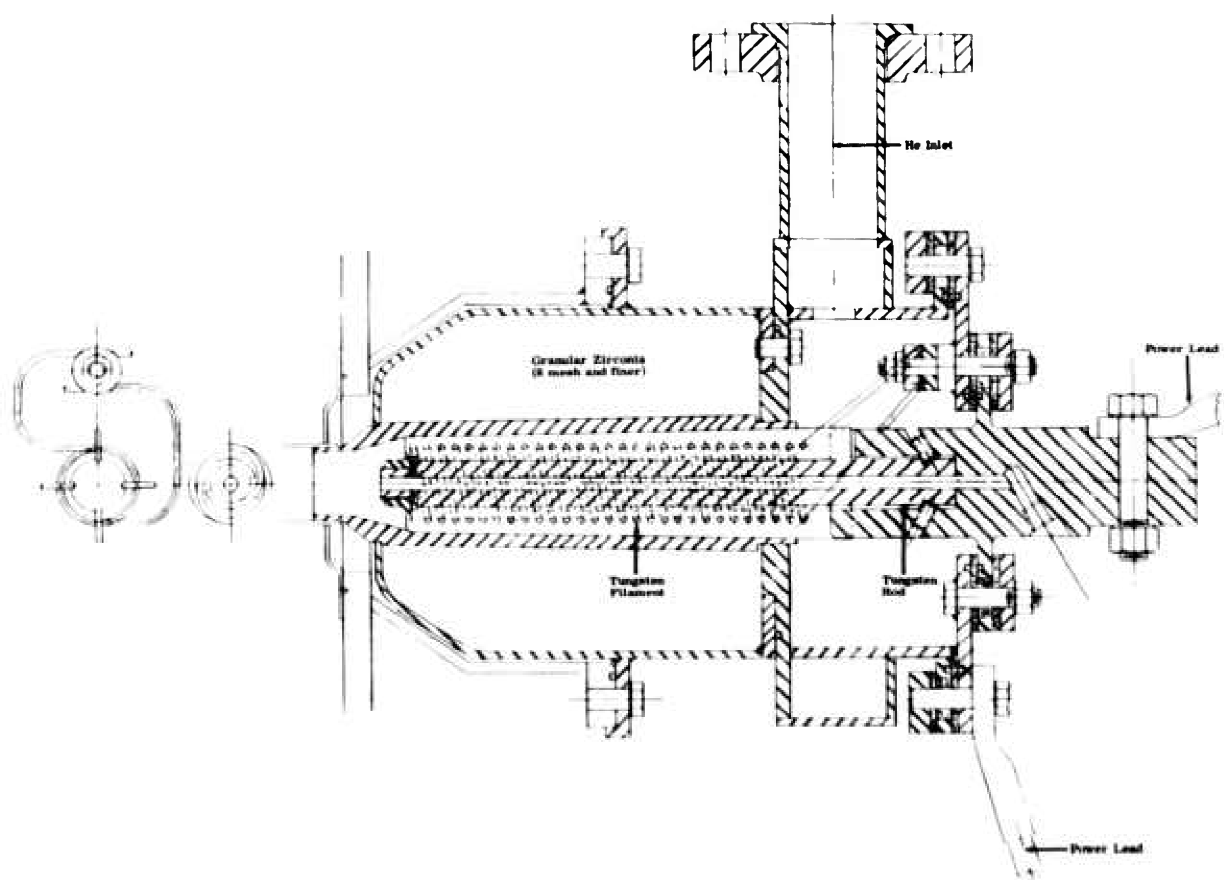

Figure 7. MPD Gas Heater Assembly

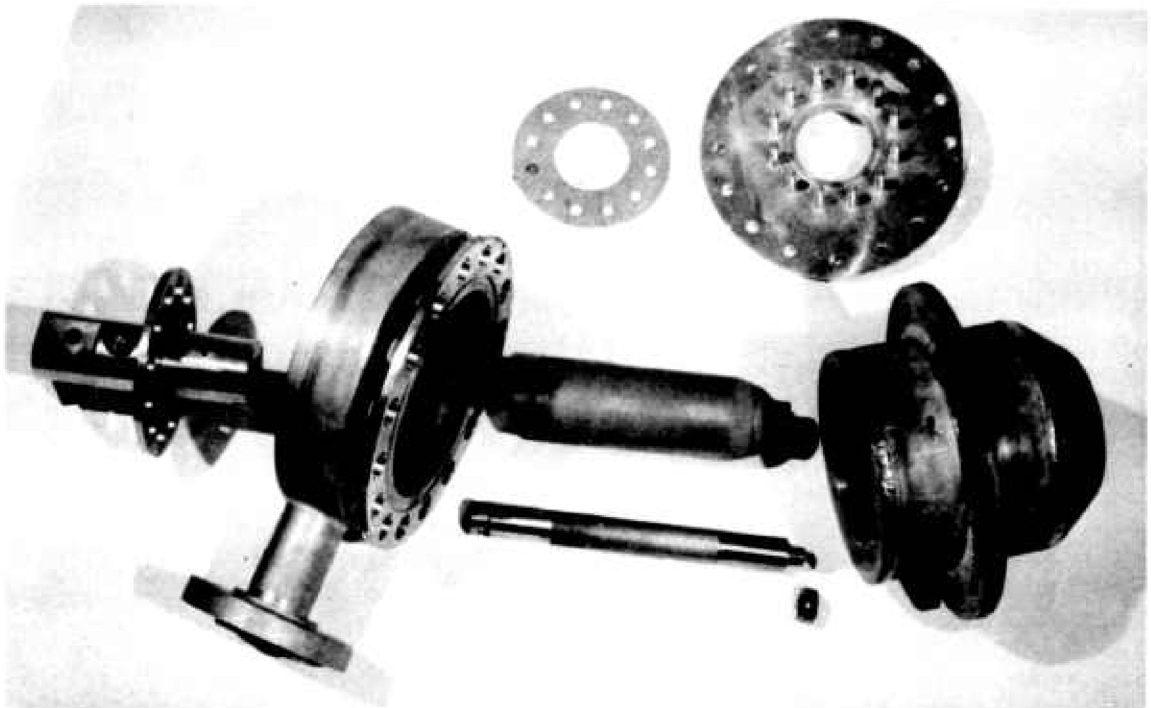

Figure 8. Heater Parts

walls upstream of the electrode blocks. This feature reduces the possibility of channel failure which could result from thermal degradation. To protect the tantalum from oxidation, the section is housed within a 1/2-in. thick stainless steel structure. In addition to providing support to the test section, it provides a helium atmosphere for the tantalum duct. An overpressure within this cavity produces a slight in-leakage of cool helium to the test section.

The electrode assembly features variable spacing through the use of a bellows sealing arrangement. Adjustment of the two jack-screws provides variation of the aspect ratio. The electrode blocks may be interchanged to allow investigation of electrode geometry on plasma properties. One of the electrode blocks being fabricated consists of 47 platinum pins shrunk into an alumina block. An additional pin of a platinum-rhodium alloy is inserted into the alumina block to allow thermometry monitoring of the test section. Electrical leads from each pin will be connected to a 50-pin hermetically sealed connector. External breadboard circuitry permits the test

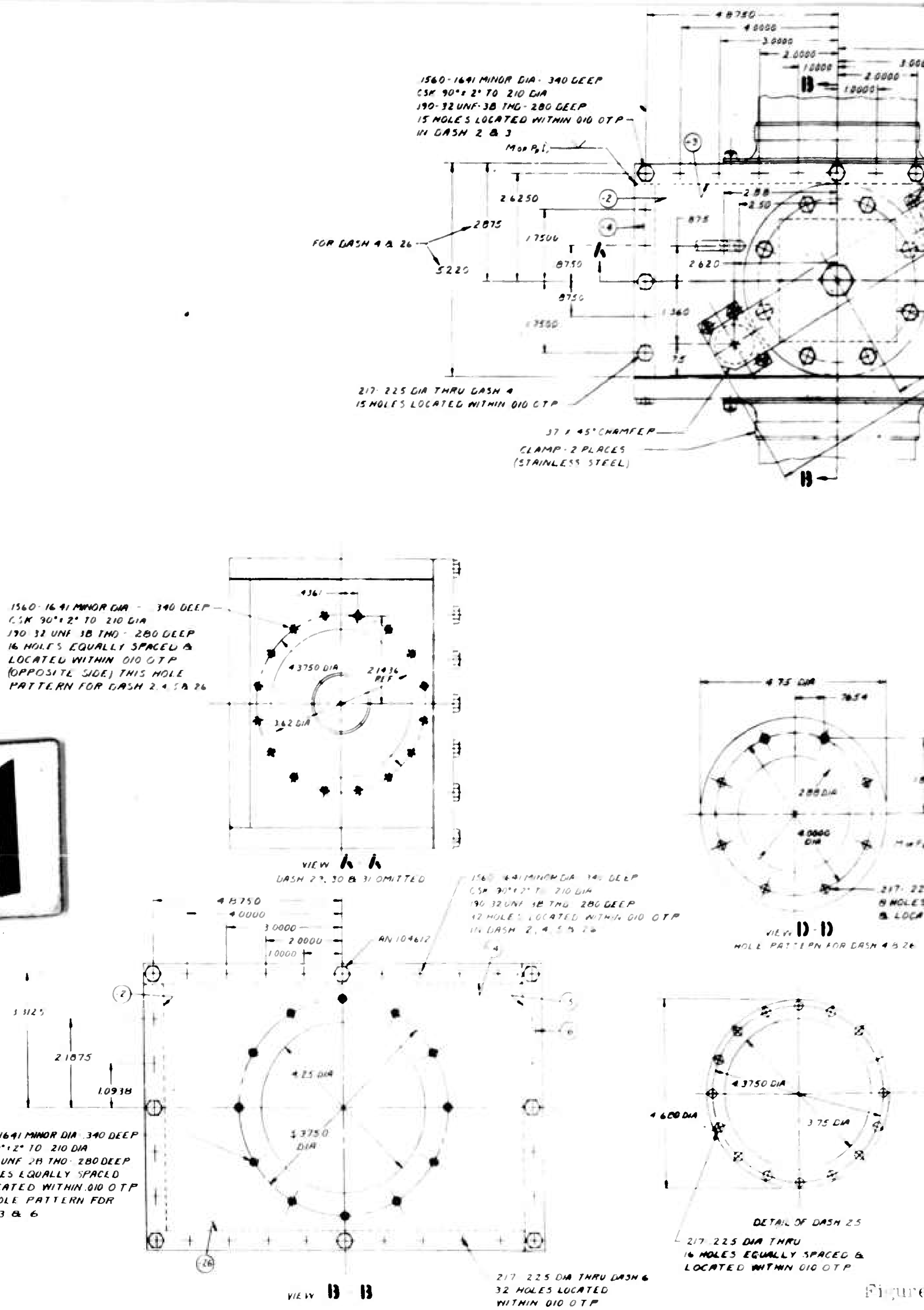

1560-1641 MINOR DIA - 340 DEEP
CSK 90° ± 2° TO 210 DIA
190-32 UNF-3B THD - 280 DEEP
15 HOLES LOCATED WITHIN 010 OTP
IN DASH 2 & 3
FOR DASH 4 & 26
217-225 DIA THRU DASH 4
15 HOLES LOCATED WITHIN 010 OTP
37 X 45° CHAMFER
CLAMP - 2 PLACES
(STAINLESS STEEL)
1560-1641 MINOR DIA - 340 DEEP
CSK 90° ± 2° TO 210 DIA
190-32 UNF-3B THD - 280 DEEP
16 HOLES EQUALLY SPACED &
LOCATED WITHIN 010 OTP
(OPPOSITE SIDE) THIS HOLE
PATTERN FOR DASH 2, 4, 5 & 26
4 3750 DIA
3 62 DIA
VIEW A-A
DASH 27, 30 & 31 OMITTED
4 75 DIA
2 88 DIA
4 0000 DIA
VIEW D-D
HOLE PATTERN FOR DASH 4 & 26
1560-1641 MINOR DIA 340 DEEP
CSK 90° ± 2° TO 210 DIA
190 32 UNF 2B THD - 280 DEEP
12 HOLES EQUALLY SPACED
& LOCATED WITHIN 010 OTP
THIS HOLE PATTERN FOR
DASH 3 & 6
4 25 DIA
3 3750 DIA
VIEW B-B
217 225 DIA THRU DASH 6
32 HOLES LOCATED
WITHIN 010 OTP
4 3750 DIA
3 75 DIA
4 620 DIA
DETAIL OF DASH 25
217 225 DIA THRU
16 HOLES EQUALLY SPACED &
LOCATED WITHIN 010 OTP

1

Figure

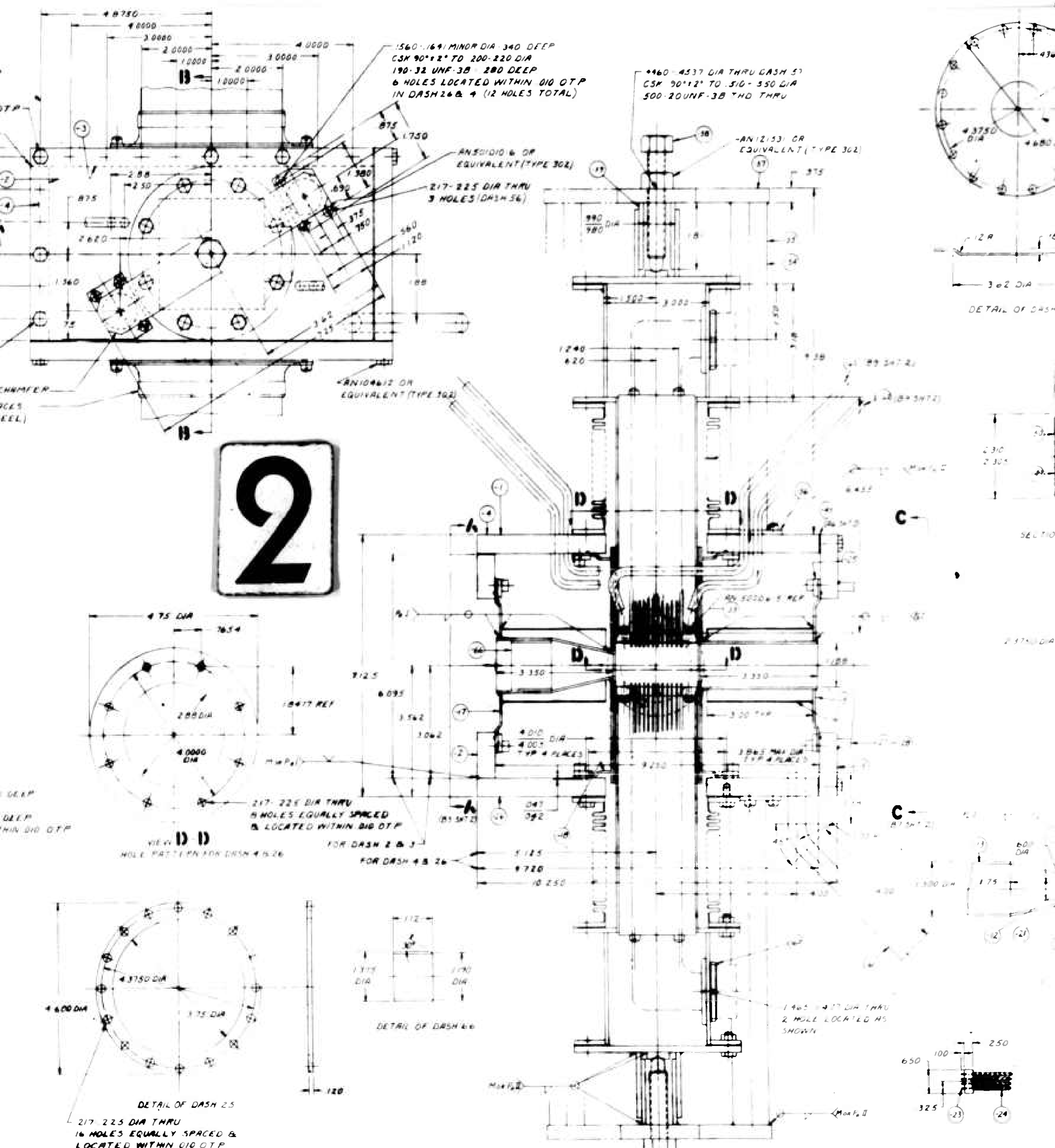

Figure 9. MPD Diagnostic Device

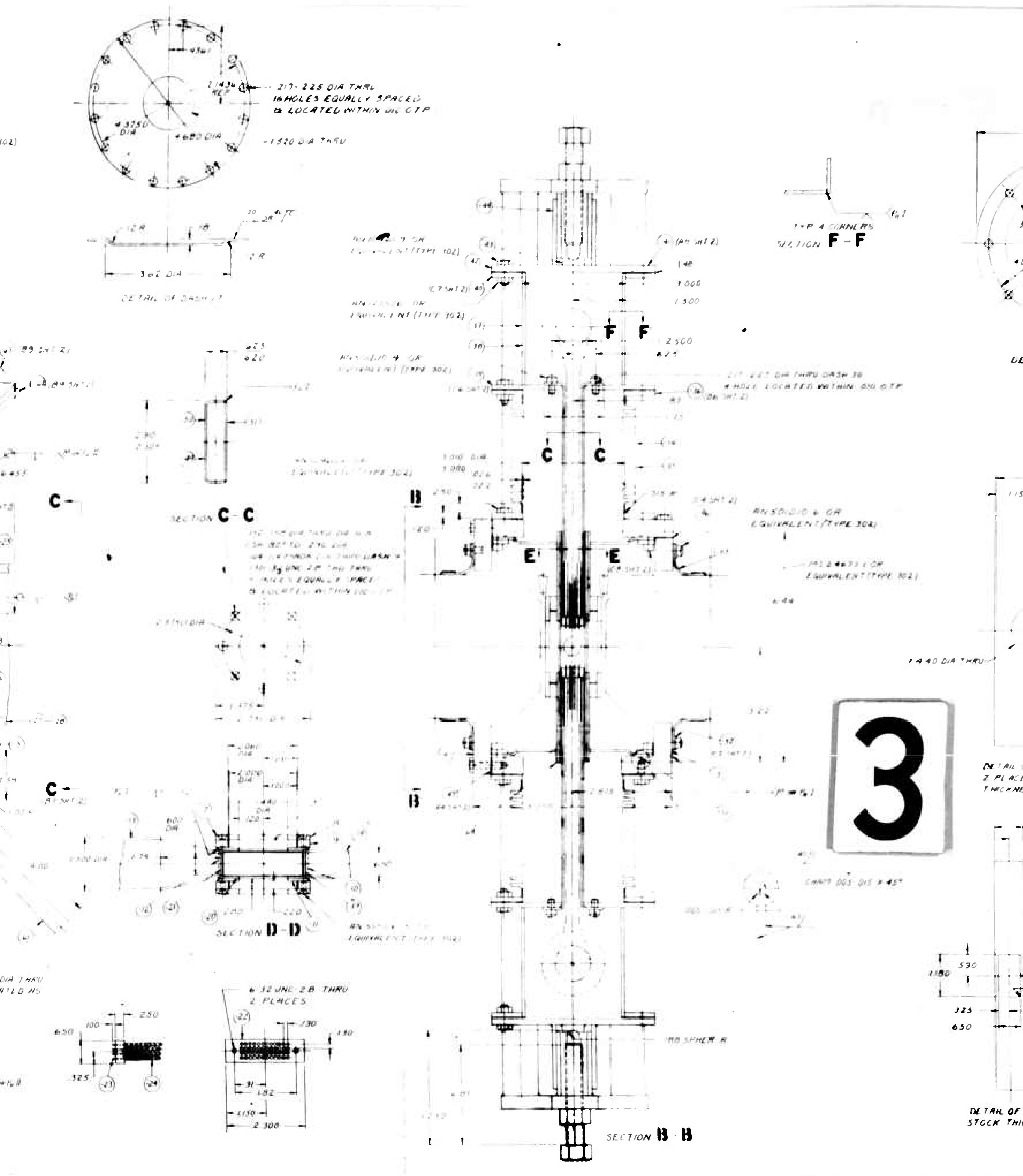

16 HOLES EQUALLY SPACED
1.520 DIA THRU
4.680 DIA
3.02 DIA
DETAIL OF DASH 17
TYP 4 CORNERS
SECTION F-F
F
C
B
E
SECTION C-C
EQUIVALENT (TYPE 302)
AN 50.0.10-6 OR
MS 24673 OR
1.440 DIA THRU
3
CHAM .005-.015 X 45°
SECTION D-D
6-32 UNC-2B THRU
2 PLACES
2.300
SECTION B-B
.590
.325
.650

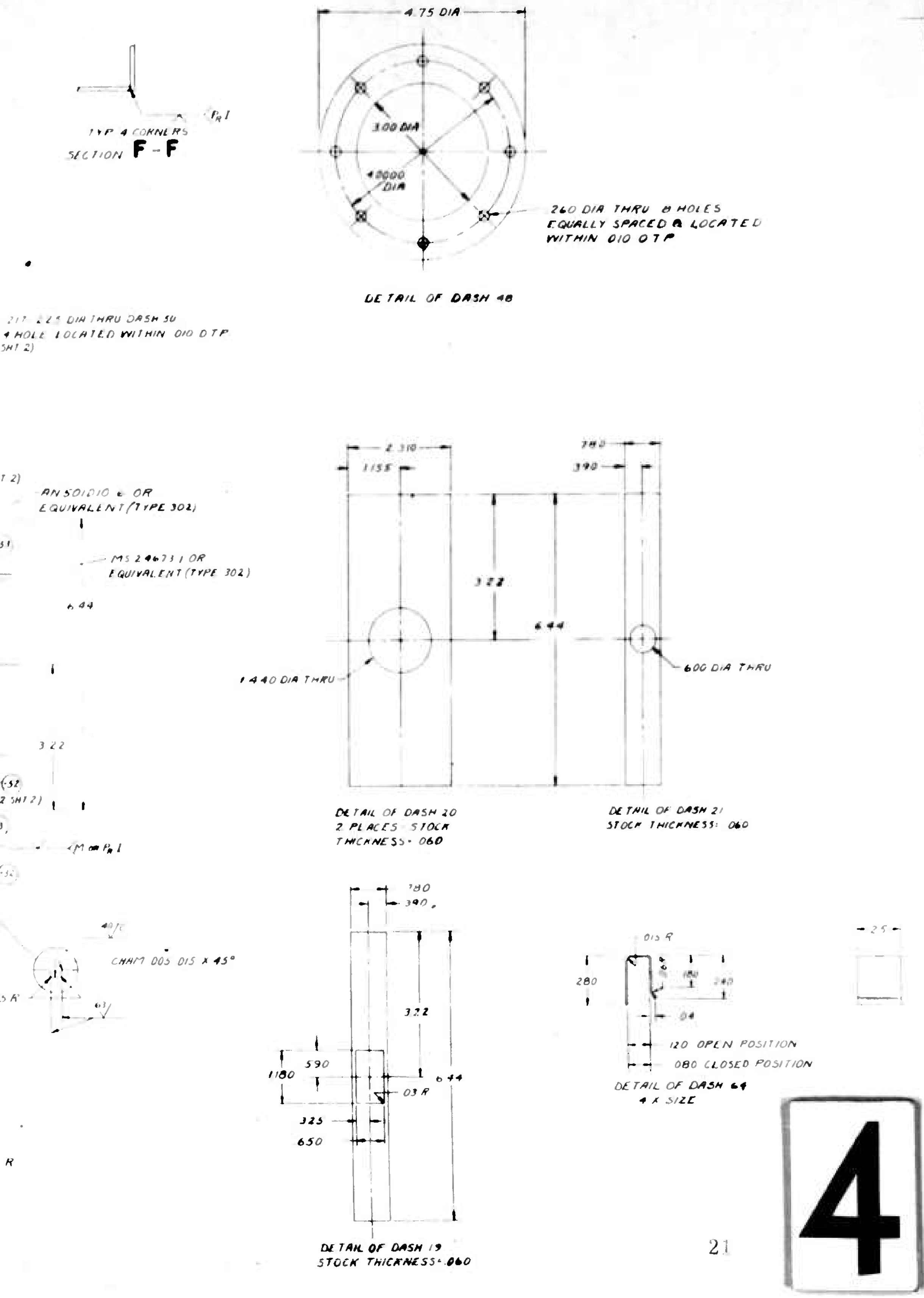

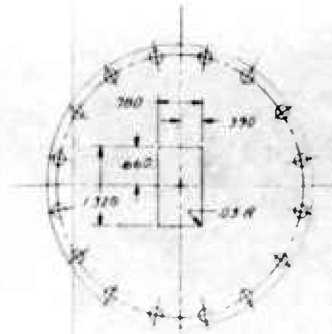

DETAIL OF DASH 15
SAME AS DASH 17 EXCEPT
AS SHOWN

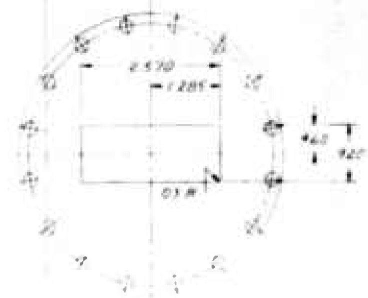

DETAIL OF DASH 18
SAME AS DASH 17 EXCEPT
AS SHOWN

NOTES

1. DASH 27 - 4 x 3 IN CONCENTRIC REDUCER SCHED 40S TYPE 316 STAINLESS STEEL
   DASH 28 FLANGE PIPE WELDING 3IN 150LB ASA STD TYPE 316 STAINLESS STEEL
   TUBE TURNS INC LOUISVILLE KY
2. DASH 61 AMS 5570 495 505 OD x 031 039 WALL THICKNESS
3. DASH 62 & 63 AMS 5570 246 254 OD x 025 031 WALL THIC[KNESS]
4. ALL BOLTS SCREWS & NUTS MUST BE TYPE 302 MATE[RIAL]
5. PURCHASED PARTS DASH 24 ALSIMAG 35 PART NO 164[...]
   AMERICAN LAVA CORP
   CHATANOOGA TENN
6. SAME AS AN 500C6 5
7. PURCHASED PARTS DASH 35 CAT NO A 10011 &
   DASH 36 TYPE 4 STAINLESS STEEL
   FLEXONICS CORP
   MAYWOOD ILL
8. 995 - 1005 x 058 072 WALL THICKNESS
9. MAKE FROM AN105132
10. PURCHASED PART CAT NO KHIO 21 P
    CANNON ELECTRIC CO
    3208 HUMBOLDT ST
    LOS ANGELES 31 CALIF

REMOVE BURRS & SHARP EDGES

MACHINED SURFACES TO BE $\overset{63}{\surd}$ UOS

WELD RODS TO BE AMS 5782 AMS 5783 AMS 5784 & AMS 5785

FILLER MATERIAL TO BE SAME COMPOSITION AS AMS 7849 (TANTALUM)

FOR STANDARD SIZE PARTS & MATERIAL (NUTS, BOLTS, SCREWS, ETC). STANDARD COMMERCIALLY AVAILABLE PARTS ARE ACCEPTABLE. AN, MS OR ALLISON STANDARDS ARE DESIREABLE BUT ONLY IF READILY AVAILABLE

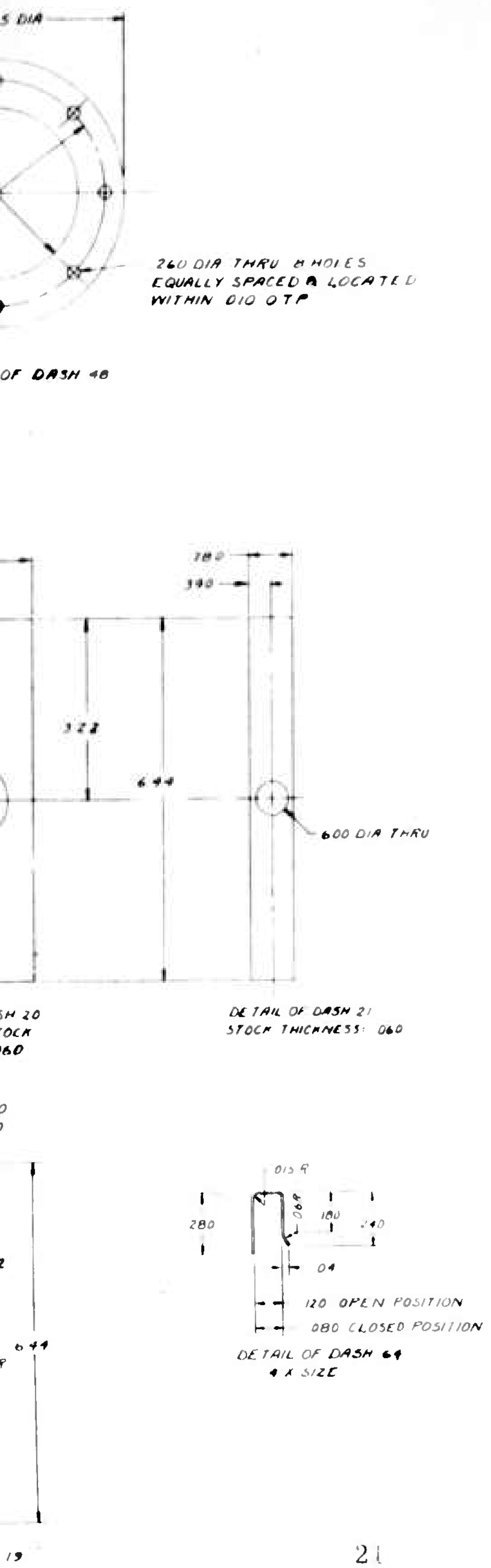

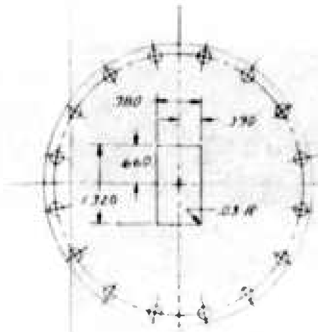

DETAIL OF DASH 15
SAME AS DASH 17 EXCEPT
AS SHOWN

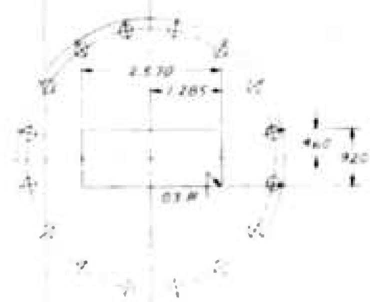

DETAIL OF DASH 18
SAME AS DASH 17 EXCEPT
AS SHOWN

NOTES

1 DASH 27 4 x 3 IN CONCENTRIC REDUCER
SCHED 40S TYPE 316 STAINLESS STEEL
DASH 28 FLANGE PIPE WELDING 3 IN 150 LB
ASA STD TYPE 316 STAINLESS STEEL
TUBE TURNS INC LOUISVILLE KY

2 DASH 61 AMS 5570 495 505 OD x 031 039 WALL THICKNESS

3 DASH 62 & 63 AMS 5570 246 254 OD x 025 031 WALL THICK

4 ALL BOLTS SCREWS & NUTS MUST BE TYPE 302 MATERIAL

5 PURCHASED PARTS DASH 24 ALSIMAG 1? PART NO 364
AMERICAN LAVA CORP
CHATANOOGA TENN

6 SAME AS AN 500C6 5

7 PURCHASED PARTS DASH 35 CAT NO A 10011 &
DASH 36 TYPE 4 STAINLESS STEEL
FLEXONICS CORP
MAYWOOD ILL

8 995 - 1.005 x 058 072 WALL THICKNESS

9 MAKE FROM AN 105132

10 PURCHASED PART CAT NO KHIO 21 P
CANNON ELECTRIC CO
3209 HUMBOLDT ST
LOS ANGELES 31 CALIF

REMOVE BURRS & SHARP EDGES

MACHINED SURFACES TO BE $\overset{63}{\surd}$ UOS

WELD RODS TO BE AMS 5782 AMS 5783
AMS 5784 & AMS 5785

FILLER MATERIAL TO BE SAME COMPOSITION
AS AMS 7849 (TANTALUM)

FOR STANDARD SIZE PARTS & MATERIAL (NUTS, BOLTS, SCREWS, ETC.) STANDARD COMMERCIALLY AVAILABLE PARTS ARE ACCEPTABLE. AN, MS OR ALLISON STANDARDS ARE DESIREABLE BUT ONLY IF READILY AVAILABLE

5

DASH NO	NUMBER REQD	MATERIAL	STOCK THICKNESS [illegible]	STOCK THICKNESS [illegible]	ZONE
1	1	ASSY OF DASH 2 THRU 6, 26, 27 THRU 31, 61 THRU 63 & BOLTS			[illegible]
2	1	CRES AMS 5521	500		[illegible]
3	1	CRES AMS 5521	500		[illegible]
4	1	CRES AMS 5521	500		[illegible]
5	1	CRES AMS 5521	500		[illegible]
6	1	CRES AMS 5521	500		[illegible]
26	1	CRES AMS 5521	500		[illegible]
27	1	SEE NOTE 1			[illegible]
28	1	SEE NOTE 1			[illegible]
29	1	CRES AMS 5510	188		[illegible]
30	1	CRES AMS 5510	188		C12
31	1	CRES AMS 5510	500		C12
61	1	SEE NOTE 2			A6 1
62	2	SEE NOTE 3			B6 1
63	2	SEE NOTE 3			C6 1
	64	BOLTS AN 104602	SEE NOTE 4		
7	1	ASSY OF DASH 8-18 & 65 & SCREWS			B6 1
8	2	Ta AMS 7849	120		A6 1
9	2	Ta AMS 7849	220		A6 1
10	1	Ta AMS 7849	060		B6 1
11	2	Ta AMS 7849	060		A6 1
12	1	Ta AMS 7849	060		B6 1
13	1	Ta AMS 7849	060		A6 1
14	1	Ta AMS 7849	060		A6 1
[illegible]	[illegible]	Ta AMS 7849	060		B6 1
[illegible]	[illegible]	Ta AMS 7849	030		A6 1
[illegible]	[illegible]	Ta AMS 7849	060		B7 1
18	2	Ta AMS 7849	060		B7 1
[illegible]	[illegible]	AN 565 [illegible]	SEE NOTE 4		B6 1
65	2	CORTZ			B6 1
19	[illegible]	SEE NOTE 5			B5 1
20	2	SEE NOTE 5			A6 1
21	1	SEE NOTE 5			B6 1
22	2	SEE NOTE 5			A6 1
23	48	PLATINUM WIRE	SEE NOTE 5		A6 1
24		AS NEEDED	SEE NOTE 5		A6 1
25	4	CRES AMS 5521	120		C6 1
32	6	MS 9142 083			B6 1
33	4	AN 500C6 5 REF	SEE NOTE 5 & 6		
34	2	ASSY OF DASH 35 & 36			E5 1
35	2	SEE NOTE 7			E5 1
36	4	SEE NOTE 7			E5 1
37	2	ASSY OF DASH 38-40			E5 1
38	5	CRES AMS 5521	094		E5 1
39	2	CRES AMS 5521	120		E5 1
40	[illegible]	CRES AMS 5521	120		E5 1
41	2	ASSY OF DASH 42-44			D5 1
42	2	CRES AMS 5521	88		D5 1
43	2	CRES AMS 5510	188		D5 1
44	2	CRES AMS 5645			D5 1
45	[illegible]	AMS 3232	030		C6 1
46	[illegible]	AMS 3232	030		B6 1
47	[illegible]	AMS 3232	030		B5 1
48	6	AMS 3232	030		C4 1
49	2	ASSY OF DASH 50 & 51			C6 1
50	2	Ta AMS 7849	060		C6 1
51	2	Ta AMS 7849	060		C6 1
52	2	CRES AMS 5521	120		B5 1
53	[illegible]	AMS 3274	[illegible]		C5 1
54	2	ASSY OF DASH 55-59			D7 1
55	4	CRES AMS 5570	SEE NOTE 8		D7 1
56	4	CRES AMS 5510			C6 1
57	2	CRES AMS 5510	375		D7 1
58	2	AN 105132 REF	SEE NOTE 9		D7 1
59	2	CRES AMS 5645			D7 1
60	2	SEE NOTE 10			A6 1
64	6	CRES AMS 5521	010		A3 1
66	1	Ta AMS 7849	060		B7 1
	16	AN 104606	SEE NOTE 4		C5 1
	8	AN 501010-4	SEE NOTE 4		C5 1
	32	AN 104609	SEE NOTE 4		D5 1
	36	AN 501010 6	SEE NOTE 4		C4 1
	64	MS 24673-1	SEE NOTE 4		B4 1
	32	AN 121526	SEE NOTE 4		C5 1
	2	AN 121531	SEE NOTE 4		D7 1

section to be operated as either a segmented or Hall current generator or as any other selected configuration. With such a pin-type configuration, the spatial variation of electrical conductivity of the plasma through the test section may be observed. Further, observance may be made of end losses which may develop in the various generator types. Since each electrode block is held in position by two ceramic setscrews, interchangeability is simplified. It is anticipated that different electrode materials, in addition to various electrode geometries, will be investigated. Aerodynamic losses may be determined by employing blocks with extruding pins and then, for comparison, pins machined flush with the electrode block.

Observation windows are necessary to allow spectroscopic investigation of plasma properties. Two quartz windows mounted flush with the channel and perpendicular to the electrode blocks are being used. The quartz windows will be replaced later by sapphire windows. A continuous flow of helium into the stainless steel structures is directed over the windows to provide cooling. A vacuum seal for the windows consists of a soft copper ring seated in a V-groove on the window. To provide safety, additional quartz windows are mounted in each of the magnet pole pieces.

The electromagnet (Figure 10) contains removable pole pieces which may be manually rotated so that eccentric holes may be used to observe the spatial variation of plasma properties. The quartz windows are mounted within the core of the pole pieces to form a gas-tight seal. The gas within the stainless steel structure thus provides cooling of the magnet pole faces. The pole pieces protrude through the stainless steel structure with an O-ring seal being used at the point of protrusion. This intermittent duty (10 min on—50 min off) magnet provides a flux density of approximately 15,000 gauss with a gap of 4.45 cm.

The exploded view of the test section hardware is shown in Figure 11.

DIAGNOSTIC EQUIPMENT

The following diagnostic equipment has been set up, calibrated, and adapted to the task:

- A 3.4-in. Ebert grating spectrograph (Figure 12) correcting to 295 lines/mm and 599 lines/mm (interchangeable) and having a theoretical resolving power (first order) of 42,000 and 72,000. Actual resolving power was measured to 75% of the theoretical resolving power. The instrument was used to obtain the spectrum picture camera data of Section IV in this report.

- Hilger two-prism spectrograph with two different cameras (Figure 13), f/1.5 and f/5.6, with a resolving power of 60,000. This instrument was used to detect very weak cesium lines for preliminary measurement of electron densities.
- Microdensitometer (Figure 14). This instrument is being used to show the feasibility of measuring the radial distribution of broadened cesium lines.
- Spectrum picture camera (Figure 15) attached to a small, high aperture monochromator. The spectrum picture camera, described in Section IV of this report, was used in connection with this small monochromator for some preliminary studies on plasma sources.

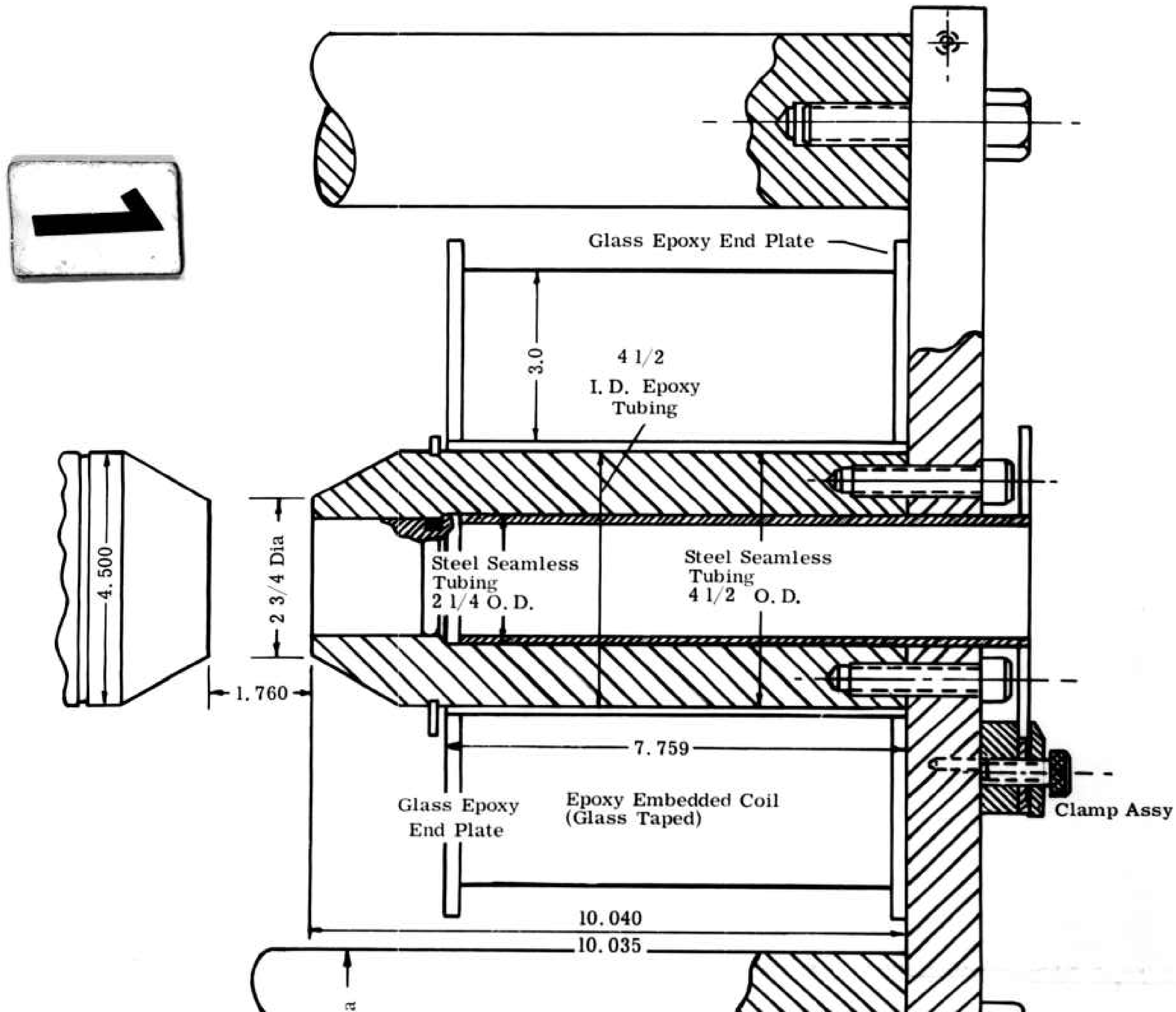

1
Glass Epoxy End Plate
3.0
4 1/2
I. D. Epoxy
Tubing
4.500
2 3/4 Dia
1.760
Steel Seamless
Tubing
2 1/4 O. D.
Steel Seamless
Tubing
4 1/2 O. D.
7.759
Glass Epoxy
End Plate
Epoxy Embedded Coil
(Glass Taped)
Clamp Assy
10.040
10.035
a

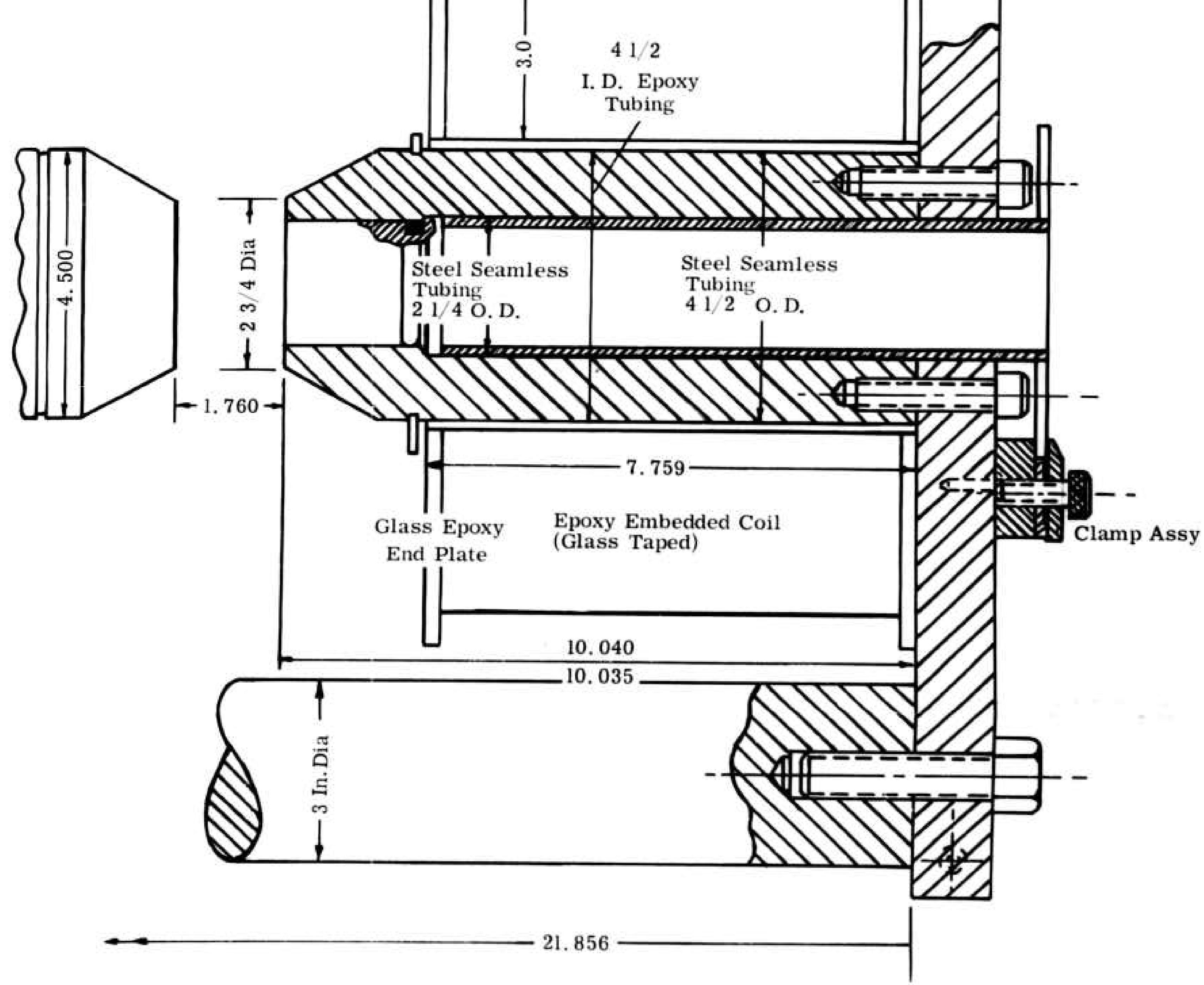

Figure 10. MPD Field Magnet

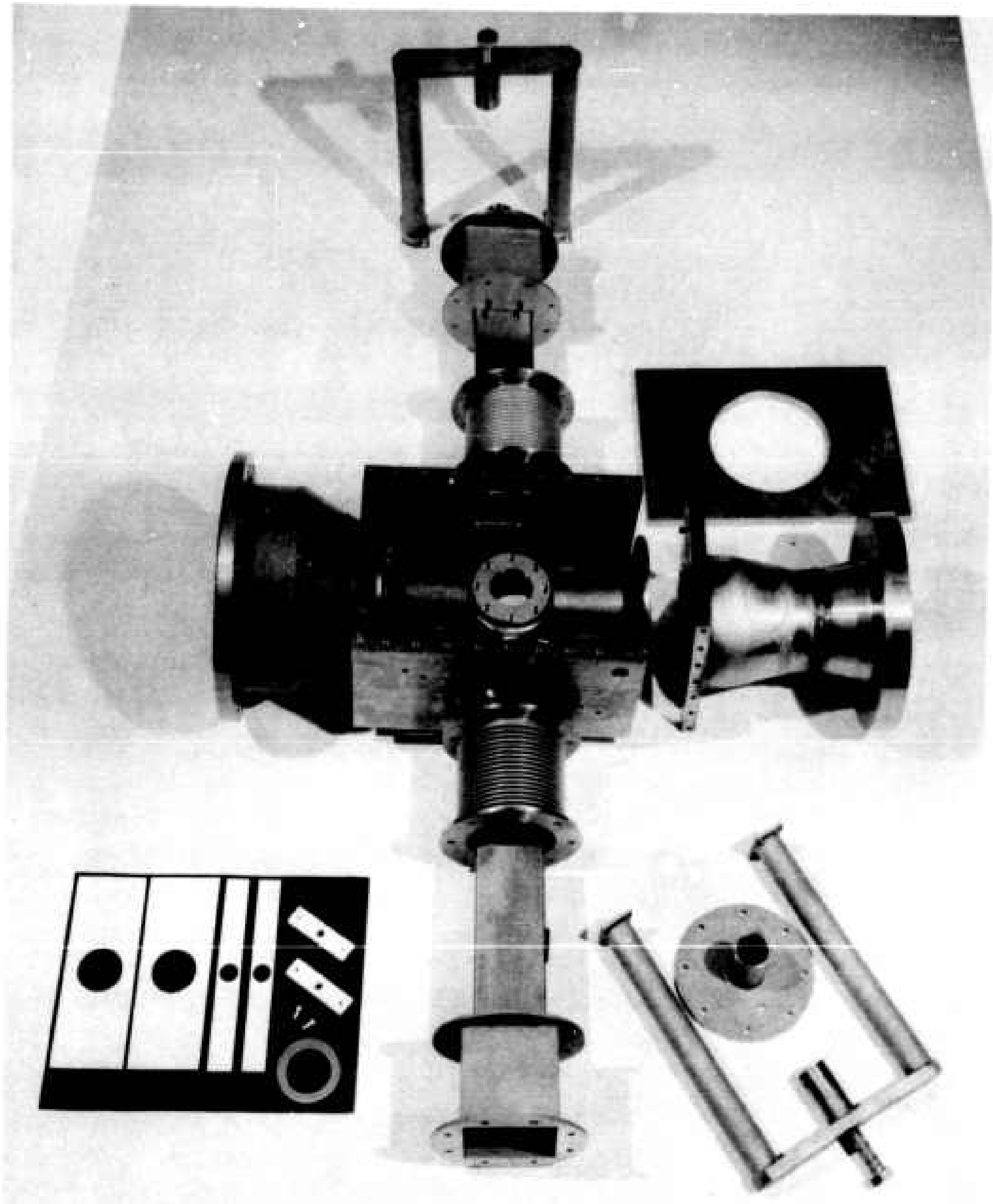

Figure 11. Test Section—Exploded View

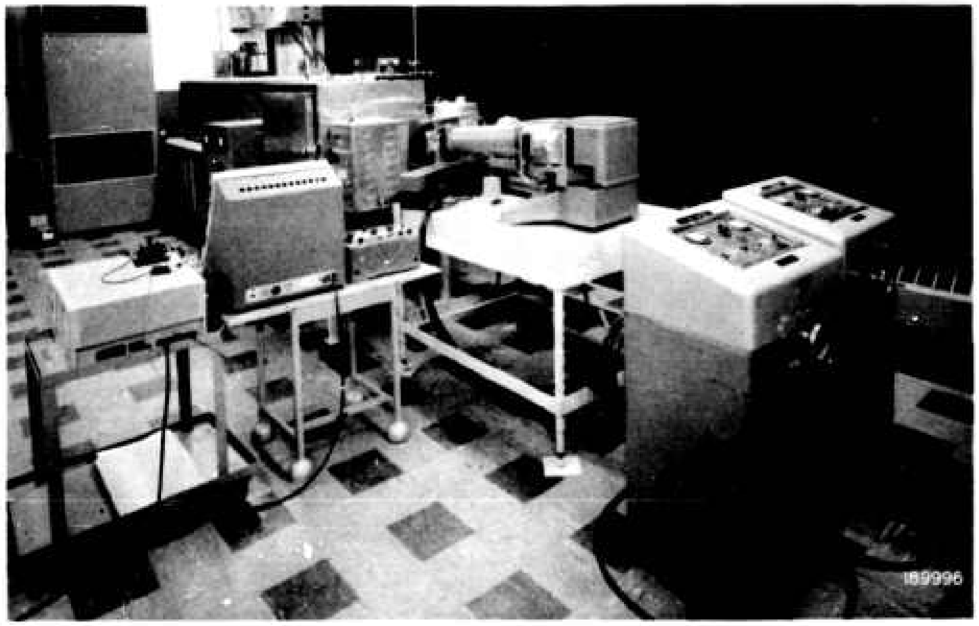

Figure 12. Ebert Grating Spectrograph

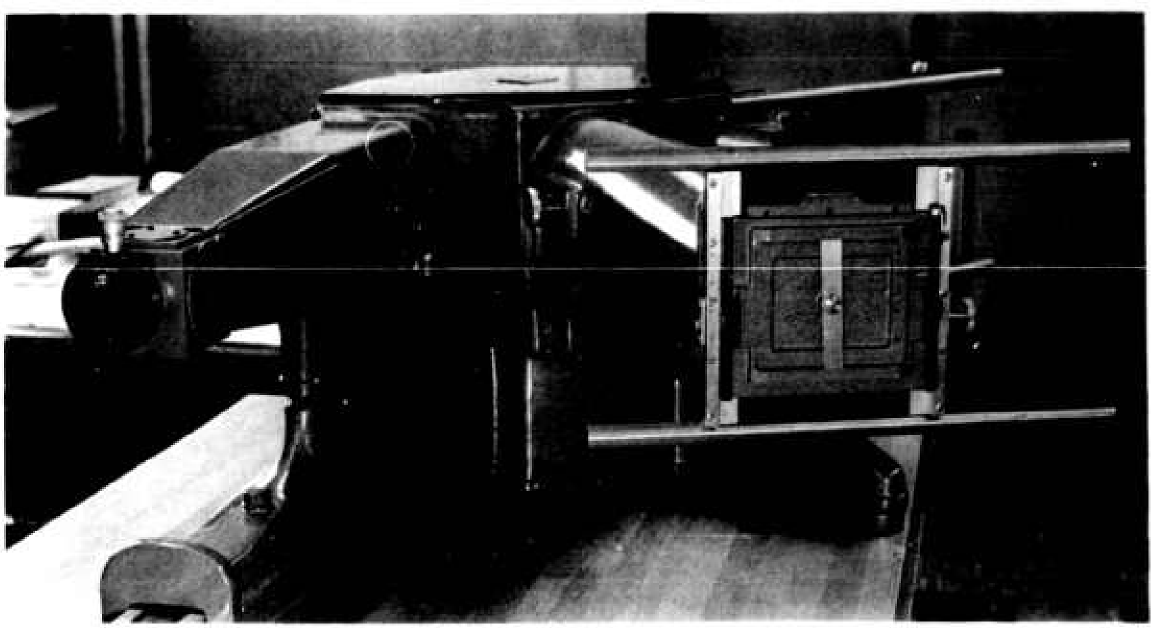

Figure 13. Hilger Two-Prism Spectrograph

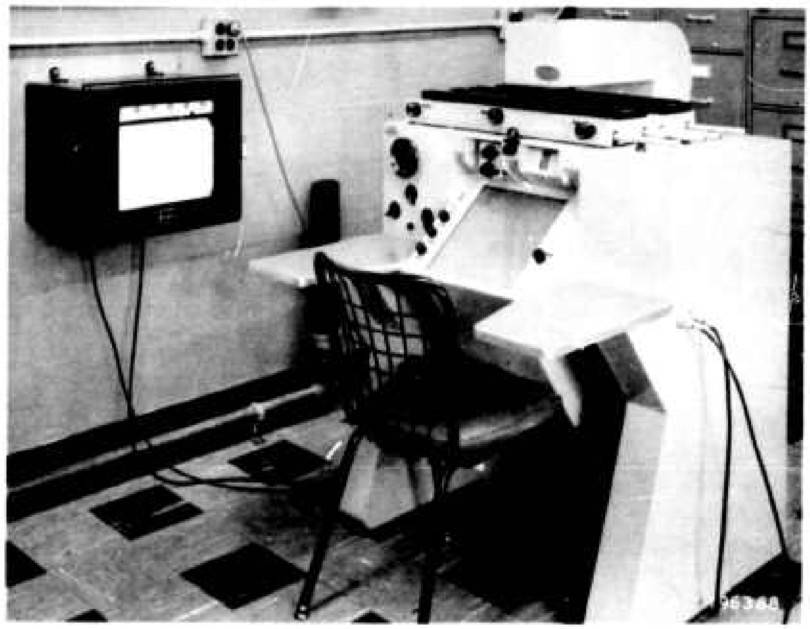

Figure 14. Microdensitometer

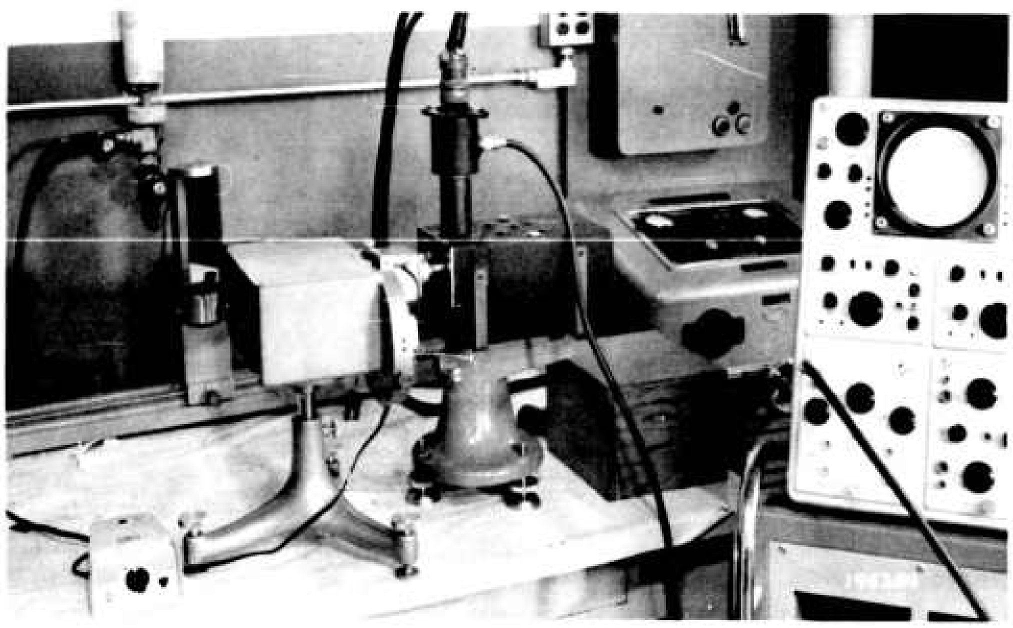

Figure 15. Spectrum Picture Camera Attached to High Aperture Monochromator

IV. RESULTS

In addition to design and fabrication of the diagnostic loop, extensive investigations have been made with respect to development and adaptation of diagnostic methods and theoretical investigations of plasma instabilities within the MPD flow channels.

Introduction to Spectroscopic Techniques

A short introduction to spectroscopic techniques is presented in the following paragraphs. This introduction includes the basic equations in this field and, therefore, provides a reference for future reports. Since the later reports will be detailed frequent references will be made to the relations presented herein.

LINE INTENSITY

The intensity of a line is related to the probability of transition between the corresponding energy levels.

The intensity of a line coming from an optically thin plasma is:

$$I_\nu = \int_0^\ell i_\nu \, d\ell \tag{1}$$

where

i = radiation power per unit volume and unit frequency
ℓ = depth of plasma

The energy of a spectral line is:

$$i_\nu = A_n^m N_m (T) h\nu \tag{2}$$

where

A_n^m = transition probability from level m to n
N_m = particle density of particles in level m
h = Planck's constant
ν = frequency

From Boltzmann's equation, the particle density is:

$$N_m = N_o(T)\frac{g_m}{U(T)} e^{-E_m/kT} \tag{3}$$

where

N_o = total particle density
g_m = statistical weight of level m
U = partition function
E_m = excitation energy
k = Boltzmann's constant
T = temperature

Substitution of Equations (2) and (3) into (1) yields the intensity of the line per unit of solid angle:

$$I = \frac{1}{4\pi} A_n^m N_o (T) \frac{g_m}{U(T)} h \nu \ell e^{-E_m/kT} \tag{4}$$

This often-used formula assumes that the radiation comes from an optically thin plasma.

If the transition probability is known, Equation (4) can be used to determine temperature from an absolute measurement of intensity. The intensity in the case where Cs is used as a seeding substance in He has been calculated and is covered in this report under subsection "Calculation of the Equilibrium Values of Line Intensities" (also see Figure 19). For a proper selected temperature range, a small change in temperature may result in a great change of intensity due to the exponential factor. For those regimes this method is very precise.

Equation (4) can be written:[1*]

$$\ln \frac{I}{A_n^m g_m \nu} = -\frac{E}{kT} + \ln C \tag{5}$$

If

$$\ln \frac{I}{A_n^m g_m \nu} = Y,$$

$$\frac{E_m}{k} = X,$$

and log C = C',

*Superscripts denote references in Section V.

A linear equation is obtained with a slope of $-\frac{1}{T}$.

$$Y = -\frac{1}{T}X + C' \tag{6}$$

In using this method the intensities of different lines are measured and plotted versus E_m/k. If a straight line is obtained in the actual plot, a criterium is established for a Maxwell-Boltzmann distribution. To measure absolute intensity, it is necessary to have a radiation standard which can be used for calibration purposes. In most cases the carbon arc with a temperature of about 4000°K can be used. The radiation of this arc has been measured with great precision by Euler.[2] To avoid the necessity of measuring the space angle and the absorption in the glass optics of the instrument, it is advantageous to image the carbon arc at the place of observation in the unknown plasma or, better yet, to remove the device containing the plasma and to locate the carbon arc in the same place.

EQUILIBRIUM

Equation (4) is valid only if the spectrum line originates from excited levels that can be assumed to be populated according to Boltzmann statistics, which implies a Maxwellian distribution of electron in the case where atoms are excited mainly by collisions with the electrons. Furthermore, excitation and de-excitation must follow the same mechanism. De-excitation by spontaneous radiation, therefore, always disturbs Boltzmann distribution of the excited levels in an optically thin plasma, where there is no compensation by the reverse processes of absorption. Thus, Equation (4) only holds if de-excitation due to spontaneous radiation can be neglected compared to de-excitation due to collisions of excited atoms with electrons. According to Finkelnburg and Maecker,[1] this is the case if

$$3 \times 10^7 \frac{N_e Q_{exc}}{A} (E_n + kT) \gg 1 \qquad \left((E_n + kT \text{ measured in eV})\right)$$

where

N_e = electron number density
Q_{exc} = collision cross section for excitation of level n
E_n = excitation energy
A = transition probability for the regarded spectroscopic line

At electron number densities, $N_e < 10^{16}$, this condition may not be fulfilled. Then, the excited levels are not populated by Boltzmann statistics, and to relate the emitted spectral radiation to plasma parameters, the cross sections of the exciting atom-electron collisions must be known.

RELATIVE INTENSITIES

If Equation (4) is applied to two different lines, the intensity ratio is

$$\frac{I_1}{I_2} = \frac{A_1 g_1}{A_2 g_2} \times h \nu \, e^{-(E_1 - E_2)/kT} \times \frac{\ell_1}{\ell_2} \tag{7}$$

The plasma depth ratio $\frac{\ell_1}{\ell_2}$ is usually assumed to be one. This is true only if the gas discharge under consideration has no temperature profile but has a uniform temperature. If a temperature profile exists, the problem must be treated with Abel's integral equation (see subsection "A Spectroscopic Method Allowing Spatial Resolution"). The advantage of the line ratio method is that the particle density does not have to be known.

If Equation (4) is applied for the same line on a gas discharge with a temperature profile on two different points:

$$\frac{I_x}{I_o} = \frac{N_x}{N_o} \frac{U_o}{U_x} \frac{\ell_x}{\ell_o} \, e^{-(E/k)\,[(1/T_x) - (1/T_o)]} \tag{8}$$

Index o: point in core
Index x: arbitrary point

From this equation the temperature ratio across the cross section of the discharge can be established. If such lines are selected which have their intensity maximum (see Figure 19) within this temperature range, the absolute value can be obtained.

MEASUREMENT OF ELECTRON DENSITY WITH THE INGLIS-TELLER TECHNIQUE

In the case of a hydrogen plasma, it is possible to obtain a rough estimate of the electron density with the very simple method of Inglis and Teller.[3] If n is the quantum number of the last visible Balmer line, the particle density, N, is

$$\log N = 23.26 - 7.5 \log n \tag{9}$$

where

$N = n_e + n_i$ if $T < 10^5/n$ $(n_e = n_i)$
$N = n_e = n_i$ if $T > 10^5/n$

Mohler[4] applied this technique to cesium and found the constant to be 23.06 rather than the aforementioned value of 23.26. Using this method, it is possible to determine the electron density with a maximum error factor of two only by observing the spectrum. It is also important to note that this method utilizes no assumptions regarding existing equilibrium.

MEASUREMENT OF ELECTRON DENSITY BY STARK BROADENING

The theory of line broadening caused by the Stark Effect has been extended significantly in recent times. In the case of hydrogen, the line profiles given by Griem and Kolb[5] can be used. For cesium, Agnew and Summes[6] and Griem[7] have made calculations. This method also does not depend on an established equilibrium. It will be used quite often in the work reported in following reports.

CONTINUUM RADIATION

Free-bound transitions and free-free interactions involve indiscrete energy levels and, therefore, result in radiation at indiscrete frequencies. This "continuum" radiation can be used to determine the plasma temperature.

Using Kramer's theory, Maecker and Peters[8] found:

$$\epsilon_\nu = C\ \overline{(Z + s)^2}\ \frac{N_e\ N_i}{(kT)^{1/2}} \tag{10}$$

where

ϵ = radiation power density per unit of frequency

$C = \dfrac{32\ \pi\ ^2 e^6}{3\sqrt{3}\ (2\ \pi\ n)^{3/2}} = 6.36 \times 10^{-47}$ cgs

s = correction factor of order 1.

DOPPLER BROADENING

In the case of a low-density plasma, it is possible to use Doppler broadening to measure ion temperature.

$$T = 7.82 \times 10^{12} \, M \left(\frac{\Delta \lambda_D}{\lambda}\right)^2 \tag{11}$$

where

M = molecular weight
$\Delta \lambda_D$ = Doppler broadening

In high-density plasmas, the broadening caused by collision and by the Stark effect is much larger than the Doppler broadening. Therefore, this method is, in general, not applicable to high-density plasmas.

However, if an atom has incompleted shells, such as the iron atom, transitions between those orbits are almost totally shielded against Stark interactions and, therefore, allow measurement of Doppler broadening in high density plasmas. In the case of cesium it may be difficult to observe such lines; however, the ordinary cesium spectrum has some lines—e.g., the second member of the sharp series where the broadening due to Stark effect is less than the Doppler broadening.

DOPPLER SHIFT

In the case of a high velocity plasma stream, the measuring of the Doppler shift of a spectrum line would be a method to determine the plasma velocity. The velocity is given by

$$V = c \frac{\Delta \lambda}{\lambda} \frac{1}{\cos a} \tag{12}$$

where

c = velocity of light
$\Delta \lambda$ = Doppler shift
λ = wavelength
$\cos a$ = angle of observation

With a Perot-Fabry interferometer, a resolution power $\frac{\lambda}{\Delta \lambda}$ of 10^6 may be achieved. Therefore, the lower limit of the detectable velocity is 10^4 cm/sec. The resolving power of the Perot-Fabry interferometer is given by

$$\frac{\lambda}{\Delta \lambda} = \frac{\pi L}{\lambda \operatorname{arc} \sin G} \tag{13}$$

where

L = Plate distance

r = reflectivity

$G = \frac{1 - r}{1.8\sqrt{r}}$

The useful dispersion is approximately

$$\Delta L = \frac{\lambda^2}{2L} \tag{14}$$

At 6500 Å, a plate distance of 40 mm would be necessary to get a resolution power of about 10^6 and the useful spectrum range would be 0.05 Å. This requires a half width of the line to be 0.01 Å or less for the line used in this type of investigation.

SPATIAL RESOLUTION

Most of the plasma devices under consideration are cylindrical and, therefore, have a temperature profile. As a consequence, in order to apply the methods previously described, it is insufficient just to measure the line intensity or line broadening. The spatial resolution of the observed data must be considered. The first approach to get a spatial resolution is to form an image of the plasma device in the plane of the entrance slit in such a manner that the axis of the cylindrical device is perpendicular to the entrance slit. Thus, a stigmatic line spectrum is obtained; the length of the spectrum lines gives a measurement for the diameter of the discharge, and the intensity distribution along the line corresponds to the intensity distribution across the diameter. This gives only the situation along a cross section of infinitesimal width. A better way to obtain spatial resolution is to use the spectrum picture method, described under "A Spectroscopic Method Allowing Spatial Resolution".

TIME RESOLUTION

Many plasma devices change their properties during time. These are pulsed discharges or fluctuating steady-state devices. Both types are important in connection with this program. For spectroscopic investigations on such devices, it is necessary to employ techniques of short-time spectroscopy. Such techniques are described in previous reports.[9,10,11,12,13]

It is necessary to have time resolution as well as spatial resolution. If this information is not available, the results are unambiguous only in special cases.

Short-time spectroscopic techniques will be employed later in this program.

Calculation of the Equilibrium Values of Line Intensities

To obtain a more fundamental foundation upon which to build the diagnostic experiments and theoretical model of the plasma flow through a magnetic field, a numerical program has been initiated on the IBM 7090 computer. This program allows the computation of line intensities through which the observed spectrum data may be interpreted. Further analyses for determination of the plasma conductivity have been provided within the program assuming equilibrium at the electron temperature. The fluid under investigation is helium seeded with cesium.

This program, based on equilibrium conditions, will provide the reference upon which to compare theoretical and experimental investigations of nonequilbrium plasmas. Such a standard or reference is of extreme importance in interpretation of observed data.

The number densities of ions and electrons are given approximately by the Saha equation,

$$\frac{n_{Cs}{}^{+}}{n_{Cs}} \cdot n_e = \frac{2U_{Cs}{}^{+}}{U_{Cs}} \frac{(2\pi m)^{3/2} (kT_e)^{3/2}}{h^3} \cdot e^{-(V_{Cs} - \Delta V)/kT_e} \tag{15}$$

Griem[7] is of the opinion that the error of number densities of ions and electrons given by the Saha equation based on electron temperatures is 10% or less if

$$N_e > 9 \times 10^{17} \left(\frac{E_2}{E_H}\right)^3 \left(\frac{kT}{E_H}\right)^{1/2} \tag{16}$$

In Equations (15) and (16), $n_{Cs}{}^{+}$, n_e, and n_{Cs} represent the number densities of the cesium ions, electrons, and cesium atoms, respectively. $U_{Cs}{}^{+}$ and U_{Cs} represent the partition functions of the cesium ion and cesium atoms. E_2 expresses the excitation energy of the resonance line whereas E_H is the ionization potential of hydrogen. The ionization potential, V_{Cs}, of the cesium atom must be corrected to incorporate the depression, ΔV, occurring as a result of electron density. The expression given by Griem[7] is

$$\Delta V = \frac{e^2}{\sqrt{\frac{kT_e}{8\pi n_e e^2}}} = 2.94 \times 10^{-8} \sqrt{\frac{n_e}{T_e(°K)}} \tag{17}$$

The partition functions for the cesium I and cesium II are computed on the basis of the statistical weights, g_s, and respective excitation energies, X_s, of the various energy states.

$$U_{Cs} = \sum_{s=o}^{\infty} g_{Cs,s}\, e^{-X_{Cs,s}/kT_e}$$

$$= g_{Cs,o} + g_{Cs,1}\, e^{-X_{Cs,1}/kT_e} + g_{Cs,2}\, e^{-X_{Cs,2}/kT_e} + \dots \tag{18}$$

$$U_{Cs^+} = \sum_{s=o}^{\infty} g_{Cs^+,s}\, e^{-X_{Cs^+,s}/kT_e}$$

$$= g_{Cs^+,o} + g_{Cs^+,1}\, e^{-X_{Cs^+,1}/kTe} + g_{Cs^+,2}\, e^{-X_{Cs^+,2}/kTe} + \dots \tag{19}$$

Within the program, 104 energy levels for cesium I and 63 levels for cesium II[14] were used to compute the ratio of partition functions employed in the Saha equation.

Letting ψ represent the right hand side of Equation (15), the Saha equation may be expressed as:

$$\frac{n_{Cs^+}}{n_{Cs}} = \frac{\psi}{n_e} \tag{20}$$

The total pressure of the plasma is given by the sum of partial pressures of the constituents, or

$$P_{TOT} = kT_g\,(n_{He} + n_{Cs}) + kT_g\,(n_{Cs^+}) + kT_e n_e \tag{21}$$

It should be recognized at this point that for the temperature range of interest in the proposed investigation the ionization of helium is negligible.

By conservation of charge of the plasma,

$$n_e = n_{Cs^+} \tag{22}$$

Letting the seeding ratio, α , be represented as

$$\alpha = \frac{n_{Cs} + n_{Cs}{}^{+}}{n_{He}} \tag{23}$$

and the ratio of electron to gas temperature be

$$\beta = T_e / T_g \tag{24}$$

the set of simultaneous Equations (19 through 23) may be solved to yield:

$$n_{Cs}{}^{+} = n_e = - \frac{\psi(1+\alpha+\alpha\beta)}{2(1+\alpha)} + \sqrt{\left[\frac{\psi(1+\alpha+\alpha\beta)}{2(1+\alpha)}\right]^2 + \frac{P_{TOT}\,\psi\beta}{kT_e\,(1+\alpha)}} \tag{25}$$

The remaining unknowns, n_{Cs}, n_{He}, and degree at ionization are readily obtained.

Line intensities are given by

$$I_{Cs} = \left(A_n^m \frac{g_{Cs}}{U_{Cs}}\right) \frac{hc}{\lambda} n_{Cs}\, e^{-E_m/kT_e} \tag{26}$$

where

A_n^m = transition probability from level m to n
E_m = energy of m-state

Twenty-seven of the strongest cesium lines have been computed based on the transition probabilities given in references 15 and 16. Should better values of transition probabilities become available, correction can be made of line intensities by simply multiplying the intensities by the ratio of probabilities.

The conductivity of the plasma has been computed on the basis of calculated electron-ion collision cross sections and assumed values of electron-neutral cross sections. Since the assumed values of cross sections are, at this time, questionable, the conductivity values represent only order of magnitude estimates. The calculation has been specifically programmed so that these values may be readily changed when better data become available.

The electron-ion cross section is given by

$$Q_i = 0.90\left(\frac{e^2}{kT_e}\right)^2 \ln\left[\frac{1.5}{\sqrt{2}e^3}\left(\frac{k^3T_e{}^3}{\pi n_e}\right)^{1/2}\right] \tag{27}$$

so that the mean free path becomes

$$\lambda_e = \frac{1}{n_e Q_i + n_{Cs} Q_s + n_{He} Q_g} \tag{28}$$

where Q_s and Q_g represent the electron-neutral cross sections of the seed and gas atoms, respectively.

The mean free time based on a Maxwellian distribution of velocity is given as

$$\tau_e = \frac{\lambda_e}{\left(\frac{8\,kT_e}{\pi m_e}\right)^{1/2}} = \frac{\lambda_e}{0.621 \times 10^6 \sqrt{T_e}} \tag{29}$$

The conductivity is then given as:

$$\sigma = \frac{0.85\, n_e\, e^2}{m_e}\, \tau_e = 2.389 \times 10^{-3}\, n_e\, \tau_e \tag{30}$$

Several runs have been made with the program over a temperature range of 1500 to 6000°K. Seeding values have ranged from 0.5% to 100% cesium. The degree of ionization for the various seed ratios is illustrated in Figure 16. As shown by Figure 17, the optimized seeding level, based on assumed cross sections for the temperature range of interest, appears to be 1.0%. On the basis of 1% seeding of a plasma with a total pressure of 1 atm under conditions of equilibrium ($T_e = T_g$) the various properties are given as shown in Table I. For the same conditions, the effect of pressure on conductivity of pure cesium is illustrated in Figure 18. As mentioned previously, the intensities of 27 of the most prominent cesium lines have been computed. These intensities are illustrated graphically in Figure 19 and listed in tabular form in Tables II through VII. With reference to the tables, it should be noted that only two significant figures should be used since the values of transition probabilities[15,16] are given to only two significant places. The data obtained through the numerical program provides the basic information for interpretation of observed spectra and further provides a reference for the continued effort on nonequilibrium plasmas.

TABLE I

Theoretical Plasma Properties—1% Seeding

Property	1500°K	1600°K	1800°K	2000°K	2200°K	3000°K	6000°K
Electron Density, cc^{-1}	7.5×10^{11}	2.0×10^{12}	9.7×10^{12}	3.5×10^{13}	1.0×10^{14}	1.7×10^{15}	1.2×10^{16}
Ion Density (n_{Cs^+}), cc^{-1}	7.5×10^{11}	2.0×10^{12}	9.7×10^{12}	3.5×10^{13}	1.0×10^{14}	1.7×10^{15}	1.2×10^{16}
Cesium Density, cc^{-1}	4.8×10^{16}	4.5×10^{16}	4.0×10^{16}	3.6×10^{16}	3.3×10^{16}	2.2×10^{16}	3.5×10^{16}
Helium Density, cc^{-1}	4.8×10^{18}	4.5×10^{18}	4.0×10^{18}	3.6×10^{18}	3.3×10^{18}	2.4×10^{18}	1.2×10^{18}
Degree of Ionization	1.5×10^{-7}	4.2×10^{-7}	2.4×10^{-6}	9.6×10^{-6}	3.0×10^{-5}	6.8×10^{-4}	9.6×10^{-3}
Mean Free Path, cm	2.3×10^{-4}	2.4×10^{-4}	2.7×10^{-4}	3.0×10^{-4}	3.1×10^{-4}	2.7×10^{-4}	2.8×10^{-4}
Mean Free Time, sec	9.5×10^{-12}	9.8×10^{-12}	1.0×10^{-11}	1.1×10^{-11}	1.1×10^{-11}	7.8×10^{-12}	5.8×10^{-12}
Conductivity, mho/m	0.171	0.460	2.40	8.96	25.8	309	1623
	$Q_s = 4 \times 10^{14}\ cm^{-2}$			$Q_g = 5 \times 10^{16}\ cm^{-2}$			

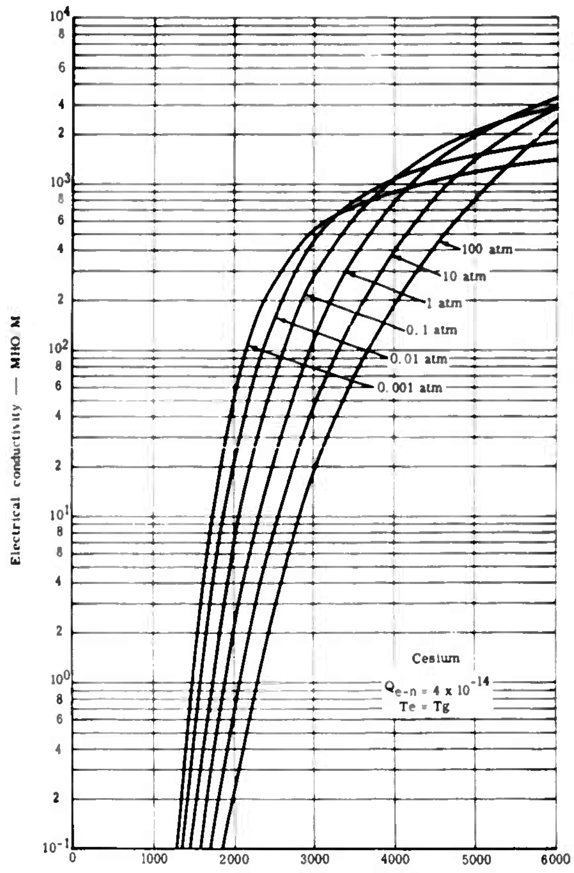

Figure 16. Electrical Conductivity of Plasmas—Pressure Effect

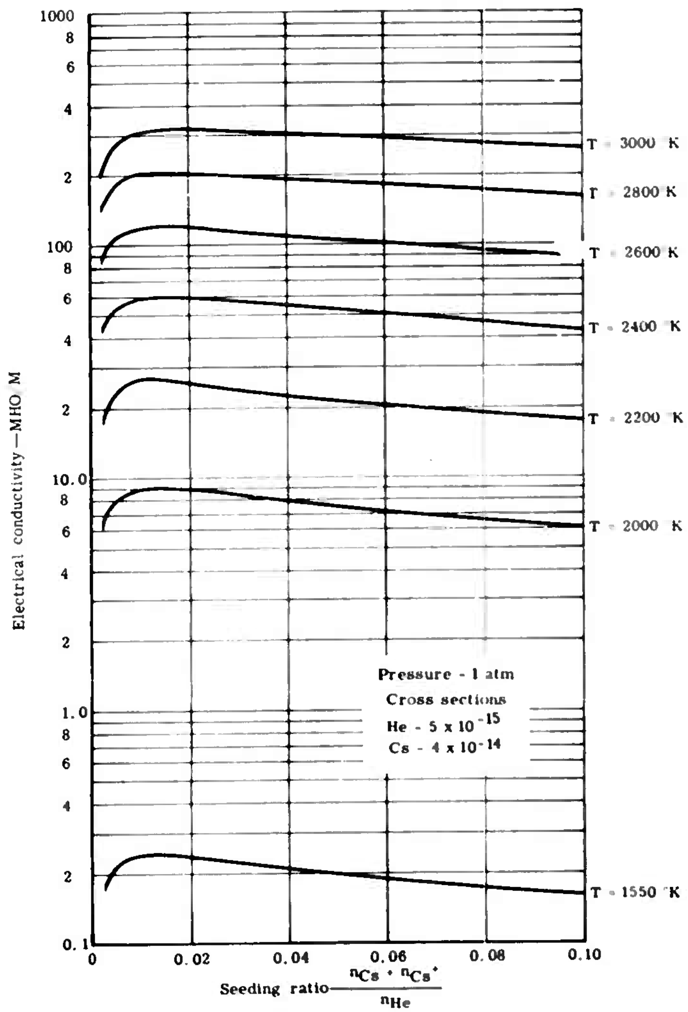

Figure 17. Electrical Conductivity of Plasmas—Seeding Effect

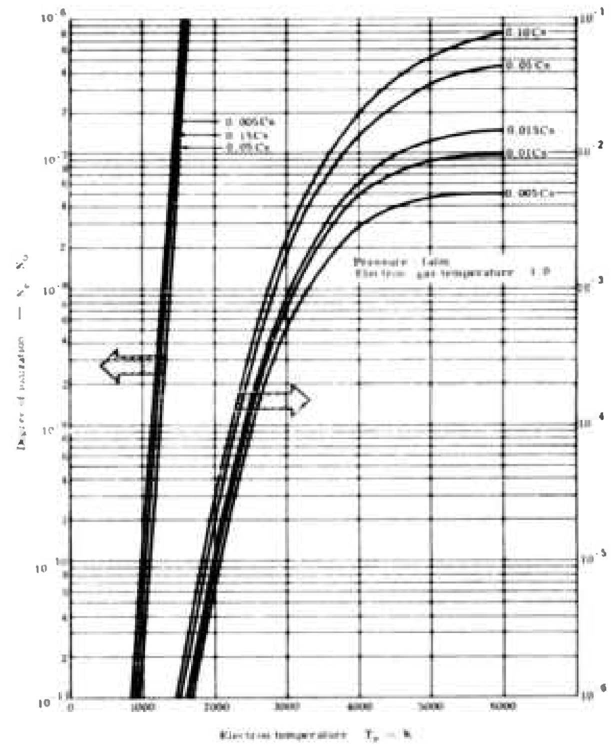

Figure 18. Ionization of He-Cs Plasmas

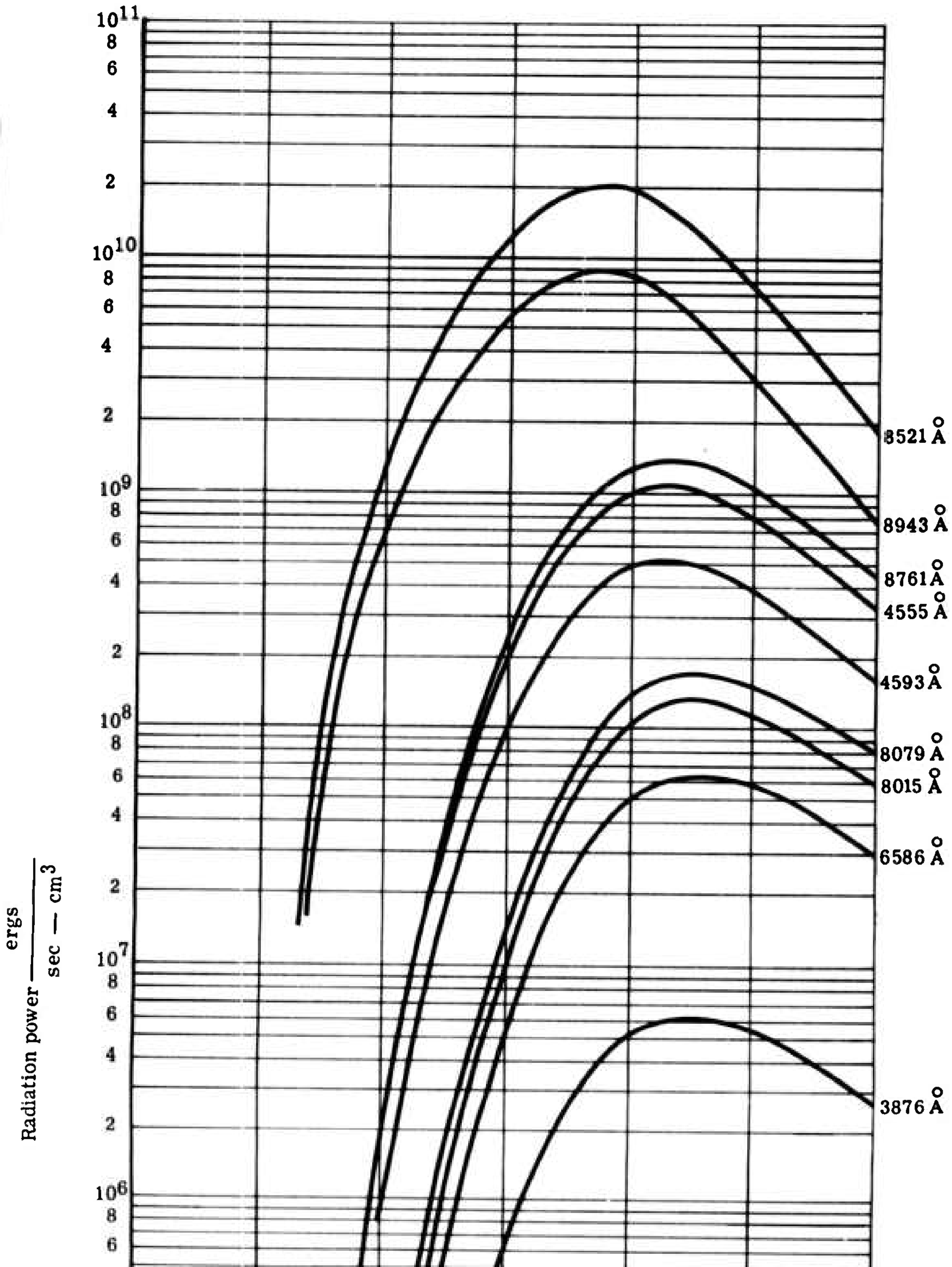

10^{11}
8
6
4
2
10^{10}
8
6
4
2
10^{9}
8
6
4
2
10^{8}
8
6
4
2
10^{7}
8
6
4
2
10^{6}
8
6
Radiation power $\frac{\text{ergs}}{\text{sec} - \text{cm}^3}$
8521 Å
8943 Å
8761 Å
4555 Å
4593 Å
8079 Å
8015 Å
6586 Å
3876 Å

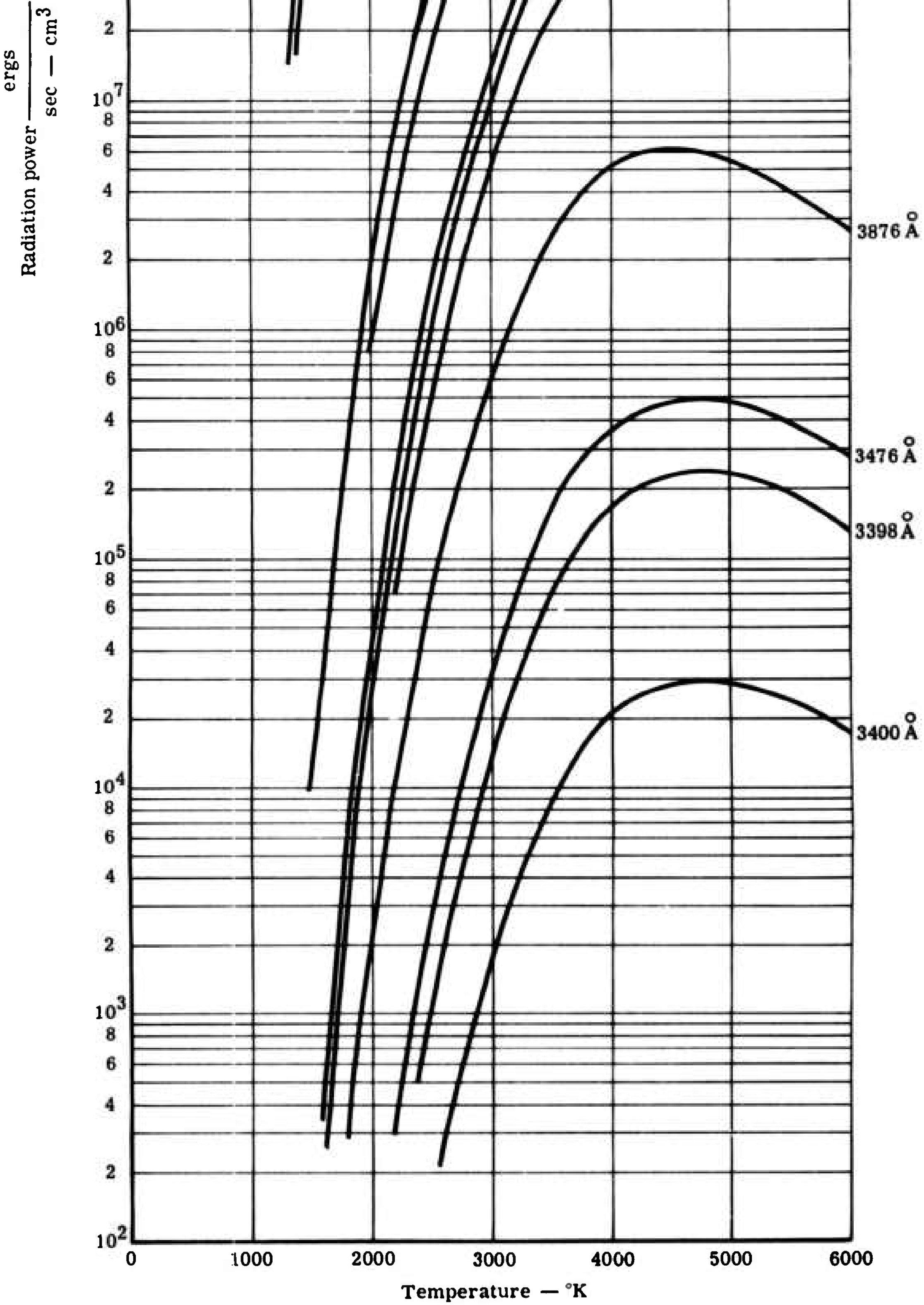

Figure 19. Cesium Line Intensities

λ (Å)	g A_n^m	Ref for g A_n^m	Cesium Line Intensities—(Cs + Cs⁺)/He = (1500°K	1600°K	1700°K	1800°K	2000°K	
8943.50	0.480000	NBS	29237934.2	53497045.0	9C825000.0	0.14489259E 09	0.31760930E 09	0.
8761.38	4.300000		4813.75354	17434.3577	54067.1870	147351.371	802761.711	31
8521.10	1.3C0000		47982763.5	90861389.0	0.15900532E 09	0.26058377E 09	0.59796485E C9	0.
8079.02	2.00C000		36.6456223	172.493023	674.116791	2256.48230	17435.4932	91
8015.71	1.50C000		27.7C12937	130.391560	5C9.580841	1705.72839	13179.9021	69
7609.C1	0.440C00		1C9.140622	438.168797	1488.12483	4396.87762	27480.2515	12
6983.49	0.58C000		29.7C09854	132.305767	492.512863	1578.83472	11334.8773	56
6973.29	3.3CC000		166.636900	743.C17555	2768.27011	888C.90100	6384C.6421	31
6723.28	3.20CC00		17C.209642	758.214493	2822.48001	9047.94543	64957.6230	32
6586.51	0.60CC00		14.3459175	67.2663336	261.986515	874.294823	672C.78571	35
6354.98	C.48CC00		11.8948641	55.7736301	217.225140	724.918297	5572.51434	29
6217.27	0.19C000		2.02321586	1C.0145884	4C.9136763	142.460934	1177.11775	65
6212.87	2.90C000		3C.6643577	151.856974	620.662460	2161.95926	17875.2288	99
6034.09	0.38C000		2.62088034	13.3548446	55.9748187	199.389788	1712.49013	98
6010.33	1.90C000		20.9287665	103.593979	423.223640	1473.65965	12176.4677	67
5844.70	0.760000		3.22249493	16.9611297	73.1516542	267.282421	2396.93781	14
5663.8C	0.88CC00		3.88C39407	20.4140179	88.0060482	321.435642	2880.71585	17
4593.18	0.650000		3C55.83450	1C534.9034	31279.3105	82011.8223	418357.074	15
4555.36	1.40CC00		5597.71173	19504.3555	58456.7866	154553.217	799666.695	30
3888.37	C.002900	RUSS	0.36912617	1.61124760	5.89139450	18.5874202	129.878883	62
3876.19	0.023700		2.80C82232	12.2849408	45.1109543	142.866436	1C04.73093	48
3617.41	C.000938		0.20352515E-01	0.99675570E-01	C.40341070	1.39299950	11.3478777	62
3611.52	0.007640		0.15850942	0.77854864	3.15904838	1C.9332218	89.4112043	49
3480.13	0.00C550		0.43646666E-02	0.22817785E-01	0.97824709E-C1	0.35554026	3.15976578	18
3476.88	0.004490		0.34846556E-01	0.18243676	0.78314693	2.84955922	25.3737025	15
3400.00	0.000320		0.13570529E-02	0.73885682E-C2	0.32832285E-01	0.12319057	1.15575330	7.
3398.0C	C.002560		0.10696013E-01	0.58291534E-01	0.25924882	0.97347017	9.14471900	56

λ (Å)	g A_n^m	Ref for g A_n^m	Cesium Line Intensities—(Cs + Cs⁺)/He = 0.005 (P 3000°K	3200°K	3400°K	3600°K	3800°K	
8943.50	0.48C000	NBS	0.27430800E 10	0.33128896E 10	C.37182711E 10	0.38684604E 10	0.37237871E 10	0.3
8761.38	4.30C000		0.10643591E 09	0.18085318E 09	0.27433823E 09	0.37305535E C9	C.45631920E 09	C.9
8521.10	1.30C000		0.59246781E 10	0.72792853E 1C	0.82947094E 1C	0.87467305E 10	0.85216622E 10	0.1
8079.02	2.00C000		6595458.56	12776051.1	21755783.2	32786860.7	43967802.0	528
8015.71	1.500000		4985663.25	9657719.50	16445711.9	24784364.2	33236302.7	399
7609.C1	0.44C000		5501153.44	9841429.88	15622604.5	22119874.2	28052652.2	320
6983.49	0.58C000		3439231.88	6481C04.75	10771049.5	15885258.4	2C894339.5	246
6973.29	3.3CCC00		19445628.5	36661721.5	6C955631.0	89932120.0	0.11833045E 09	0.1
6723.28	3.2CC000		19709461.5	37141175.5	61726453.5	91034831.0	0.11974074E 09	0.1
6586.51	0.6CC000		2503285.56	4839740.13	8227329.69	1238C127.4	16579464.7	199
6354.98	0.48C000		2075589.92	4C12852.47	6821659.81	1C264936.5	13746801.4	165
6217.27	C.190000		.544498.070	1C81605.03	1883140.31	2894496.59	3950677.81	482
6212.87	2.900000		8284534.19	16460592.0	28665009.7	44068150.0	60158510.0	734
6034.C9	C.38CC00		889626.664	1793001.03	3161940.88	4915702.31	6778C61.CC	839
601C.33	1.90C000		5632455.25	11186455.0	19479781.7	29941561.7	40867024.5	499
5844.70	C.76C000		1417490.30	2903543.16	5194087.44	8178225.75	11405548.4	143
5663.80	0.880000		1700292.31	3481984.59	6227519.94	9803532.75	13669919.5	170
4593.18	0.65CC00		45536867.0	75490177.0	0.11204694E 09	0.14944671E C9	0.17966587E C9	C.1
4555.36	1.40C000		90825170.0	0.15137134E C9	0.22573122E 09	0.30233602E 09	0.36482975E 09	C.3
3888.37	0.002900	RUSS	36332.9712	67775.3174	111633.812	163332.637	213310.590	250
3876.19	0.023700		286558.117	535837.852	884472.125	1296537.14	1696138.33	199
3617.41	0.C00938		5030.48535	9939.67371	17224.5444	26364.9067	35851.1943	436
3611.52	C.007640		40098.4419	79345.0352	137673.799	210971.584	287172.918	349
3480.13	0.00C550		1818.68480	3712.74881	6621.85071	10398.6322	14467.7711	179
3476.88	0.004490		14689.4844	3C009.5654	53557.6406	84152.1807	117141.789	149
3400.C0	0.000320		782.586266	1630.38770	2960.44901	4723.59314	6666.34448	838
3398.C0	0.002560		6216.09351	12956.4569	23536.2993	37567.9785	53037.1880	661

References:

NBS Corliss, C. H. and Bozman, W. R., Experimental Transition Probabilities for Spectral Lines of Seventy Elements, NBS Monograph 53 (July 1962)

RUSS Kvater, G. S. and Meister, Probabilities for Members Leningrad Universitet, Ves

1

TABLE II

Cesium Line Intensities—$(Cs + Cs^{+})/He = 0.005$ (P = 1 atm, Te = Tg)

1700°K	1800°K	2000°K	2200°K	2400°K	2600°K	2800°K
0825000.0	0.14489259E 09	0.31760930E 09	0.59654800E 09	0.99560561E 09	0.15107201E 10	0.21129211E 10
4067.1870	147351.371	802761.711	3175674.47	9859590.25	25296621.7	55498607.5
.15900532E 09	0.26058377E 09	0.59796485E 09	0.11659887E 10	0.20076671E 10	0.31279394E 10	0.44749587E 10
74.116791	2256.48230	17435.4932	91803.4102	361710.504	1135335.36	2960702.09
09.580841	1705.72839	13179.9021	69396.3711	273425.531	858226.875	2238064.78
488.12483	4396.87762	27480.2515	121638.072	414723.555	1151787.14	2704493.81
92.512863	1578.83472	11334.8773	56198.3267	210601.090	633588.281	1593279.86
768.27011	8880.90100	63840.6421	316856.035	1188450.33	3578085.66	9003525.00
822.48001	9047.94543	64957.6230	322059.922	1206907.30	3630951.50	9130727.13
61.986515	874.294823	6720.78571	35238.0435	138352.406	432969.637	1126212.17
17.225140	724.918297	5572.51434	29217.4927	114714.383	358995.160	933794.633
0.9136763	142.460934	1177.11775	6547.43945	27004.0920	88103.6211	237500.887
20.662460	2161.95926	17875.2288	99479.2100	410469.934	1339698.48	3612575.91
5.9748187	199.389788	1712.49013	9831.64148	41633.1611	138898.166	381659.645
23.223640	1473.65965	12176.4677	67728.7256	279338.625	911370.930	2456782.13
3.1516542	267.282421	2396.93781	14256.2335	62174.1641	212662.439	596963.812
8.0060482	321.435642	2880.71585	17124.5554	74650.6396	255242.406	716261.422
1279.3105	82011.8223	418357.074	1568294.67	4655610.13	11500116.6	24422934.7
8456.7866	154553.217	799666.695	3032702.97	9090318.63	22639083.5	48417322.5
.89139450	18.5874202	129.878883	629.829033	2317.08096	6862.82159	17028.3210
5.1109543	142.866436	1004.73093	4898.07037	18098.9236	53805.8809	133931.770
.40341070	1.39299950	11.3478777	62.3915701	254.849472	824.695992	2207.59293
.15904838	10.9332218	89.4112043	493.148666	2019.67365	6550.29138	17567.7668
.97824709E-01	0.35554026	3.15976578	18.6550081	80.8588791	275.135662	768.892288
.78314693	2.84955922	25.3737025	150.041611	651.203445	2218.30142	6205.18298
.32832285E-01	0.12319057	1.15575330	7.13264418	32.0789495	112.618453	323.265686
.25924882	0.97347017	9.14471900	56.4955139	254.311152	893.465706	2566.28519

Cesium Line Intensities—$(Cs + Cs^{+})/He = 0.005$ (P = 1 atm, Te = Tg)

3400°K	3600°K	3800°K	4000°K	5000°K	6000°K	8000°K
.37182711E 10	0.38684604E 10	0.37237871E 10	0.33211881E 10	0.88993466E 09	0.20489991E 09	23387257.5
.27433823E 09	0.37305535E 09	0.45631920E 09	0.50491852E 09	0.30699608E 09	0.12205280E 09	27575558.5
.82947094E 10	0.87467305E 10	0.85216622E 10	0.76831919E 10	0.21453565E 10	0.50770554E 09	59973638.0
1755783.2	32786860.7	43967802.0	52848514.5	44008551.5	21578131.5	6336037.69
16445711.9	24784364.2	33236302.7	39949443.5	33267106.2	16311420.5	4789560.88
15622604.5	22119874.2	28052652.2	32066578.7	22061935.5	9524557.75	2385361.84
10771049.5	15885258.4	20894339.5	24681193.2	19237145.2	9025351.75	2507994.16
60955631.0	89932120.0	0.11833045E 09	0.13981918E 09	0.10910514E 09	51227690.5	14249091.4
61726453.5	91034831.0	0.11974074E 09	0.14144234E 09	0.11024373E 09	51722254.5	14372748.2
8227329.69	12380127.4	16579464.7	19903890.7	16497805.0	8064154.19	2358753.94
6821659.81	10264936.5	13746801.4	16503236.7	13679093.6	6686363.50	1955752.06
1883140.31	2894496.59	3950677.81	4824662.13	4267572.31	2178365.69	672629.781
28665009.7	44068150.0	60158510.0	73478229.0	65031638.5	33207990.0	10258831.7
3161940.88	4915702.31	6778061.00	8353720.81	7650943.13	3997104.34	1270549.48
19479781.7	29941561.7	40867024.5	49907787.0	44145079.5	22533683.7	6957889.13
5194087.44	8178225.75	11405548.4	14201495.5	13522411.4	7250056.81	2380446.53
6227519.94	9803532.75	13669919.5	17018355.7	16195175.1	8679702.63	2848471.53
0.11204694E 09	0.14944671E 09	0.17966587E 09	0.19572825E 09	0.11216552E 09	42868392.5	9219182.38
0.22573122E 09	0.30233602E 09	0.36482975E 09	0.39878350E 09	0.23146611E 09	89219843.0	19392641.0
111633.812	163332.637	213310.590	250359.740	190438.293	87906.5713	23936.6379
884472.125	1296537.14	1696138.33	1993776.83	1525409.73	706860.453	193408.523
17224.5444	26364.9067	35851.1943	43635.4932	38107.4189	19286.9331	5892.34546
137673.799	210971.584	287172.918	349846.598	306591.000	155532.480	47654.7500
6621.85071	10398.6322	14467.7711	17975.9172	16977.8591	9053.53125	2952.53360
53557.6406	84152.1807	117141.789	145613.033	137767.932	73550.7773	24021.1694
2960.44901	4723.59314	6666.34448	8389.73242	8319.73157	4583.07874	1556.59377
23536.2993	37567.9785	53037.1880	66768.7871	66288.5840	36544.5610	12423.9799

Transition
, NBS Monograph 53

RUSS Kvater, G. S. and Meister, T. G., Absolute Values of Transition Probabilities for Members of the Principal Series of Cesium, Leningrad Universitet, Vestnik, No. 9, p. 137-158 (1952)

λ (Å)	$g A_n^m$	Ref for $g A_n^m$	Cesium Line Intensities—(Cs + Cs⁺)/He = 0.01 1500°K	1600°K	1700°K	1800°K	2000°K
8943.50	C.48C000	NBS	58186753.5	0.10646629E 09	0.18075861E 09	0.28837886E C9	0.63232221E 09
8761.38	4.300000		9579.90698	34696.7090	107603.742	293272.551	1598202.72
8521.10	1.300000		95491057.0	0.18082634E 09	0.31645013E 09	0.51863834E 09	0.11904766E 10
8079.C2	2.00C000		72.9288788	343.284245	1341.61758	4491.06317	34711.9854
8015.71	1.50C000		55.1286659	259.496685	1014.16051	3394.90103	26239.6116
7609.01	0.44C000		217.202023	872.014656	2961.64474	8751.07922	54709.8994
6983.49	0.580000		59.1082764	263.306217	980.192055	3142.34528	22566.3872
6973.29	3.300000		331.626038	1478.70453	5509.37152	17675.6038	127099.094
6723.28	3.20CC00		338.736187	1508.94850	5617.25940	18008.0715	129322.872
6586.51	0.60C000		28.5499773	133.869024	521.401810	174C.10378	13380.2817
6354.98	0.48C000		23.6721075	110.997003	432.318367	1442.80055	11094.2107
6217.27	C.19C000		4.02642542	19.9303734	81.4258127	283.539139	2343.50092
6212.87	2.900C00		61.0254941	3C2.215733	1235.23355	4302.93457	35587.4468
6034.C9	0.38C000		5.21584451	26.5779314	111.400282	396.844307	3409.36337
6010.33	1.900000		41.6505818	2C6.165907	842.293617	2933.01602	24241.8933
5844.70	0.76C000		6.41312468	33.7549219	145.585375	531.970604	4772.01703
5663.80	C.88C000		7.72241735	4C.6266322	175.148376	639.751434	5735.16132
4593.18	0.650000		6C81.45172	2C965.8704	62251.6367	163227.639	832898.984
4555.36	1.400000		1114C.0713	38816.2822	116339.861	307606.348	1592040.91
3888.37	0.002900	RUSS	0.73460229	3.20659876	11.7249689	36.9944310	258.573349
3876.19	0.023700		5.57394910	24.4486794	89.7791758	284.346210	2C0C.29932
3617.41	0.00C938		0.4C503777E-01	0.19836774	0.80286220	2.77247861	22.5922692
3611.52	0.007640		0.31545144	1.54941617	6.28709286	21.7603259	178.007034
3480.13	0.000550		0.86861737E-02	0.45410451E-01	0.19468933	0.70762967	6.29071647
3476.88	0.004490		0.69348538E-01	0.36307361	1.55860782	5.67146063	5C.5160117
3400.00	0.000320		0.27006868E-02	0.14704241E-01	0.65342344E-01	0.24518547	2.30096683
3398.C0	0.002560		0.21286260E-01	0.11600797	0.51595329	1.93749183	18.2060437

λ (Å)	$g A_n^m$	Ref for $g A_n^m$	Cesium Line Intensities—Cs + Cs⁺/He = 0.01 3000°F	3200°K	3400°K	3600°K	3800°K
8943.50	C.48CC00	NBS	0.56154466E 10	0.69230193E 10	0.80090708E 10	0.86881527E 10	0.88264045E 10
8761.38	4.30C000		0.21788834E 09	0.37793291E C9	0.59091827E 09	0.83784281E C9	0.10816026E 10
8521.10	1.300000		0.12128597E 11	0.15211684E 11	0.17866614E 11	0.19644231E 11	0.20198694E 11
8079.C2	2.000000		13501773.5	26698398.2	46861459.0	73635818.0	0.10421584E C9
8015.71	1.50C000		1C2C6310.1	20181951.0	35423686.5	55663058.5	78779222.0
7609.C1	0.44C000		11261586.6	2C565855.0	33650732.0	49678896.5	66492537.5
6983.49	0.58C000		7C40561.19	13543499.9	23200593.7	35676608.5	49525358.5
6973.29	3.30CC00		39807766.0	76612815.C	0.13129703E 09	0.20197801E 09	0.28047587E 09
6723.28	3.20CC00		4C347867.0	77614740.0	0.13295736E 09	0.20445459E 09	0.28381865E 09
6586.51	0.600000		5124555.69	1C113712.5	17721479.7	27804455.2	39297913.0
6354.98	0.48C000		4249006.25	8385747.13	14693698.9	23053960.5	32553718.2
6217.27	0.19C000		1114659.34	226C254.09	4C56241.06	6500732.88	9364198.13
6212.87	2.90C000		16959534.0	34398064.5	61743774.5	98972402.0	0.14259229E 09
6034 9	0.38C000		1821183.11	3746874.16	6810748.13	11C4C147.C	16065877.6
6010.33	1.900000		11530378.7	2338C763.0	41959003.5	67245577.0	96866142.0
5844.70	C.760000		2901789.56	6C67598.69	11187945.1	18367429.2	27034301.2
5663.80	0.88CC00		3480722.59	7276380.63	13413935.4	22017696.7	32401486.7
4593.18	0.65C000		93219973.0	0.15775350E 09	0.24134655E C9	0.33564150E 09	0.42585777E 09
4555.36	1.40C000		0.18593109E 09	0.31632407E 09	0.48621987E 09	0.67901470E 09	0.86474733E 09
3888.37	0.002900	RUSS	74378.3848	141631.588	240456.674	366827.812	5C5605.047
3876.19	0.023700		586622.258	1119752.28	1905132.69	2911885.13	4C20316.56
3617.41	0.000938		10298.0668	2C771.1575	37101.2744	59212.790C	84977.2383
3611.52	0.007640		82086.7988	165809.086	296546.203	473819.840	680679.172
3480.13	0.000550		3723.08768	7758.61377	14263.3148	23354.2271	34292.6157
3476.88	0.004490		30071.3118	62711.6563	115361.931	188996.891	277658.410
3400.00	0.000320		1602.05728	3407.05746	6376.73938	1C608.6902	15801.0787
3398.C0	0.002560		12725.1632	27075.3965	50696.6499	84373.7021	125712.792

References:

NBS Corliss, C. H. and Bozman, W. R., Experimental Transition Probabilities for Spectral Lines of Seventy Elements, NBS Monograph 53 (July 1962)

RUSS Kvater,
Probab
Leningr

TABLE III

	1700°K	1800°K	2000°K	2200°K	2400°K	2600°K	2800°K
	Cesium Line Intensities—(Cs + Cs⁺)/He = 0.01 (P = 1atm, Te = Tg)						
09	0.18075861E 09	0.28837886E 09	0.63232221E 09	0.11886595E 10	0.19678074E 10	0.30288845E 10	0.42691333E 10
	107603.742	293272.551	1598202.72	6327731.94	19685472.5	50717896.0	0.11213431E 09
09	0.31645013E 09	0.51863834E 09	0.11904766E 10	0.23233061E 10	0.40084703E 10	0.62712921E 10	0.90416037E 10
	1341.61758	4491.06317	34711.9854	182924.092	722184.383	2276265.25	5982065.13
	1014.16051	3394.90103	26239.6116	138276.652	545916.266	1720682.80	4521984.63
	2961.64474	8751.07922	54709.8994	242371.543	828029.258	2309249.84	5464399.25
	980.192055	3142.34528	22566.3872	111978.715	420482.168	1270298.66	3219204.00
	5509.37152	17675.6038	127099.094	631355.672	2372837.56	7173802.69	18191520.7
	5617.25940	18008.0715	129322.872	641724.734	2409688.41	7279794.94	18448531.2
	521.401810	1740.10378	13380.2817	70214.0273	276231.812	868072.781	2275499.00
	432.318367	1442.80055	11094.2107	58217.7002	229036.580	719759.320	1886721.52
	81.4258127	283.539139	2343.50092	13046.1868	53915.8618	176641.385	479867.859
	1235.23355	4302.93457	35587.4468	198218.611	819536.562	2685998.53	7299168.81
	111.400282	396.844307	3409.36337	19590.1665	83123.9844	278480.777	771139.008
	842.293617	2933.01602	24241.8933	134953.764	557722.242	1827232.73	4963900.56
	145.585375	531.970604	4772.01703	28406.4460	124135.767	426372.801	1206158.66
	175.148376	639.751434	5735.16132	34121.7583	149046.062	511742.555	1447198.13
	62251.6367	163227.639	832898.984	3124926.22	9295303.75	23056901.7	49346264.5
	116339.861	307606.348	1592040.91	6042852.19	18149559.2	45389724.0	97826654.0
	11.7249689	36.9944310	258.573349	1254.97414	4626.24030	13759.4607	34405.5313
	89.7791758	284.346210	2000.29932	9759.71460	36135.9702	107876.897	270607.629
	0.80286220	2.77247861	22.5922692	124.319143	508.827663	1653.45580	4460.41656
	6.28709286	21.7603259	178.007034	982.629875	4032.44241	13132.8601	35495.4751
-01	0.19468933	0.70762967	6.29071647	37.1712823	161.441317	551.627098	1553.53819
	1.55860782	5.67146063	50.5160117	298.967388	1300.18056	4447.53375	12537.5022
-01	0.65342344E-01	0.24518547	2.30096683	14.2122442	64.0482264	225.791849	653.154671
	0.51595329	1.93749183	18.2060437	112.570880	507.752865	1791.33409	5185.15033

	3400°K	3600°K	3800°K	4000°K	5000°K	6000°K	8000°K
	Cesium Line Intensities—Cs + Cs⁺/He = 0.01 (P = 1 atm, Te = Tg)						
10	0.80090708E 10	0.86881527E 10	0.88264045E 10	0.83958603E 10	0.30288873E 10	0.76446094E 09	90098597.0
09	0.59091827E 09	0.83784281E 09	0.10816026E 10	0.12764183E 10	0.10448594E 10	0.45536669E 09	0.10623388E 09
11	0.17866614E 11	0.19644231E 11	0.20198694E 11	0.19422870E 11	0.73017084E 10	0.18941982E 10	0.23104635E 09
	46861459.0	73635818.0	0.10421584E 09	0.13359940E 09	0.14978284E 09	80505835.0	24409364.7
	35423686.5	55663058.5	78779222.0	0.10099095E 09	0.11322439E 09	60856266.5	18451616.7
	33650732.0	49678896.5	66492537.5	81063314.0	75087666.0	35535165.0	9189523.63
	23200593.7	35676608.5	49525358.5	62393289.5	65473509.5	33672678.5	9661960.38
	0.13129703E 09	0.20197801E 09	0.28047587E 09	0.35345853E 09	0.37133871E 09	0.19112535E 09	54894129.5
	0.13295736E 09	0.20445459E 09	0.28381865E 09	0.35756186E 09	0.37521390E 09	0.19297051E 09	55370513.5
	17721479.7	27804455.2	39297913.0	50316417.0	56150182.5	30086547.0	9087017.63
	14693698.9	23053960.5	32583718.2	41719669.5	46556714.0	24946148.5	7534466.81
	4056241.06	6500732.88	9364198.13	12196596.0	14524657.2	8127262.88	2591282.84
	61743774.5	98972402.0	0.14259229E 09	0.18575068E 09	0.22133479E 09	0.12389566E 09	39521793.0
	6810748.13	11040147.0	16065877.6	21117946.7	26039939.5	14912793.6	4894747.75
	41959003.5	67245577.0	96866142.0	0.12616533E 09	0.15024751E 09	84070905.0	26805026.2
	11187945.1	18367429.2	27034301.2	35900939.5	46023447.5	27049231.5	9170587.50
	13413935.4	22017696.7	32401486.7	43021874.5	55120182.5	32383096.7	10973637.6
09	0.24134655E 09	0.33564150E 09	0.42585777E 09	0.49479494E 09	0.38175469E 09	0.15993765E 09	35516579.5
09	0.48621987E 09	0.67901470E 09	0.86474733E 09	0.10081123E 10	0.78779357E 09	0.33287024E 09	74709476.0
	240456.674	366827.812	505605.047	632901.641	648155.609	327970.559	92215.0664
	1905132.69	2911885.13	4020316.56	5040205.88	5191723.00	2637225.09	745099.625
	37101.2744	59212.7900	84977.2383	110309.170	129698.377	71957.6045	22700.0559
	296546.203	473819.840	680679.172	884401.328	1043480.06	580276.016	183588.268
	14263.3148	23354.2271	34292.6157	45442.5605	57784.0439	33777.8125	11374.5331
	115361.931	188996.891	277658.410	368105.223	468892.344	274410.543	92540.7207
	6376.73938	10608.6902	15801.0787	21208.9829	28316.1572	17099.0051	5996.72333
	50696.6499	84373.7021	125712.792	168789.420	225612.807	136344.074	47862.9512

2

...ental Transition ...ements, NBS Monograph 53

RUSS Kvater, G. S. and Meister, T. G., Absolute Values of Transition Probabilities for Members of the Principal Series of Cesium, Leningrad Universitet, Vestnik, No. 9, p. 137-158 (1952)

1

λ (Å)	$g A_n^m$	Ref for $g A_n^m$	Cesium Line Intensities - $(Cs + Cs^+)/He = 0.02$ (P = 1					
			1500°K	1600°K	1700°K	1800°K	2000°K	
8943.50	0.480000	NBS	0.27985289E 09	0.51206393E 09	0.86941234E 09	0.13871424E 10	0.30427295E 10	0.5
8761.38	4.300000		46075.1719	166878.482	517552.215	1410681.80	7690539.00	304
8521.10	1.300000		0.45927031E 09	0.86970861E 09	0.15220610E 10	0.24947226E 10	0.57285642E 10	0.1
8079.02	2.000000		350.756084	1651.07166	6452.90900	21602.6389	167033.803	881
8015.71	1.500000		265.144829	1248.08415	4877.90668	16329.9462	126264.806	666
7609.01	0.440000		1044.64694	4194.07159	14244.9115	42093.9087	263263.605	116
6983.49	0.580000		284.285015	1266.40660	4714.52533	15115.1182	108589.279	539
6973.29	3.300000		1594.97650	7112.02808	26498.9617	85022.1143	611599.844	304
6723.28	3.200000		1629.17326	7257.49042	27017.8806	86621.3301	622300.641	309
6586.51	0.600000		137.312931	643.861046	2507.83713	8370.14124	64385.8115	338
6354.98	0.480000		113.852507	533.854988	2079.36380	6940.07147	53385.2559	280
6217.27	0.190000		19.3653493	95.8578081	391.641678	1363.86273	11276.9080	628
6212.87	2.900000		293.506001	1453.54716	5941.22333	20697.7139	171246.516	954
6034.09	0.380000		25.0859356	127.830130	535.812805	1908.87631	16405.8298	943
6010.33	1.900000		200.321121	991.582603	4051.26181	14108.2151	116651.800	650
5844.70	0.760000		30.8443310	162.348831	700.236176	2558.85263	22962.9084	136
5663.80	0.880000		37.1414576	195.399244	842.428230	3077.29343	27597.5510	164
4593.18	0.650000		29249.1289	100838.169	299417.762	785147.648	4007903.41	150
4555.36	1.400000		53578.8818	186692.121	559571.172	1479629.33	7660888.31	291
3888.37	0.002900	RUSS	3.53311646	15.4225672	56.3947272	177.948362	1244.25293	604
3876.19	0.023700		26.8082628	117.589207	431.819660	1367.74484	9625.42468	470
3617.41	0.000938		0.19480549	0.95407632	3.86160463	13.3360077	108.713824	598
3611.52	0.007640		1.51718378	7.45212507	30.2396441	104.670197	856.568451	473
3480.13	0.000550		0.41776705E-01	0.21840766	0.93641630	3.40379712	30.2708781	179
3476.88	0.004490		0.33353621	1.74625129	7.49658805	27.2805154	243.082655	144
3400.00	0.000320		0.12989125E-01	0.70722023E-01	0.31428345	1.17937623	11.0722344	68.
3398.00	0.002560		0.10237762	0.55795590	2.48163086	9.31960535	87.6073399	542

λ (Å)	$g A_n^m$	Ref for $g A_n^m$	Cesium Line Intensities—$(Cs + Cs^+)/He = 0.02$ (P =					
			3000°K	3200°K	3400°K	3600°K	3800°K	
8943.50	0.480000	NBS	0.28027876E 11	0.35505467E 11	0.42761311E 11	0.49074227E 11	0.53721947E 11	0.5
8761.38	4.300000		0.10875265E 10	0.19382706E 10	0.31549777E 10	0.47324777E 10	0.65831785E 10	0.8
8521.10	1.300000		0.60536384E 11	0.78014799E 11	0.95391822E 11	0.11095862E 12	0.12293943E 12	0.1
8079.02	2.000000		67390194.0	0.13692567E 09	0.25019849E 09	0.41592510E 09	0.63431013E 09	0.8
8015.71	1.500000		50941842.5	0.10350536E 09	0.18913097E 09	0.31440763E 09	0.47949005E 09	0.6
7609.01	0.440000		56208949.5	0.10547425E 09	0.17966496E 09	0.28060664E 09	0.40470709E 09	0.5
6983.49	0.580000		35140922.5	69459331.0	0.12387053E 09	0.20151602E 09	0.30143629E 09	0.4
6973.29	3.300000		0.19868894E 09	0.39291726E 09	0.70100934E 09	0.11408541E 10	0.17071175E 10	0.2
6723.28	3.200000		0.20138469E 09	0.39805575E 09	0.70987404E 09	0.11548428E 10	0.17274633E 10	0.2
6586.51	0.600000		25577736.2	51869289.5	94616936.0	0.15705089E 09	0.23918691E 09	0.3
6354.98	0.480000		21207684.7	43007228.0	78451279.0	0.13021816E 09	0.19832093E 09	0.2
6217.27	0.190000		5563499.38	11591962.4	21656718.2	36718788.0	56995229.5	815
6212.87	2.900000		84648603.0	0.17641426E 09	0.32965682E 09	0.55903644E 09	0.86788855E 09	0.1
6034.09	0.380000		9089908.25	19216257.0	36363335.5	62359249.5	97785029.0	0.1
6010.33	1.900000		57550547.0	0.11991081E 09	0.22402374E 09	0.37983043E 09	0.58957615E 09	0.8
5844.70	0.760000		14483442.6	31118348.7	59733673.5	0.10374672E 09	0.16454438E 09	0.2
5663.80	0.880000		17373019.0	37317720.0	71618480.0	0.12436492E 09	0.19721177E 09	0.2
4593.18	0.650000		0.46528051E 09	0.80905623E 09	0.12885758E 10	0.18958399E 10	0.25919850E 10	0.3
4555.36	1.400000		0.92802126E 09	0.16223028E 10	0.25959814E 10	0.38353518E 10	0.52632881E 10	0.6
3888.37	0.002900	RUSS	371238.172	726373.211	1283824.69	2071992.97	3077367.13	423
3876.19	0.023700		2927955.19	5742772.94	10171713.5	16447514.0	24469672.5	336
3617.41	0.000938		51399.8193	106527.170	198087.795	334457.965	517214.297	737
3611.52	0.007640		409712.492	850370.164	1583292.89	2676327.50	4142956.47	591
3480.13	0.000550		18582.7141	39790.9058	76153.4111	131914.191	208722.143	303
3476.88	0.004490		150092.246	321623.641	615930.078	1067531.45	1689969.02	246
3400.00	0.000320		7996.20514	17473.4697	34046.1143	59922.2056	96173.3281	141
3398.00	0.002560		63513.9688	138859.152	270675.004	476577.055	765151.406	112

References:

NBS Corliss, C. H. and Bozman, W. R., Experimental Transition Probabilities for Spectral Lines of Seventy Elements, NBS Monograph 53 (July 1962)

RUSS K
P
L

TABLE IV

Cesium Line Intensities - $(Cs + Cs^{+})/He = 0.02$ (P = 1 atm, Te = Tg)

	1700°K	1800°K	2000°K	2200°K	2400°K	2600°K	2800°K
09	0.86941234E 09	0.13871424E 10	0.30427295E 10	0.57261435E 10	0.96011716E 10	0.14709788E 11	0.20944415E 11
	517552.215	1410681.80	7690539.00	30482656.5	95081444.0	0.24631163E 09	0.55013215E 09
09	0.15220610E 10	0.24947226E 10	0.57285642E 10	0.11192089E 11	0.19361036E 11	0.30456552E 11	0.44358207E 11
	6452.90900	21602.6389	167033.803	881202.344	3488173.03	11054690.1	29348077.0
	4877.90668	16329.9462	126264.806	666121.711	2636792.59	8356502.06	22184906.5
	14244.9115	42093.9087	263263.605	1167579.23	3999407.03	11214880.1	26808402.5
	4714.52533	15115.1182	108589.279	539436.359	2030941.98	6169209.94	15793450.0
	26498.9617	85022.1143	611599.844	3041436.97	11460879.2	34839598.0	89247801.0
	27017.8806	86621.3301	622300.641	3091388.00	11638870.0	35354349.5	90508696.0
	2507.83713	8370.14124	64385.8115	338242.848	1334208.25	4215798.56	11163623.0
	2079.36380	6940.07147	53385.2559	280452.801	1106253.81	3495513.69	9256276.50
	391.641678	1363.86275	11276.9080	62847.5464	260415.291	857859.508	2354236.97
	5941.22333	20697.7139	171246.516	954880.805	3958387.06	13044561.4	35809802.0
	535.812805	1908.87631	16405.8298	94371.9365	401491.434	1352442.86	3783216.41
	4051.26181	14108.2151	116651.800	650114.320	2693815.78	8873962.38	24352950.5
	700.236176	2558.85263	22962.9084	136842.699	599579.609	2070681.02	5917427.50
	842.428230	3077.29343	27597.5510	164375.141	719897.117	2485279.53	7099969.88
	299417.762	785147.648	4007903.41	15053743.4	44896606.5	0.11197592E 09	0.24209331E 09
	559571.172	1479629.33	7660888.31	29110301.7	87662936.0	0.22043535E 09	0.47993863E 09
	56.3947272	177.948362	1244.25293	6045.60138	22344.8845	66822.8691	168793.912
	431.819660	1367.74484	9625.42468	47015.5859	174537.859	523904.531	1327604.00
	3.86160463	13.3360077	108.713824	598.884048	2457.65344	8030.01385	21882.8530
	30.2396441	104.670197	856.568451	4733.63422	19476.8220	63779.7813	174141.189
	0.93641630	3.40379712	30.2708781	179.065645	779.766579	2678.97894	7621.67542
	7.49658805	27.2805154	243.082655	1440.21906	6279.91254	21599.4639	61509.1235
-01	0.31428345	1.17937623	11.0722344	68.4648075	309.354923	1096.55890	3204.38400
	2.48163086	9.31960535	87.6073399	542.289001	2452.46210	8699.62036	25438.4045

Cesium Line Intensities—$(Cs + Cs^{+})/He = 0.02$ (P = 1 atm, Te = Tg)

	3400°K	3600°K	3800°K	4000°K	5000°K	6000°K	8000°K
11	0.42761311E 11	0.49074227E 11	0.53721947E 11	0.56124306E 11	0.36709824E 11	0.12940989E 11	0.17828683E 10
10	0.31549777E 10	0.47324777E 10	0.65831785E 10	0.85325494E 10	0.12663595E 11	0.77085629E 10	0.21021529E 10
11	0.95391822E 11	0.11095862E 12	0.12293943E 12	0.12983721E 12	0.88496006E 11	0.32065468E 11	0.45719382E 10
09	0.25019849E 09	0.41592510E 09	0.63431013E 09	0.89307987E 09	0.18153536E 10	0.13628232E 10	0.48301177E 09
09	0.18913097E 09	0.31440763E 09	0.47949005E 09	0.67510021E 09	0.13722688E 10	0.10301903E 10	0.36512004E 09
09	0.17966496E 09	0.28060664E 09	0.40470709E 09	0.54188875E 09	0.91005532E 09	0.60154831E 09	0.18184201E 09
	0.12387053E 09	0.20151602E 09	0.30143629E 09	0.41708414E 09	0.79353265E 09	0.57001965E 09	0.19119058E 09
09	0.70100934E 09	0.11408541E 10	0.17071175E 10	0.23627852E 10	0.45005895E 10	0.32354184E 10	0.10862433E 10
09	0.70987404E 09	0.11548428E 10	0.17274633E 10	0.23902150E 10	0.45475564E 10	0.32666539E 10	0.10956700E 10
	94616936.0	0.15705089E 09	0.23918691E 09	0.33635314E 09	0.68053481E 09	0.50931271E 09	0.17981363E 09
	78451279.0	0.13021816E 09	0.19832093E 09	0.27888595E 09	0.56426289E 09	0.42229474E 09	0.14909180E 09
	21656718.2	36718788.0	56995229.5	81531309.0	0.17603745E 09	0.13758036E 09	51276227.5
09	0.32965682E 09	0.55903644E 09	0.86788855E 09	0.12416986E 10	0.26825564E 10	0.20973372E 10	0.78205606E 09
	36363335.5	62359249.5	97785029.0	0.14116839E 09	0.31560156E 09	0.25244756E 09	96857122.0
09	0.22402374E 09	0.37983043E 09	0.58957615E 09	0.84338491E 09	0.18209855E 10	0.14231736E 10	0.53041705E 09
	59733673.5	0.10374672E 09	0.16454438E 09	0.23998914E 09	0.55779976E 09	0.45789626E 09	0.18146731E 09
	71618480.0	0.12436492E 09	0.19721177E 09	0.28759088E 09	0.66805132E 09	0.54618929E 09	0.21714601E 09
09	0.12885758E 10	0.18958399E 10	0.25919850E 10	0.33075851E 10	0.46268301E 10	0.27074652E 10	0.70280100E 09
10	0.25959814E 10	0.38353518E 10	0.52632881E 10	0.67389882E 10	0.95479824E 10	0.56349121E 10	0.14783488E 10
	1283824.69	2071992.97	3077367.13	4230795.25	7855583.75	5551969.06	1824748.97
	10171713.5	16447514.0	24469672.5	33692563.5	62923185.0	44643617.0	14744009.0
	198087.795	334457.965	517214.297	737390.266	1571931.86	1218116.61	449188.027
	1583292.89	2676327.50	4142956.47	5912010.06	12646885.5	9823059.75	3632839.13
	76153.4111	131914.191	208722.143	303772.586	700337.062	571799.398	225078.916
	615930.078	1067531.45	1689969.02	2460694.84	5682930.19	4645291.38	1831193.00
	34046.1143	59922.2056	96173.3281	141776.949	343189.105	289456.305	118662.981
	270675.004	476577.055	765151.406	1128316.66	2734405.53	2308067.16	947110.641

2

...rimental Transition
Elements, NBS Monograph 53

RUSS Kvater, G. S. and Meister, T. G., Absolute Values of Transition Probabilities for Members of the Principal Series of Cesium, Leningrad Universitet, Vestnik, No. 9, p. 137-158 (1952)

λ (Å)	$g A_n^m$	Ref for $g A_n^m$	Cesium Line Intensities—(Cs + Cs⁺)/He = 0.05 (P - 1 atm,					
			1500°K	1600°K	1700°K	1800°K	2000°K	
8943.50	0.480000	NBS	0.11523309E 09	0.21084760E 09	0.35798386E 09	0.57114239E 09	0.12525903E 10	0
8761.38	4.300000	↓	18972.0564	68713.9346	213104.109	580834.477	3165938.69	1
8521.10	1.300000	↓	0.18911057E 09	0.35811148E 09	0.62671447E 09	0.10271776E 10	0.23582590E 10	0
8079.02	2.000000	↓	144.428419	679.845772	2657.01001	8894.67615	68762.2510	3
8015.71	1.500000	↓	109.176862	513.911514	2008.49678	6723.69623	51979.0142	2
7609.01	0.440000	↓	430.147083	1726.95221	5865.39691	17331.7566	108376.856	4
6983.49	0.580000	↓	117.058085	521.455971	1941.22389	6223.50256	44702.5884	2
6973.29	3.300000	↓	656.752502	2928.45084	10911.0491	35007.0269	251775.283	1
6723.28	3.200000	↓	670.833466	2988.34650	11124.7158	35665.4888	256180.443	1
6586.51	0.600000	↓	56.5404010	265.116421	1032.61156	3446.32413	26505.4934	1
6354.98	0.480000	↓	46.8802629	219.820292	856.186020	2857.50681	21976.9312	1
6217.27	0.190000	↓	7.97393668	39.4704399	161.259960	561.557198	4642.32739	2
6212.87	2.900000	↓	120.854946	598.513023	2446.32150	8522.08203	70496.4854	3
6034.09	0.380000	↓	10.3294631	52.6353731	220.622976	785.961227	6753.73358	3
6010.33	1.900000	↓	82.4848509	408.294357	1668.12257	5808.92010	48021.6602	2
5844.70	0.760000	↓	12.7005581	66.8488035	288.324932	1053.58264	9453.06445	5
5663.80	0.880000	↓	15.2934824	80.4576530	346.873055	1267.04558	11360.9924	6
4593.18	0.650000	↓	12043.7126	41521.1553	123286.413	323276.895	1649920.31	6
4555.36	1.400000	↓	22061.8074	76872.4053	230405.576	609222.961	3153732.50	1
3888.37	0.002900	RUSS	1.45480706	6.35040104	23.2207451	73.2685041	512.217476	2
3876.19	0.023700	↓	11.0386539	48.4185677	177.803400	563.155617	3962.46664	1
3617.41	0.000938	↓	0.80213717E-01	0.39285076	1.59003051	5.49097127	44.7538595	2
3611.52	0.007640	↓	0.62472033	3.06848931	12.4512893	43.0969334	352.620697	1
3480.13	0.000550	↓	0.17202106E-01	0.89931606E-01	0.38557300	1.40148030	12.4615121	7
3476.88	0.004490	↓	0.13733791	0.71903696	3.08674890	11.2324862	100.069031	5
3400.00	0.000320	↓	0.53484429E-02	0.29120522E-01	0.12940741	0.48559668	4.55807000	2
3398.00	0.002560	↓	0.42155328E-01	0.22974409	1.02182102	3.83725673	36.0650234	2

λ (Å)	$g A_n^m$	Ref for $g A_n^m$	Cesium Line Intensities—Cs + Cs⁺/He = 0.05 (P - 1 atm -					
			3000°K	3200°K	3400°K	3600°K	3800°K	
8943.50	0.480000	NBS	0.11343690E 11	0.14189580E 11	0.16771754E 11	0.18747070E 11	0.19812579E 11	0
8761.38	4.300000	↓	0.44015341E 09	0.77462003E 09	0.12374389E 10	0.18078754E 10	0.24278671E 10	0
8521.10	1.300000	↓	0.24500822E 11	0.31178220E 11	0.37414385E 11	0.42387810E 11	0.45339894E 11	0
8079.02	2.000000	↓	27274756.5	54721654.0	98132342.0	0.15888945E 09	0.23393270E 09	0
8015.71	1.500000	↓	20617633.7	41365393.5	74180561.0	0.12010829E 09	0.17683527E 09	0
7609.01	0.440000	↓	22749384.0	42152251.0	70467826.0	0.10719582E 09	0.14925542E 09	0
6983.49	0.580000	↓	14222545.7	27759070.0	48584245.0	76982058.0	0.11116929E 09	0
6973.29	3.300000	↓	80415148.0	0.15702739E 09	0.27494844E 09	0.43582292E 09	0.62958260E 09	0
6723.28	3.200000	↓	81506199.0	0.15908096E 09	0.27842534E 09	0.44116680E 09	0.63708609E 09	0
6586.51	0.600000	↓	10352048.0	20729299.0	37110460.5	59995731.0	88211800.0	0
6354.98	0.480000	↓	8583362.13	17187620.7	30769999.7	49745236.5	73140485.0	9
6217.27	0.190000	↓	2251708.78	4632669.00	8494153.75	14027112.4	21019762.0	2
6212.87	2.900000	↓	34259733.0	70503069.0	0.12929732E 09	0.21356007E 09	0.32007610E 09	0
6034.09	0.380000	↓	3678948.25	7679679.88	14262352.9	23822142.2	36062983.5	4
6010.33	1.900000	↓	23292367.7	47921752.0	87866136.0	0.14510076E 09	0.21743488E 09	0
5844.70	0.760000	↓	5861867.25	12436290.5	23428618.7	39632761.0	60683741.5	8
5663.80	0.880000	↓	7031362.19	14913837.7	28090053.7	47509212.5	72731431.0	0
4593.18	0.650000	↓	0.18831245E 09	0.32333522E 09	0.50540259E 09	0.72423851E 09	0.95592051E 09	0
4555.36	1.400000	↓	0.37559699E 09	0.64834514E 09	0.10181905E 10	0.14651603E 10	0.19410934E 10	0
3888.37	0.002900	RUSS	150250.805	290291.375	503539.090	791531.508	1134928.75	1
3876.19	0.023700	↓	1185027.97	2295070.16	3989528.63	6283190.00	9024381.50	1
3617.41	0.000938	↓	20802.9905	42573.0439	77693.5889	127767.817	190747.920	2
3611.52	0.007640	↓	165822.471	339846.133	620995.898	1022396.13	1527916.64	2
3480.13	0.000550	↓	7520.96075	15902.2340	29868.7344	50393.1431	76976.4375	1
3476.88	0.004490	↓	60746.6646	128535.260	241578.830	407812.570	623258.250	8
3400.00	0.000320	↓	3236.29498	6983.18372	13353.4973	22891.1558	35468.5908	4
3398.00	0.002560	↓	25705.9360	55494.3574	106163.595	182059.383	282186.781	3

References:

NBS Corliss, C. H. and Bozman, W. R., Experimental Transition Probabilities for Spectral Lines of Seventy Elements, NBS Monograph 53 (July 1962)

RUSS Kvater, G. S
Probabilities
Leningrad U

1

TABLE V

esium Line Intensities—$(Cs + Cs^+)/He = 0.05$ (P - 1 atm, Te = Tg)

	1700°K	1800°K	2000°K	2200°K	2400°K	2600°K	2800°K
09	0.35798386E 09	0.57114239E 09	0.12525903E 10	0.23560538E 10	0.39456215E 10	0.60296888E 10	0.85449511E 10
	213104.109	580834.477	3165938.69	12542259.7	39073917.5	0.10096559E 09	0.22444420E 09
09	0.62671447E 09	0.10271776E 10	0.23582590E 10	0.46050479E 10	0.79564583E 10	0.12484444E 11	0.18097364E 11
	2657.01001	8894.67615	68762.2510	362575.645	1433471.97	4531427.63	11973496.9
	2008.49678	6723.69623	51979.0142	274079.512	1083595.39	3425413.44	9051049.75
	5865.39691	17331.7566	108376.856	480407.020	1643564.64	4597091.06	10937354.4
	1941.22389	6223.50256	44702.5884	221954.113	834619.820	2528820.59	6443448.50
	10911.0491	35007.0269	251775.283	1251416.28	4709872.13	14281098.4	36411525.0
	11124.7158	35665.4888	256180.443	1271968.92	4783017.81	14492100.2	36925948.5
	1032.61156	3446.32413	26505.4934	139171.916	548295.656	1728097.81	4554560.88
	856.186020	2857.50681	21976.9312	115393.876	454617.301	1432845.88	3776397.25
	161.259960	561.557198	4642.32739	25858.9751	107018.206	351645.160	960487.078
	2446.32150	8522.08203	70496.4854	392891.062	1626707.39	5347095.56	14609766.5
	220.622976	785.961227	6753.73358	38829.8618	164993.738	554379.797	1543485.44
	1668.12257	5808.92010	48021.6602	267493.180	1107029.19	3637525.56	9935573.38
	288.324932	1053.58264	9453.06445	56304.6958	246398.490	848792.781	2414205.84
	346.873055	1267.04558	11360.9924	67633.0732	295843.215	1018740.83	2896662.25
	123286.413	323276.895	1649920.31	6193947.00	18450353.5	45900046.5	98769794.0
	230405.576	609222.961	3153732.50	11977596.7	36025266.0	90358647.0	0.19580647E 09
	23.2207451	73.2685041	512.217476	2487.49655	9182.67664	27391.3599	68864.9326
	177.803400	563.155617	3962.46664	19344.8262	71726.6973	214753.686	541638.961
	1.59003051	5.49097127	44.7538595	246.414198	1009.97780	3291.58267	8927.81726
	12.4512893	43.0969334	352.620697	1947.68031	8004.04059	26143.9675	71046.5273
-01	0.38557300	1.40148030	12.4615121	73.6775637	320.446697	1098.14015	3109.50888
	3.08674890	11.2324862	100.069031	592.586197	2580.74310	8853.83521	25094.6353
-01	0.12940741	0.48559668	4.55807000	28.1702285	127.130052	449.490421	1307.33203
	1.02182102	3.83725673	36.0650234	223.127846	1007.84440	3566.06100	10378.4193

esium Line Intensities—$Cs + Cs^+/He = 0.05$ (P - 1 atm - Te = Tg)

	3400°K	3600°K	3800°K	4000°K	5000°K	6000°K	8000°K
11	0.16771754E 11	0.18747070E 11	0.19812579E 11	0.19793040E 11	0.94856726E 10	0.27206392E 10	0.33746164E 09
09	0.12374389E 10	0.18078754E 10	0.24278671E 10	0.30091257E 10	0.32722227E 10	0.16206039E 10	0.39789587E 09
11	0.37414385E 11	0.42387810E 11	0.45339894E 11	0.45788953E 11	0.22867016E 11	0.67412601E 10	0.86537732E 09
	98132342.0	0.15888945E 09	0.23393270E 09	0.31495740E 09	0.46908017E 09	0.28651212E 09	91424558.0
	74180561.0	0.12010829E 09	0.17683527E 09	0.23808376E 09	0.35458881E 09	0.21658130E 09	69109988.0
	70467826.0	0.10719582E 09	0.14925542E 09	0.19110482E 09	0.23515467E 09	0.12646606E 09	34419090.5
	48584245.0	76982058.0	0.11116929E 09	0.14709069E 09	0.20504568E 09	0.11983766E 09	36188588.0
09	0.27494844E 09	0.43582292E 09	0.62958260E 09	0.83327005E 09	0.11629344E 10	0.68019579E 09	0.20560434E 09
09	0.27842534E 09	0.44116680E 09	0.63708609E 09	0.84294356E 09	0.11750705E 10	0.68676257E 09	0.20738862E 09
	37110460.5	59995731.0	88211800.0	0.11861975E 09	0.17584749E 09	0.10707498E 09	34035157.0
	30769999.7	49745236.5	73140485.0	98353126.0	0.14580329E 09	88780821.0	28220123.7
	8494153.75	14027112.4	21019762.0	28753184.0	45487377.0	28924107.2	9705573.75
	0.12929732E 09	0.21356007E 09	0.32007610E 09	0.43790279E 09	0.69316191E 09	0.44093214E 09	0.14802771E 09
	14262352.9	23822142.2	36062983.5	49785056.0	81550190.0	53073125.0	18333133.7
	87866136.0	0.14510076E 09	0.21743488E 09	0.29743177E 09	0.47053540E 09	0.29919985E 09	0.10039743E 09
	23428618.7	39632761.0	60683741.5	84635609.0	0.14413324E 09	96265481.0	34348166.0
	28090053.7	47509212.5	72731431.0	0.10142304E 09	0.17262180E 09	0.11524817E 09	41101437.0
09	0.50540259E 09	0.72423851E 09	0.95592051E 09	0.11664672E 10	0.11955545E 10	0.56920193E 09	0.13302630E 09
09	0.10181905E 10	0.14651603E 10	0.19410934E 10	0.23766007E 10	0.24671607E 10	0.11846515E 10	0.27982213E 09
	503539.090	791531.508	1134928.75	1492050.53	2029851.61	1167214.08	345388.820
	3989528.63	6283190.00	9024381.50	11882165.1	16259100.7	9385617.63	2790748.72
	77693.5889	127767.817	190747.920	260051.238	406180.941	256089.840	85022.3916
	620995.898	1022396.13	1527916.64	2084955.03	3267904.88	2065143.67	687624.453
	29868.7344	50393.1431	76976.4375	107129.755	180964.311	120211.822	42602.9790
	241578.830	407812.570	623258.250	867799.289	1468446.56	976599.383	346608.547
	13353.4973	22891.1558	35468.5908	49999.6724	88678.7002	60853.6304	22460.5510
	106163.595	182059.383	282186.781	397917.035	706559.516	485234.777	179269.273

2

imental Transition Elements, NBS Monograph 53

RUSS Kvater, G. S. and Meister, T. G., Absolute Values of Transition Probabilities for Members of the Principal Series of Cesium, Leningrad Universitet, Vestnik, No. 9, p. 137-158 (1952)

λ (Å)	$g A_n^m$	Ref for $g A_n^m$	Cesium Line Intensities—$(Cs + Cs^+)/He$ = 0.10 (P = 1 atm, T					
			1500°K	1600°K	1700°K	1800°K	2000°K	
8943.50	0.48C000	NBS	0.53426557E 09	0.97758156E 09	0.16598081E 10	0.26482560E 10	0.58095073E 10	0.
8761.38	4.300000		87961.8506	318587.812	988066.672	2693196.00	14683606.4	5
8521.10	1.300000		0.87679034E 09	0.16603611E 10	0.29057894E 10	0.47627870E 10	0.10937592E 11	0.
8079.C2	2.000000		669.626457	3152.06189	12319.3451	41242.5698	318918.949	1
8015.71	1.500000		5C6.186497	2382.71823	9312.48462	31176.2346	241078.387	1
7609.01	0.44C000		1994.32959	8006.90466	27195.1736	80363.3740	5C2651.277	2
6983.49	0.58C000		542.726921	2417.69760	9000.57080	28856.9519	2C7330.363	1
6973.29	.3.30000Q		3044.96066	13577.5771	50589.5640	162319.543	1167732.39	5
6723.28	3.200000		3110.24545	13855.2794	51580.2393	165372.676	1188163.50	5
6586.51	0.600000		262.143337	1229.19551	4787.74933	15979.8130	122932.335	6
6354.98	0.48C000		217.355175	1019.18288	3969.74451	13249.6025	1C1928.888	5
6217.27	0.190000		36.9702792	183.002199	747.688980	2603.81168	21531.0891	1
6212.87	2.900000		560.330643	2774.96777	11342.4783	39514.9360	326962.316	1
6034.C9	0.380000		47.8914180	244.C40581	1C22.92823	3644.32162	31323.7798	1
6010.33	1.90C000		382.431927	1893.03096	7734.32452	26934.6279	222724.199	1
5844.70	0.760000		58.8847375	309.940250	1 36.83136	4885.22064	43843.2617	2
5663.80	C.88C000		70.9065466	373.036816	1608.29234	5874.99927	52692.2217	3
4593.18	0.650000		55839.3472	192510.211	571622.937	1498960.70	7652321.44	2
4555.36	1.40C000		1C2287.140	356414.043	1068285.70	2824826.88	14626994.1	5
3888.37	0.002900	RUSS	6.74505275	29.4432325	107.664016	339.729218	2375.66190	1
3876.19	C.023700		51.1795030	224.489628	824.393372	2611.22318	18377.8989	8
3617.41	0.000938		0.37190206	1.82142769	7.37224710	25.4603722	2C7.568157	1
3611.52	0.007640		2.89644700	14.2268566	57.7309561	199.830578	1635.45288	9
3480.13	0.00C550		0.79755672E-01	0.41696220	1.78772636	6.49834222	57.7964258	3
3476.88	0.004490		0.63675208	3.33376935	14.3118484	52.0824585	464.119621	2
34C0.00	0.000320		0.24797466E-01	0.13501546	0.60000323	2.25160021	21.1403039	1
3398.C0	0.002560		0.19544853	1.06519394	4.73771858	17.7924776	167.269382	1

λ (Å)	$g A_n^m$	Ref for $g A_n^m$	Cesium Line Intensities—$(Cs + Cs^+)/He$ = 01.0 (P = 1 atm, T					
			3000°K	3200°K	3400°K	3600°K	3800°K	
8943.5C	0.48C000	NBS	0.53950512E 11	0.68759070E 11	0.83559418E 11	0.97120731E 11	0.10815014E 12	0.
8761.38	4.30C000		0.20933665E 10	0.37536102E 10	0.61651082E 10	0.93658466E 10	0.13252901E 11	0.
8521.10	1.30C000		0.11652574E 12	0.15108166E 12	C.18640413E 12	0.21959352E 12	C.24749507E 12	0.
8079.02	2.000000		0.12971855E 09	0.26516711E 09	0.48891018E 09	0.82313981E 09	0.12769591F 10	0.
8015.71	1.50C000		98057325.0	0.20044609E 09	0.36957879E 09	0.62223087E C9	0.96528365E 09	0.
7609.C1	0.440000		0.10819591E 09	0.20425901E 09	0.35108137E 09	0.55533676E 09	0.81473460E 09	0.
6983.49	C.58C000		67642329.0	0.13451333E 09	0.24205407E 09	0.39881185E 09	0.60683537E 09	0.
6973.29	3.300000		0.38245388E 09	0.76091453E 09	0.13698348E 10	0.22578163E 10	0.34366774E 10	C.
6723.28	3.20C000		0.38764291E 09	0.77C86560E 09	0.13871572E 10	0.22855007E 10	0.34776364E 10	0.
6586.51	0.600000		49234269.0	0.1C044887E 09	0.18488993E 09	0.31081279E 09	0.48151825E C9	0.
6354.98	C.48CC00		4C822411.0	83286807.0	0.15330080E 09	0.25770926E 09	0.39924905E 09	0.
6217.27	0.19C000		1C7C9111.4	22448727.2	42319159.5	72668603.0	C.11473973E 09	C.
6212.87	2.900000		0.16293905E 09	C.34163980E 09	0.64417884E 09	C.11C63654E 10	0.17471866E 10	C.
6034.C9	C.38C000		17497052.2	37213760.5	71C57202.C	0.12341255E 09	0.19685557E 09	0.
6010.33	1.900C00		0.11077833E 09	0.23221653E 09	0.43776239E C9	0.75170635E 09	0.11869030E 10	0.
5844.70	0.760000		27878999.7	6C263077.0	0.11672492E 09	0.2C532076E 09	0.33125192E 09	0.
5663.80	0.88C000		33441109.7	72268637.0	0.13994890E 09	0.24612536E 09	0.39701617E 09	0.
4593.18	C.650000		0.89561271E 09	0.15667997E 10	0.25179923E 10	0.37519769E 10	0.52180451E 10	0.
4555.36	1.40CC00		0.17863367E 10	0.31417144E 10	C.50727794E 10	0.75903826E 10	0.1C595769E 11	0.
3888.37	0.002900	RUSS	714591.773	1406677.63	2508708.00	4100593.75	6195190.31	87
3876.19	C.023700		5635984.81	11121322.0	19876435.7	3255C580.0	49261032.5	69
3617.41	0.000938		98938.8779	206298.062	387081.227	661911.633	1041228.08	15
3611.52	0.007640		788650.523	1646807.30	3C93895.63	5296606.81	8340377.81	12
3480.13	0.000550		35769.6372	77058.1514	148810.559	261065.803	420188.215	62
3476.88	0.004490		288910.711	622848.945	1203582.33	2112706.38	3402154.94	5C
3400.C0	0.000320		15391.7968	33838.7188	66529.1455	118589.506	193610.984	29
3398.C0	C.002560		122257.254	268911.434	528923.1C9	943173.516	1540361.75	23

References:

NBS Corliss, C. H. and Bozman, W. R., Experimental Transition Probabilities for Spectral Lines of Seventy Elements, NBS Monograph 53 (July 1962)

RUSS Kvater, Probabi Leningr

ine Intensities—(Cs + Cs+)/He = 0.10 (P = 1 atm, Te = Tg)

1700°K	1800°K	2000°K	2200°K	2400°K	2600°K	2800°K
.16598081E 10	0.26482560E 10	0.58095073E 10	0.10935647E 11	0.18346806E 11	0.28142945E 11	0.40161510E 11
68066.672	2693196.00	14683606.4	58215024.5	0.18169041E 09	0.47124642E 09	0.10548940E 10
.29057894E 10	0.47627870E 10	0.10937592E 11	0.21374376E 11	0.36996858E 11	0.58269846E 11	0.85058120E 11
2319.3451	41242.5698	318918.949	1682898.50	6665523.44	21149968.0	56275771.0
312.48462	31176.2346	241078.387	1272142.83	5038627.00	15987761.4	42540188.0
7195.1736	80363.3740	502651.277	2229814.00	7642436.63	21456445.0	51405873.0
000.57080	28856.9519	207330.363	1030202.25	3880911.63	11803007.6	30284388.7
0589.5640	162319.543	1167732.39	5808461.25	21900507.5	66655543.5	0.17113519E 09
1580.2393	165372.676	1188163.50	5903856.50	22240628.5	67640372.0	0.17355299E 09
787.74933	15979.8130	122932.335	645967.852	2549528.47	8065717.00	21406564.2
969.74451	13249.6025	101928.888	535601.844	2113932.00	6687659.25	17749173.0
47.688980	2603.81168	21531.0891	120024.693	497625.602	1641267.25	4514316.19
1342.4783	39514.9360	326962.316	1823607.83	7564051.88	24957013.2	68666312.0
022.92823	3644.32162	31323.7798	180229.195	767206.937	2587510.19	7254424.88
734.32452	26934.6279	222724.199	1241572.31	5147592.13	16977772.5	46697474.0
336.83136	4885.22064	43843.2617	261336.812	1145732.14	3961652.16	11346835.2
608.29234	5674.99927	52692.2217	313919.594	1375645.97	4754867.00	13614393.6
71622.937	1498960.70	7652321.44	28749267.7	85792585.0	0.21423370E 09	0.46422081E 09
068285.70	2824826.88	14626994.1	55594136.5	0.16751444E 09	0.42173960E 09	0.92029595E 09
07.664016	339.729218	2375.66190	11545.7404	42698.6704	127846.328	323667.121
24.393372	2611.22318	18377.8989	89789.2061	333523.078	1002340.52	2545718.38
.37224710	25.4603722	207.568157	1143.73398	4696.31128	15363.1204	41960.9912
7.7309561	199.830578	1635.45288	9040.17786	37218.1118	122024.254	333920.676
.78772636	6.49834222	57.7964258	341.975155	1490.05005	5125.45508	14614.7789
4.3118484	52.0824585	464.119621	2750.49481	12000.2372	41324.3564	117945.489
.60000323	2.25160021	21.1403039	130.752399	591.143997	2097.94986	6144.49731
.73771858	17.7924776	167.269382	1035.65016	4686.39124	16644.2195	48778.8628

Line Intensities—(Cs + Cs+)/He = 01.0 (P = 1 atm, Te = Tg)

3400°K	3600°K	3800°K	4000°K	5000°K	6000°K	8000°K
.83559418E 11	0.97120731E 11	0.10815014E 12	0.11549637E 12	0.89699551E 11	0.36901361E 11	0.56386092E 10
.61651082E 10	0.93658466E 10	0.13252901E 11	0.17558855E 11	0.30943184E 11	0.21981045E 11	0.66483982E 10
.18640413E 12	0.21959352E 12	0.24749507E 12	0.26718776E 12	0.21623781E 12	0.91435009E 11	0.14459494E 11
.48891018E 09	0.82313981E 09	0.12769591E 10	0.18378399E 10	0.44357721E 10	0.38861042E 10	0.15276028E 10
.36957879E 09	0.62223087E 09	0.96528365E 09	0.13892666E 10	0.33531051E 10	0.29375982E 10	0.11547511E 10
.35108137E 09	0.55533676E 09	0.81473460E 09	0.11151351E 10	0.22236977E 10	0.17153211E 10	0.57510477E 09
.24205407E 09	0.39881185E 09	0.60683537E 09	0.85830382E 09	0.19389775E 10	0.16254168E 10	0.60467111E 09
.13698348E 10	0.22578163E 10	0.34366774E 10	0.48622985E 10	0.10997079E 11	0.92258286E 10	0.34354203E 10
.13871572E 10	0.22855007E 10	0.34776364E 10	0.49187454E 10	0.11111842E 11	0.93148968E 10	0.34652337E 10
.18488993E 09	0.31081279E 09	0.48151825E 09	0.69217014E 09	0.16628700E 10	0.14523103E 10	0.56868967E 09
.15330080E 09	0.25770926E 09	0.39924905E 09	0.57391029E 09	0.13787625E 10	0.12041777E 10	0.47152692E 09
2319159.5	72668603.0	0.11473973E 09	0.16778062E 09	0.43014318E 09	0.39231182E 09	0.16216936E 09
.64417884E 09	0.11063654E 10	0.17471866E 10	0.25552510E 10	0.65547607E 10	0.59805785E 10	0.24733786E 10
1057202.0	0.12341255E 09	0.19685557E 09	0.29050583E 09	0.77116467E 09	0.71985677E 09	0.30632630E 09
.43776239E 09	0.75170635E 09	0.11869030E 10	0.17355742E 10	0.44495332E 10	0.40581940E 10	0.16775296E 10
.11672492E 09	0.20532076E 09	0.33125192E 09	0.49386582E 09	0.13629699E 10	0.13056958E 10	0.57391970E 09
.13994890E 09	0.24612536E 09	0.39701617E 09	0.59182388E 09	0.16323669E 10	0.15631673E 10	0.68675937E 09
.25179923E 10	0.37519769E 10	0.52180451E 10	0.68065714E 10	0.11305545E 11	0.77203646E 10	0.22227217E 10
.50727794E 10	0.75903826E 10	0.10595769E 11	0.13867943E 11	0.23330260E 11	0.16068009E 11	0.46755172E 10
508708.00	4100593.75	6195190.31	8706415.38	19194925.5	15831495.9	5771063.63
9876435.7	32550580.0	49261032.5	69334826.0	0.15375125E 09	0.12730172E 09	46630311.5
87081.227	661911.633	1041228.08	1517451.34	3840976.88	3473471.88	1420629.75
093895.63	5296606.81	8340377.81	12166132.5	30902353.5	28010554.7	11489441.0
48810.559	261065.803	420188.215	625123.687	1711256.39	1630491.78	711848.469
203582.33	2112706.38	3402154.94	5063783.56	13886100.0	13246095.5	5791443.94
6529.1455	118589.506	193610.984	291758.152	838574.148	825387.594	375290.859
528923.109	943173.516	1540361.75	2321926.00	6681452.75	6581476.94	2995390.50

nental Transition
ements, NBS Monograph 53

RUSS Kvater, G. S. and Meister, T. G., Absolute Values of Transition Probabilities for Members of the Principal Series of Cesium Leningrad Universitet, Vestnik, No. 9, p. 137-158 (1952)

2

λ (Å)	$g A_n^m$	Ref for $g A_n^m$	Cesium Line Intensities—100% Cesium (P = 1atm,					
			1500°K	1600°K	1700°K	1800°K	2000°K	
8943.50	0.480000	NBS	0.58769301E 10	0.10753460E 11	0.18258183E 11	0.29131910E 11	0.63914370E 11	0.
8761.38	4.300000	↓	967581.797	3504486.66	10868909.0	29626268.7	0.16154440E 09	0.
8521.10	1.300000		0.96447081E 10	0.18264081E 11	0.31964201E 11	0.52392624E 11	0.12033194E 12	0.
8079.02	2.000000		7365.90210	34672.8857	135514.986	453685.301	3508645.78	18
8015.71	1.500000		5568.05981	26210.0557	102438.986	342951.461	2652268.41	14
7609.01	0.440000		21937.6580	88076.4707	299151.746	884030.320	5530010.94	24
6983.49	0.580000		5970.00500	26594.8311	99007.8799	317438.387	2280983.31	11
697[illegible].29	3.300000		33494.6167	149354.230	556494.195	1785582.00	12847023.7	63
6723.28	3.200000		34212.7515	152408.975	567391.805	1819167.77	13071800.5	64
6586.51	0.600000		2883.58105	13521.2305	52666.0947	175784.543	1352462.81	71
6354.98	0.480000		2390.91052	11211.0779	43667.8955	145751.100	1121389.48	58
6217.27	0.190000		406.673676	2013.03607	8224.71167	28643.0037	236878.256	13
6212.87	2.900000		6163.64630	30524.8259	124769.278	434680.617	3597136.34	20
6034.09	0.380000		526.806389	2684.46225	11252.3923	40089.0435	344614.352	19
6010.33	1.900000		4206.75739	20823.4636	85078.9434	296292.027	2450341.44	13
5844.70	0.760000		647.733078	3409.36288	14705.3827	53739.4448	482349.742	28
5663.80	0.880000		779.973183	4103.42920	17691.5015	64627.4185	579703.211	34
4593.18	0.650000		614233.734	2117624.84	6287953.94	16489186.6	84188429.0	0.
4555.36	1.400000	↓	1125160.22	3920577.69	11751332.5	31074262.2	0.16092158E 09	0.
3888.37	0.002900	RUSS	74.1956911	323.877468	1184.32333	3737.16174	26136.2834	12
3876.19	0.023700	↓	562.975380	2469.40045	9068.47375	28724.5334	202187.852	98
3617.41	0.000938		4.09092879	20.0358229	81.0960274	280.074608	2283.59946	12
3611.52	0.007640		31.8609645	156.496346	635.050789	2198.21890	17992.7371	99
3480.13	0.000550		0.87731371	4.58661133	19.6653080	71.4844475	635.858055	37
3476.88	0.004490		7.00428343	36.6716800	157.432877	572.928551	5106.09784	30
3400.00	0.000320		0.27277254	1.48517881	6.60014212	24.7685323	232.578960	14
3398.00	0.002560	↓	2.14993712	11.7172027	52.1157470	195.724604	1840.24504	11

λ (Å)	$g A_n^m$	Ref for $g A_n^m$	Cesium Line Intensities—100 % Cesium (P = 1 atm,					
			3000°K	3200°K	3400°K	3600°K	3800°K	
8943.50	0.480000	NBS	0.59995540E 12	0.77069185E 12	0.94756636E 12	0.11195204E 13	0.12743291E 13	0.
8761.38	4.300000	↓	0.23279233E 11	0.42072657E 11	0.69912515E 11	0.10796106E 12	0.15615844E 12	0.
8521.10	1.300000		0.12958217E 13	0.16934116E 13	0.21138285E 13	0.25312766E 13	0.29162252E 13	0.
8079.02	2.000000		0.14425320E 10	0.29721480E 10	0.55442564E 10	0.94884158E 10	0.15046361E 11	0.
8015.71	1.500000		0.10904441E 10	0.22467170E 10	0.41910347E 10	0.71725181E 10	0.11373901E 11	0.
7609.01	0.440000		0.12031900E 10	0.22894543E 10	0.39812735E 10	0.64014230E 10	0.95999875E 10	0.
6983.49	0.580000		0.75221490E 09	0.15077041E 10	0.27449005E 10	0.45971444E 10	0.71503185E 10	0.
6973.29	3.300000		0.42530693E 10	0.85287748E 10	0.15533968E 11	0.26026076E 11	0.40494242E 11	0.
6723.28	3.200000		0.43107737E 10	0.86403121E 10	0.15730405E 11	0.26345197E 11	0.40976861E 11	0.
6586.51	0.600000		0.54750851E 09	0.11258896E 10	0.20966575E 10	0.35827704E 10	0.56737115E 10	0.
6354.98	0.480000		0.45396464E 09	0.93352722E 09	0.17384357E 10	0.29706407E 10	0.47043367E 10	0.
6217.27	0.190000		0.11909042E 09	0.25161846E 09	0.47990056E 09	0.83765834E 09	0.13519740E 10	0.
6212.87	2.900000		0.18119598E 10	0.38292986E 10	0.73050077E 10	0.12753186E 11	0.20587035E 11	0.
6034.09	0.380000		0.19457555E 09	0.41711359E 09	0.80579083E 09	0.14225890E 10	0.23195419E 10	0.
6010.33	1.900000		0.12319078E 10	0.26028186E 10	0.49642388E 10	0.86649950E 10	0.13985234E 11	0.
5844.70	0.760000		0.31002775E 09	0.67546379E 09	0.13236642E 10	0.23667531E 10	0.39031290E 10	0.
5663.80	0.880000		0.37188106E 09	0.81002913E 09	0.15870248E 10	0.28371119E 10	0.46780267E 10	0.
4593.18	0.650000		0.99596396E 10	0.17561606E 11	0.28554109E 11	0.43249416E 11	0.61484032E 11	0.
4555.36	1.400000	↓	0.19864914E 11	0.35214171E 11	0.57525475E 11	0.87495108E 11	0.12484955E 12	0.
3888.37	0.002900	RUSS	7946600.81	15766865.1	28448825.2	47267959.0	72997698.0	0.
3876.19	0.023700	↓	62674834.0	0.12465427E 09	0.22539939E 09	0.37521382E 09	0.58044090E 09	0.
3617.41	0.000938		1100247.44	2312309.28	4389512.94	7629922.38	12268751.7	18
3611.52	0.007640		8770169.25	18458378.5	35084871.0	61054522.5	98274360.0	0.
3480.13	0.000550		397775.395	863712.805	1687516.28	3009331.88	4951062.13	75
3476.88	0.004490		3212824.69	6981254.94	13648660.1	24353380.2	40087465.5	61
3400.00	0.000320		171164.105	379284.141	754442.539	1366993.22	2281311.03	35
3398.00	0.002560	↓	1359558.88	3014116.59	5998004.19	10872056.5	18150025.2	28

References:

NBS Corliss, C. H. and Bozman, W. R., Experimental Transition Probabilities for Spectral Lines of Seventy Elements, NBS Monograph 53 (July 1962)

RUSS Kvater, G. S.
Probabilities
Leningrad Un

1

TABLE VII

Cesium Line Intensities—100% Cesium (P = 1atm, Te = Tg)

1700°K	1800°K	2000°K	2200°K	2400°K	2600°K	2800°K
0.18258183E 11	0.29131910E 11	0.63914370E 11	0.12035028E 12	0.20207082E 12	0.31046635E 12	0.44437475E 12
10868909.0	29626268.7	0.16154440E 09	0.64067488E 09	0.20011292E 10	0.51986794E 10	0.11672077E 11
0.31964201E 11	0.52392624E 11	0.12033194E 12	0.23523182E 12	0.40748159E 12	0.64281920E 12	0.94114193E 12
135514.986	453685.301	3508645.78	18520833.7	73413750.0	0.23332145E 09	0.62267409E 09
102438.986	342951.461	2652268.41	14000336.9	55495191.5	0.17637321E 09	0.47069409E 09
299151.746	884030.320	5530010.94	24539813.2	84173423.0	0.23670243E 09	0.56879017E 09
99007.8799	317438.387	2280983.31	11337703.7	42744171.0	0.13020799E 09	0.33508743E 09
556494.195	1785582.00	12847023.7	63923966.0	0.24121112E 09	0.73532823E 09	0.18935582E 10
567391.805	1819167.77	13071800.5	64973821.5	0.24495719E 09	0.74619263E 09	0.19203104E 10
52666.0947	175784.543	1352462.81	7109081.81	28080382.0	88979090.0	0.23685704E 09
43667.8955	145751.100	1121389.48	5894468.75	23282744.5	73776681.0	0.19638913E 09
8224.71167	28643.0037	236878.256	1320909.95	5480824.19	18106073.2	49949520.0
124769.278	434680.617	3597136.34	20069384.5	83310098.0	0.27531988E 09	0.75977162E 09
11252.3923	40089.0435	344614.352	1983479.69	8449979.75	28544802.2	80267979.0
85078.9434	296292.027	2450341.44	13663898.6	56695329.0	0.18729478E 09	0.51669318E 09
14705.3827	53739.4448	482349.742	2876116.84	12619037.9	43704012.5	0.12554924E 09
17691.5015	64627.4185	579703.211	3454785.06	15151297.2	52454572.5	0.15063907E 09
6287953.94	16489186.6	84188429.0	0.31639484E 09	0.94491532E 09	0.23633756E 10	0.51364604E 10
11751332.5	31074262.2	0.16092158E 09	0.61183117E 09	0.18449958E 10	0.46525318E 10	0.10182791E 11
1184.32333	3737.16174	26136.2834	127064.550	470281.070	1410370.55	3581277.06
9068.47375	28724.5334	202187.852	988158.805	3673406.81	11057584.4	28167590.2
81.0960274	280.074608	2283.59946	12587.1567	51724.9438	169482.320	464285.461
635.050769	2198.21890	17992.7371	99490.0361	409918.469	1346142.81	3694729.50
19.6653080	71.4844475	635.858055	3763.54547	16411.3386	56542.8125	161708.031
157.432877	572.928551	5106.09784	30270.0715	132170.027	455880.562	1305030.55
6.60014212	24.7685323	232.578960	1438.97180	6510.83099	23144.0881	67986.9717
52.1157470	195.724604	1840.24504	11397.6598	51615.6846	183615.105	539723.102

Cesium Line Intensities—100 % Cesium (P = 1 atm, Te = Tg)

3400°K	3600°K	3800°K	4000°K	5000°K	6000°K	8000°K
0.94756636E 12	0.11195204E 13	0.12743291E 13	0.13999344E 13	0.13772138E 13	0.74806639E 12	0.15306485E 12
0.69912515E 11	0.10796106E 12	0.15615844E 12	0.21283131E 12	0.47509023E 12	0.44560093E 12	0.18047643E 12
0.21138285E 13	0.25312766E 13	0.29162252E 13	0.32385895E 13	0.33200356E 13	0.18535754E 13	0.39251529E 12
0.55442564E 10	0.94884158E 10	0.15046361E 11	0.22276502E 11	0.68105210E 11	0.78779314E 11	0.41468081E 11
0.41910347E 10	0.71725181E 10	0.11373901E 11	0.16839335E 11	0.51482341E 11	0.59551149E 11	0.31346703E 11
0.39812735E 10	0.64014230E 10	0.95999875E 10	0.13516580E 11	0.34141836E 11	0.34773081E 11	0.15611709E 11
0.27449005E 10	0.45971444E 10	0.71503185E 10	0.10403521E 11	0.29770345E 11	0.32950537E 11	0.16414312E 11
0.15533968E 11	0.26026076E 11	0.40494242E 11	0.58936041E 11	0.16884510E 12	0.18702649E 12	0.93257412E 11
0.15730405E 11	0.26345197E 11	0.40976861E 11	0.59620234E 11	0.17060713E 12	0.18883209E 12	0.94066722E 11
0.20966575E 10	0.35827704E 10	0.56737115E 10	0.83898114E 10	0.25531094E 11	0.29441313E 11	0.15437566E 11
0.17384357E 10	0.29706407E 10	0.47043367E 10	0.69563808E 10	0.21169011E 11	0.24411155E 11	0.12800000E 11
0.47990056E 09	0.83765834E 09	0.13519740E 10	0.20336730E 10	0.66042597E 10	0.79529663E 10	0.44022254E 10
0.73050077E 10	0.12753186E 11	0.20587035E 11	0.30972260E 11	0.10063937E 12	0.12123860E 12	0.67141973E 11
0.80579083E 09	0.14225890E 10	0.23195419E 10	0.35212282E 10	0.11840177E 11	0.14592975E 11	0.83154886E 10
0.49642388E 10	0.86649950E 10	0.13985234E 11	0.21036938E 11	0.68316492E 11	0.82267927E 11	0.45537972E 11
0.13236642E 10	0.23667531E 10	0.39031290E 10	0.59861597E 10	0.20926539E 11	0.26469136E 11	0.15579540E 11
0.15870248E 10	0.28371119E 10	0.46780267E 10	0.71735118E 10	0.25062760E 11	0.31688612E 11	0.18642668E 11
0.28554109E 11	0.43249416E 11	0.61484032E 11	0.82502621E 11	0.17358118E 12	0.15650764E 12	0.60337678E 11
0.57525475E 11	0.87495108E 11	0.12484955E 12	0.16809368E 12	0.35820422E 12	0.32573154E 12	0.12692089E 12
28448825.2	47267959.0	72997698.0	0.10553067E 09	0.29471181E 09	0.32093693E 09	0.15666044E 09
0.22539939E 09	0.37521382E 09	0.58044090E 09	0.84040913E 09	0.23606400E 10	0.25806674E 10	0.12658195E 10
4389512.94	7629922.38	12268751.7	18393065.2	58972943.0	70414408.0	38564205.5
35084871.0	61054522.5	98274360.0	0.14746599E 09	0.47446334E 09	0.56783147E 09	0.31189066E 09
1687516.28	3009331.88	4951062.13	7577139.69	26274000.0	33053417.5	19323733.5
13648660.1	24353380.2	40087465.5	61378246.0	0.21320206E 09	0.26852556E 09	0.15721368E 09
754442.539	1366993.22	2281311.03	3536407.81	12875158.4	16732301.7	10187590.4
5998004.19	10872056.5	18150025.2	28144122.7	0.10258456E 09	0.13342005E 09	81312428.0

nental Transition
lements, NBS Monograph 53

RUSS Kvater, G. S. and Meister, T. G., Absolute Values of Transition Probabilities for Members of the Principal Series of Cesium, Leningrad Universitet, Vestnik, No. 9, p. 137-158 (1952)

A Spectroscopic Method Allowing Spatial Resolution*

The thermionic energy converter has a plasma between the two electrodes which are only some 50 microns apart. In addition, there is an electrode sheath on both electrodes. Consequently, changes in the properties of the plasma occur within a very short distance. It is highly desirable to investigate these changes.

Even if the plasma is not confined in an extremely narrow space, changes in properties still may happen within short distances. An example is the electrode sheaths on an MPD-power generator.

To spectroscopically observe these changes in properties, a stigmatic line spectrum is commonly used. An image of the device under investigation is formed in the plane of the entrance slit of the spectrograph. The length of the lines obtained corresponds to the diameter of the discharge; the intensity distribution along the lines is related to the intensity distribution across the diameter. The true radial intensity-density distribution i(r) can be found from the intensity distribution along a line, which may be called I(x), by solution of Abel's integral equation:[17,18,19]

$$I(x) = 2 \int_{r=x}^{R} \frac{i(r)\, dr}{\sqrt{r^2 - x^2}} \quad dr \tag{30}$$

where R = radius of the discharge.

If a drastic change in intensity takes place within a short distance, it is necessary to enlarge the picture of the device. However, enlargement is limited by the height of the entrance slit of the spectrograph, even if the intensity of the discharge would allow a greater enlargement. This, in turn, usually causes the electrode sheaths to appear as tiny knots in the stigmatic line spectrum. The diffusion effects of the photographic emulsion, due to the large density gradient, then tend to falsify the measurement. To transform the axial intensity distribution into radial distribution, the height or the width of the densitometer slit must be made extremely small to resolve the sheath structure.

This paper describes a method to avoid these difficulties.

---

*The material covered in this subsection was presented by R. T. Schneider as a paper at the VI International Conference on Ionization Phenomena in Gases, Paris, France, 1963.

EXPERIMENTAL SETUP

As stated previously, it is important that the axis of the cylindrical discharge be parallel, not perpendicular, to the entrance slit of the spectrograph. The limitation of the enlargement by the height of the entrance slit can thus be avoided.

The experimental setup is shown in Figure 20. Axes of the device and entrance slit are parallel (or, in the illustration, perpendicular to the paper plane). A lens forms an enlarged image of the device in the plane of the entrance slit. A slowly rotating mirror is located in the light path. The rotation of this mirror causes slow motion of the image of the device across the entrance slit. An exit slit in the focal plane of the spectrograph is located where a spectrum line of interest appears. Also in the focal plane of the spectrograph is a photographic plate which can be moved slowly in the direction of the dispersion. When the mirror is rotated while the plate is moved, a photographic picture of the device is obtained in the light of one specific spectrum line.

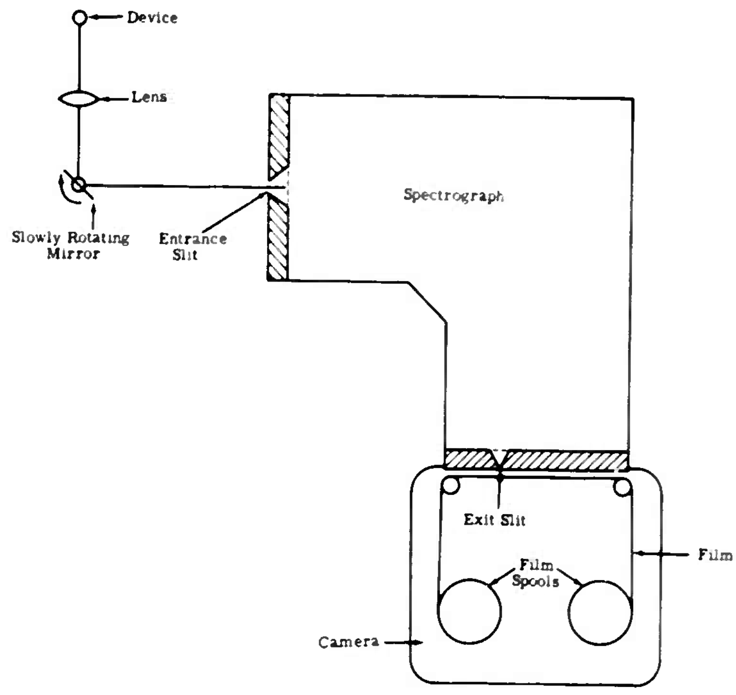

Figure 20. Schematic Diagram of Optical Arrangement

A film instead of a photographic plate proved to be more advantageous. The required low film speed of approximately 1 cm/minute caused problems of jerking. Experience showed that 70-mm film was better than 35-mm film in this respect; therefore, a 70-mm camera was modified to incorporate a continuous drive mechanism.

The exit slit is variable, and the mount rotates to bring the exit slit parallel to the entrance slit. The exit slit mount is attached directly to the film window of the camera case, reducing the distance between the film and exit slit to 1/10 mm.

If the camera is used in connection with a high dispersion spectrograph, the spectrum lines are sufficiently separated so that the exit slit serves only as an aperture and the image of the entrance slit is used as an exit slit. The exit slit must then be chosen wider than the line width. The curvature and the titlt of the focal plane can be neglected over this short distance.

A 7102 photomultiplier was used to check spectrum line adjustment with respect to the exit slit. A slot was machined into the plate which presses the film against the ducts. The photomultiplier tube was mounted behind this slot so that it looked directly into the exit slit. To permit this alignment, a hole is punched in the film and the hole is then located in front of the slot. The grating is rotated until the spectrum line is in the exit slit, as indicated by obtaining the maximum signal output of the photomultiplier. Movement of the film can then be started to obtain the spectrum picture. Because the photomultiplier also provides information concerning intensity, the proper film speed can be selected for obtaining a correct exposure.

The rotating mirror mechanism was designed so that two hours are required for one revolution. Use of a 24-v d-c motor with a high gear reduction permits fine speed adjustments with a variable resistor, and coarse speed adjustments by varying the focal length of the lens. To avoid distortion, mirror rotational speed is ratioed to film drive speed in accordance with the different enlargement factors of the optical system. This can be checked easily with two marks placed a defined distance on the discharge tube.

APPLICATION

This method was developed for use with thermionic energy converters and MPD-power generators. Investigations on both types will be reported in the near future. This paper, however, reports the application to a Cs diode which served as a checkout.

The result for the 8521 Å cesium line is shown in Figure 21. The cathode with an electrode sheath and the anode are visible. Also shown in Figure 21 is the density distribution of atoms which have a single energy—for this case, 1.45 ev. As long as the radiation is from an optically thin layer, the intensity is given by:

$$I = A_n^m \, h \, \nu \, n^* \ell \tag{31}$$

where

A_n^m = transition probability
h = Planck's constant
ν = frequency
n^* = number of radiating particles
ℓ = geometrical sheat thickness

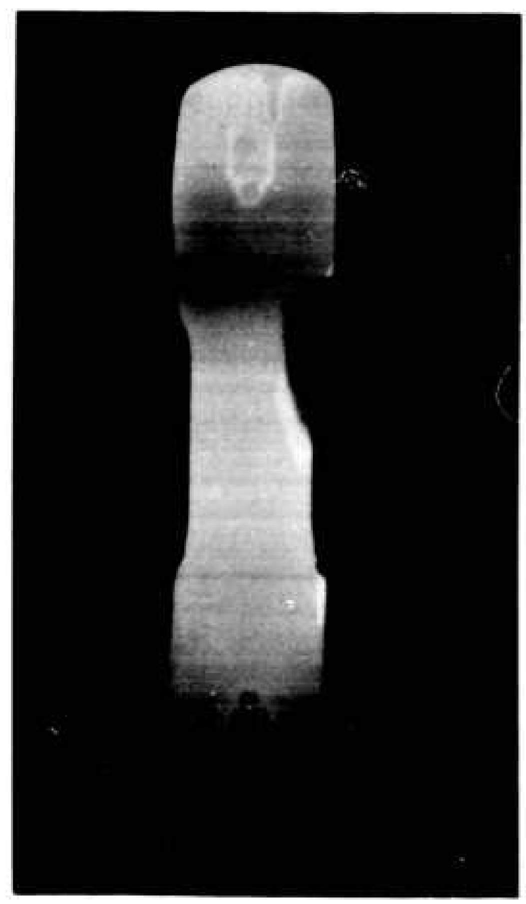

Figure 21. Density Distribution of Atoms Having a Single Energy

Even if the temperature or temperature gradient which may exist across the diode is not known, the number of particles in the excited state can be measured with this relationship if (1) the film has been calibrated with the aid of a standard lamp and (2) the transition probability is known.

The length of the geometrical sheath can be obtained by using Abel's transformation equation—Equation (30).

Figure 22 is a comparison of electrode sheaths with the stigmatic line spectrum. The improvement in accuracy can be readily noted. The sheath appears in the line spectrum only as two little knots. In order to find the intensity of the sheaths, the microdensitometer slit has to be appropriately small---whether it is parallel or perpendicular to the line. In the case of Figure 22, however, the microdensitometer slit can be chosen parallel to the sheath so that a convenient slit height can be applied.

For both the electrode sheath and stigmatic line methods, the diode is assumed not to change the intensity with time. However, if deviations occur, the error introduced in the analysis is much more severe for the stigmatic line spectrum.

Figure 23 indicates the variations which accompany a sudden increase (top of illustration) or decrease (bottom) in intensity. Using the picture method, the variation shows up as a bright or dark strip across the diode. The striations in Figure 23 do not represent a real geometrical structure. The device could have increased its intensity for a short moment, during which time the slit was passing across the diode and happened to be at the geometrical location where the bright strip now appears. If .his were the case, the stigmatic line spectrum would have caught all these sudden intensity increases which appear in the picture as bright strips and would have added them together. These strips in the picture, of course, make these parts of the picture unusable for the analysis. However, they do reveal what happens to the device with respect to time.

Using the intensity ratio method, the electron temperature was determined. The result was 3000°K ± 20 percent. Nine different intensity ratios were used, and the results agreed within the experimental error. The results obtained using line intensities of the stigmatic line were higher but did not agree with each other. It can be assumed that the fluctuations observed in Figure 23 are responsible for this.

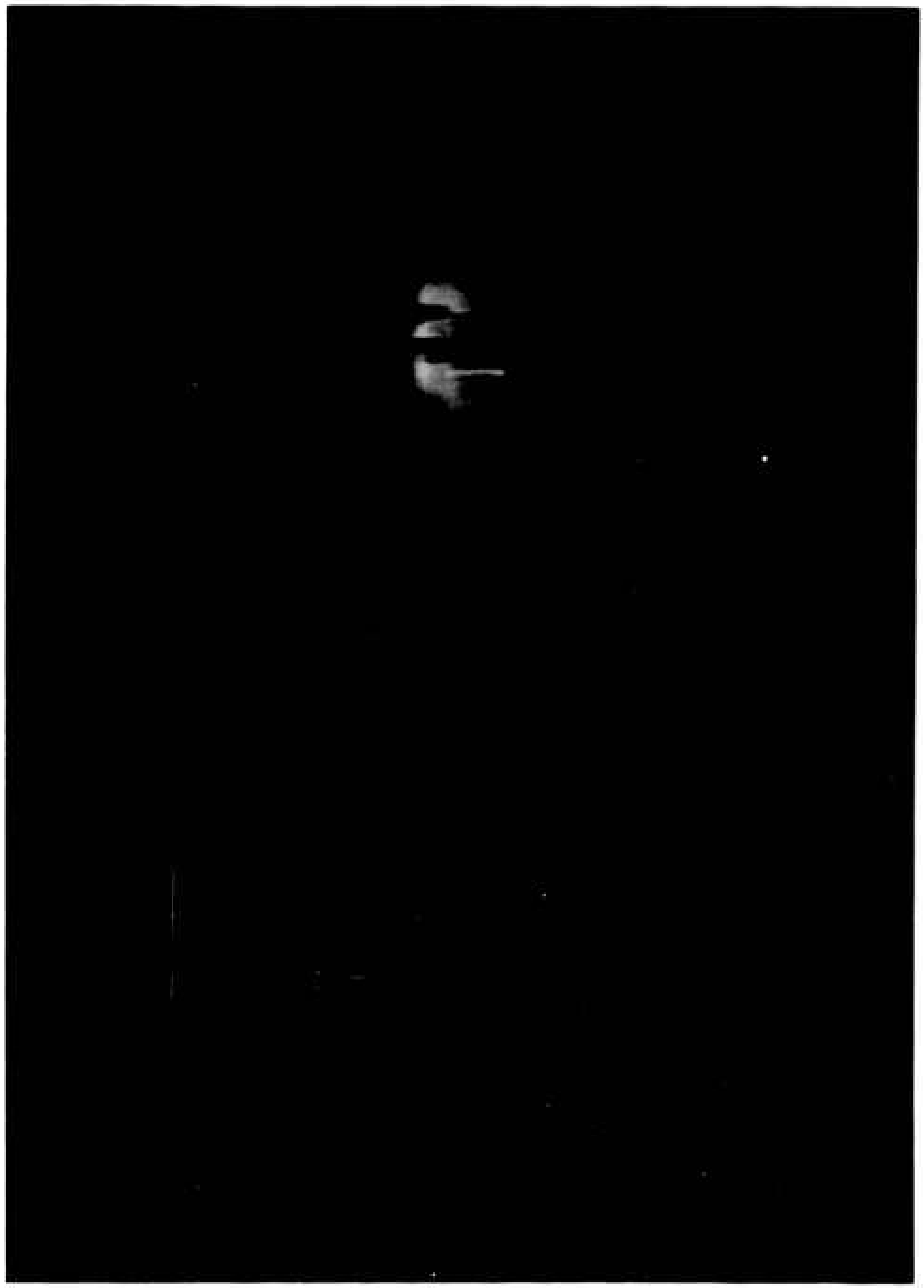

Figure 22. Luminous Electrode Sheath as a Spectrum (Upper Part) and as a Stigmatic Line Spectrum (Lower Part)

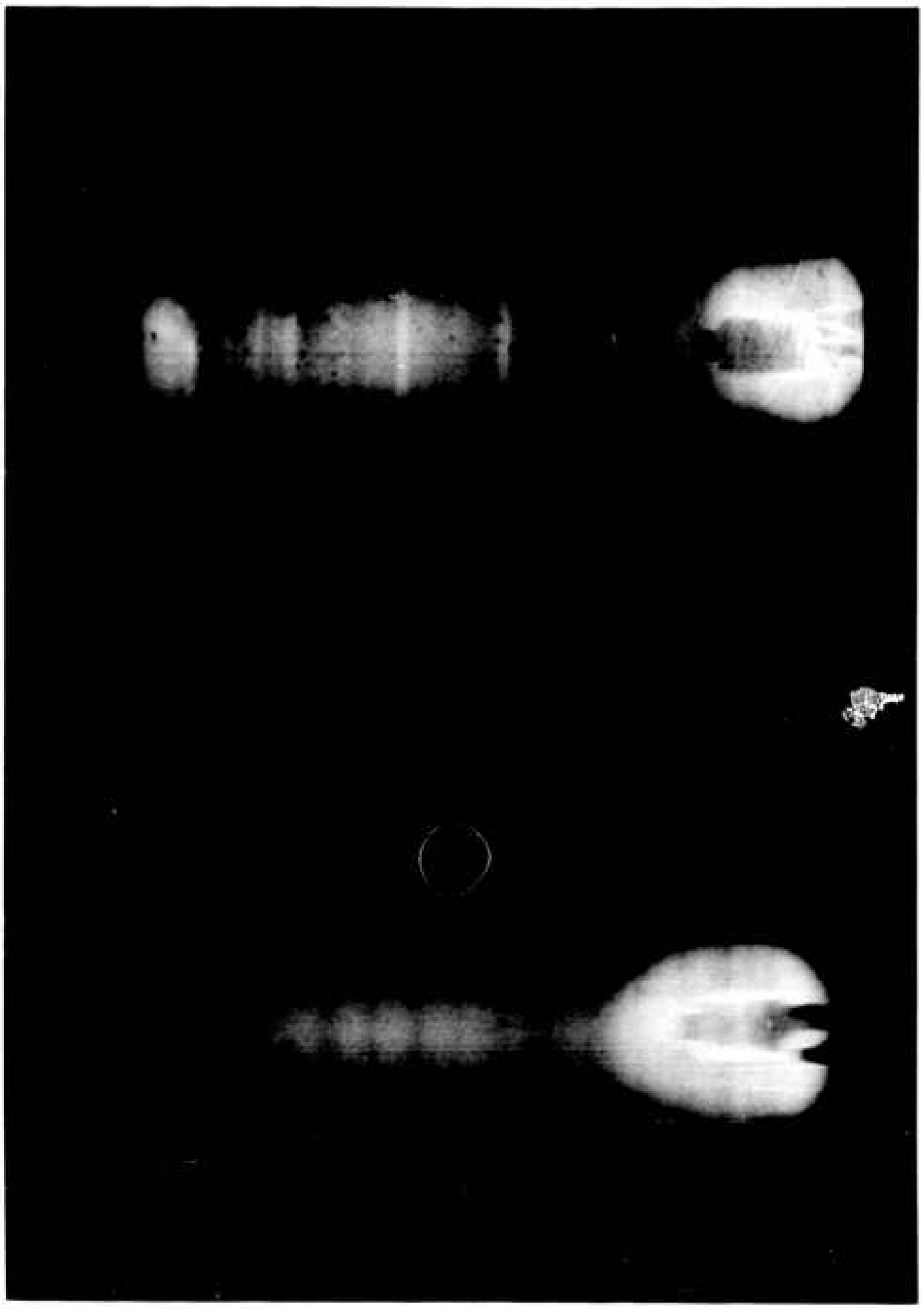

Figure 23. Striations Caused by Short-Time Increase and Decrease of Intensity

The difficulty of measuring line profiles is a disadvantage of the picture method. But the transition from the picture method to the stigmatic line spectrum is easily accomplished by stopping the motion of the rotating mirror and, a short time later, the film. Of course, the exit slit has to be larger than the line width. In Figure 22, the location where the line profile was taken can be determined exactly. This profile also should be treated with Abel's transformation, Equation (30), as further described in Reference 20.

If line radiation of the nonvisible range is under consideration, it is advisable to take a spectrum picture before taking line profiles. This is a good way to determine if the image of the device is sharp in the entrance slit plane. It is very difficult to make this judgment from the appearance of the line alone. The picture of the device in the plane of the entrance slit must be sharp because a homogeneous illumination of the slit would give only an average profile.

A compilation of the pictures taken by the described method is shown in Figure 24. The pictures were taken with the Ebert-Grating spectrograph. Although only the stronger cesium lines were used, a considerable change in the parameters can be seen. As the excitation energy rises, the electrode sheath density first increases and then decreases. This detail can be seen better in Figure 25. The transitions shown are:

$$5^2F_{7/2} - 5^2D_{5/2};\ 7^2\ P_{3/2} - 6^2\ S_{1/2};\ \text{and}\ 6^2P_{3/2} - 6^2S_{1/2}$$

Figure 24 also shows that radiation from higher excitation levels come more from the center of the tube due to the temperature profile of the discharge. The tube is filled with cesium metal. As can be seen in Figure 21, part of the cesium metal is evaporated; the rest is molten and sticks to the walls of the tube. The anode, illuminated by the ambient radiation, can be seen clearly. Because the cathode is surrounded by a sheath which is nearly optically thick, no details of the cathode structure can be seen.

Figure 26 shows the change of the cathode sheath due to variation of voltage and current for one spectrum line. Table VIII lists the points on the iv-characteristic (arc mode) where the pictures in Figure 26 were taken. A considerable increase in the sheath thickness with increasing voltage is visible in Figure 26.

The described method has these features: (1) it has a considerable advantage over the stigmatic line spectrum if details of the discharge are of interest; (2) it serves as an adjustment aid for line broadening investigations; and (3) it gives the exact location where the line profile was taken.

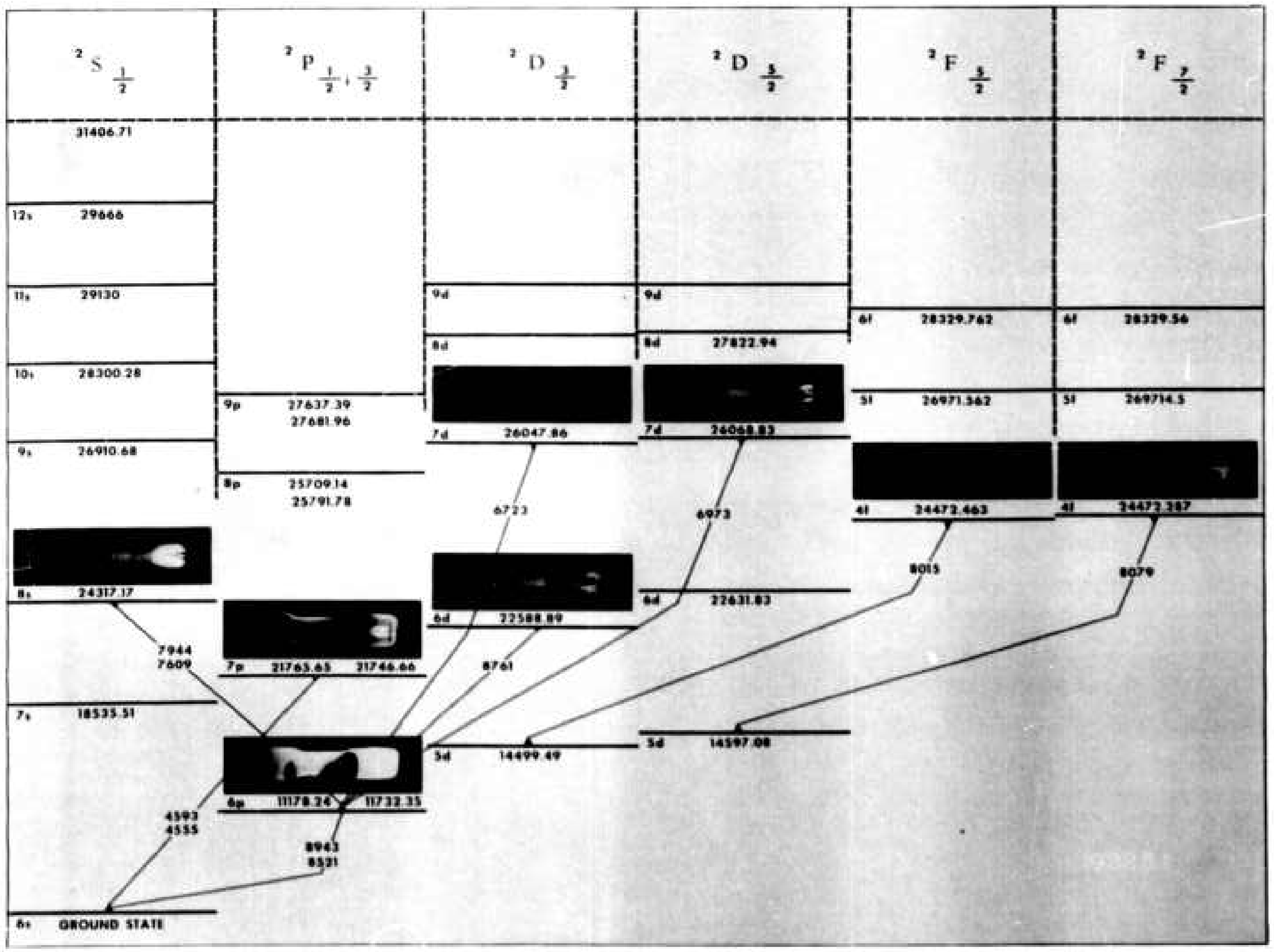

Figure 24. Energy Level Diagram of the Cesium Atom with Spectrum Pictures of Different Excited States

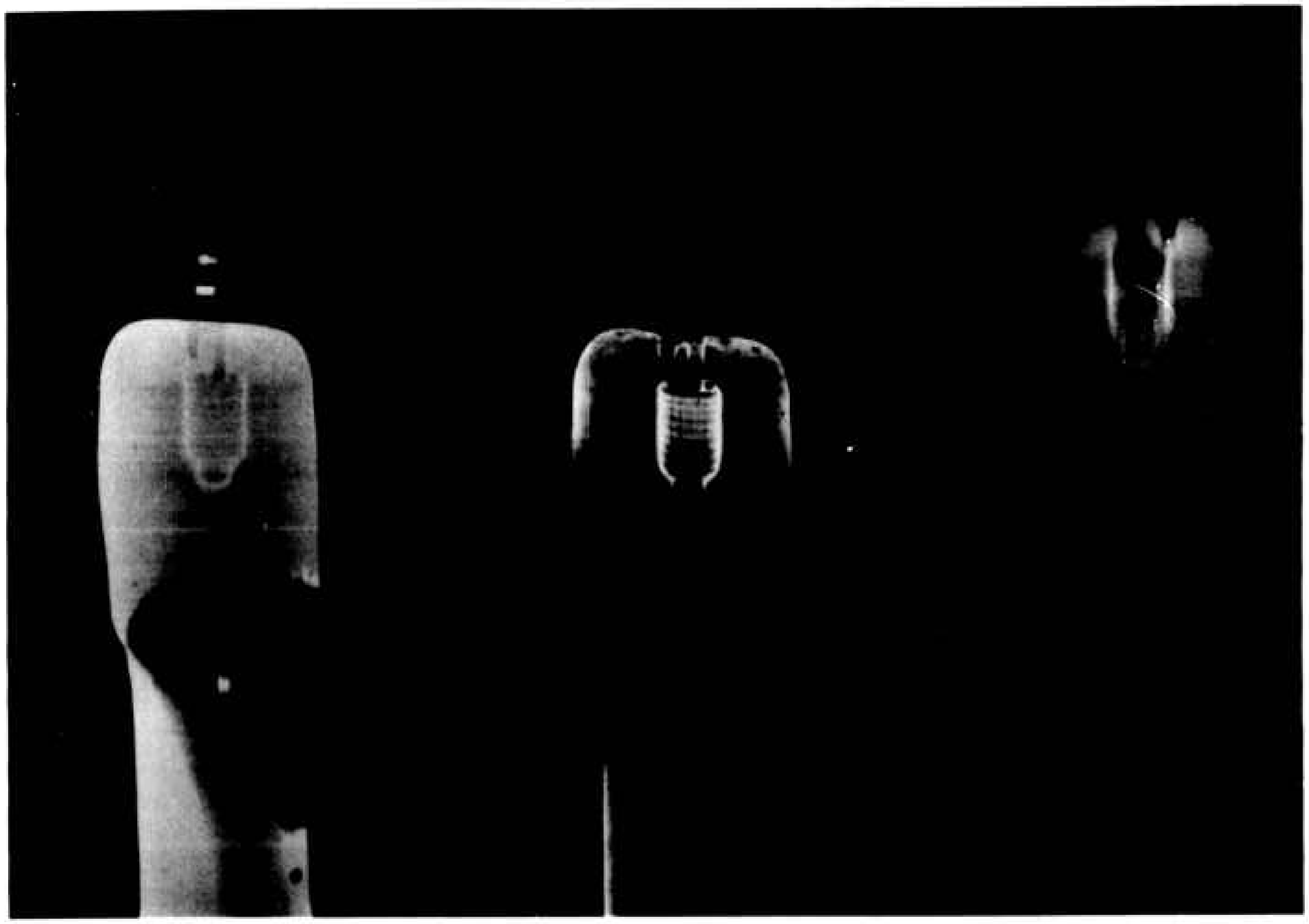

Figure 25. Details of the Electrode Sheath of Figure 24

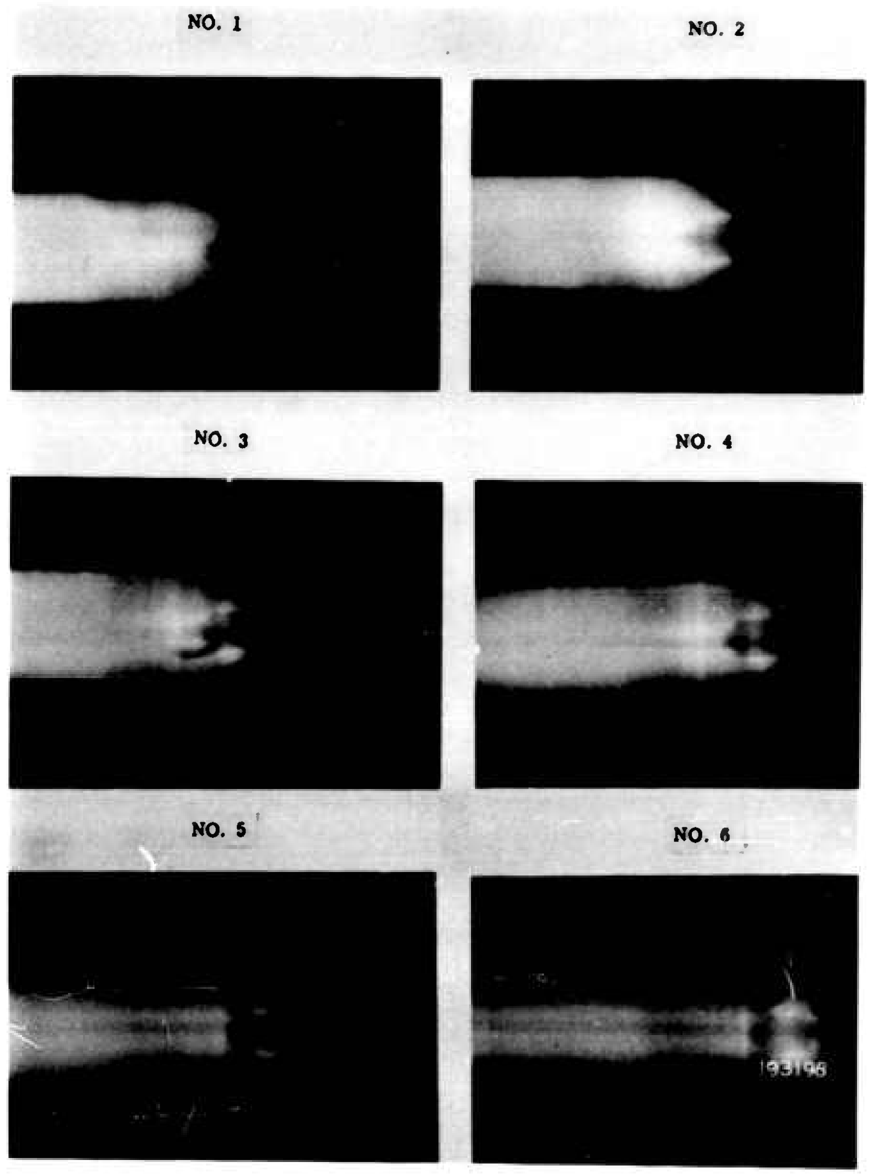

Figure 26. Change in the Electrode Sheath Caused by Variation of the Voltage Across the Tube

TABLE VIII

Position on the iv-Characteristic Mode

Point No.*	Volts	Amperes
1	8.1	1.5
2	8.2	1.5
3	8.3	1.1
4	8.5	0.8
5	9.0	0.5
6	10.0	0.4

*Point numbers correspond to photo numbers in Figure 26.

In conclusion, the described method is advantageous for several reasons:

1. A single component of a mixed gas can be photographed.

2. In the case of nonequilibrium investigations, the population density vs excitation energy can be determined more precisely. This is true because a suitable location can be selected, avoiding inhomogeneities like sheaths and dark spaces.

3. The composition of the sheath can be determined more precisely.

4. Occasional sudden changes in intensity can be detected.

5. The summation of the undesired intensities can be avoided.

Magnetohydrodynamic Instability of Viscous Plasma Flow

As is well known from ordinary hydrodynamics, the laminar viscous velocity profile of a fluid becomes instable when in the perturbed state of the flow the inertia force density is large compared to the viscous force density. This condition becomes:

$$\left[\rho_o (\vec{v}_o \cdot \nabla)\tilde{\vec{v}}\right] \gg \left[\mu \nabla^2 \tilde{\vec{v}}\right] \tag{32}$$

where ρ = density field, $\vec{v}$ = velocity field, and μ = viscosity, where quantities referring to the unperturbed flow are designated by zero index and perturbations by tilde. As a result of this instability, an anomalous fluctuating or turbulent flow is observed. According to Equation (32), the onset of turbulence can be expressed in terms of a critical Reynolds number, Re_{cr}, its numerical value being of order of magnitude[21]

$$Re_{cr} = \left(\frac{\bar{v}_o D \bar{\rho}_o}{\bar{\mu}}\right)_{cr} \cong 2500 \tag{33}$$

In Equation (33), D = the characteristic dimension of the channel; spatial mean values over this length are marked by a bar. The actual range of Re_{cr} varies up to $\approx$ 50, 000 due to the dependence on the conditions prevailing in the channel, in particular, on the magnitude of the initial perturbations (Re_{cr} increases strongly for decreasing perturbation amplitudes).

In the case of an ionized gas, it is to be expected that the viscous flow instability is remarkably influenced by a strong magnetic field. With regard to MPD energy converters, plasma flows with constant magnetic fields $\vec{B}_o$ applied perpendicular to the velocity field $\vec{v}_o$ ($\vec{B}_o \perp \vec{v}_o$) are of interest. In the equilibrium state of the flow, the magnetic field lines are pulled out in the flow direction in a proportion corresponding to the local strength of the velocity field—i.e., a magneto-viscous boundary layer is formed near the channel wall. Its thickness, D_B, can be calculated approximately by equating the viscous force density to the magnetic induction drag:

$$\left[\mu \nabla^2 \vec{v}_o\right] \cong \left[\sigma (\vec{v}_o \times \vec{B}_o) \times \vec{B}_o\right] \tag{34}$$

i.e.,

$$D_B = \frac{1}{\bar{B}_o}\sqrt{\frac{\bar{\mu}}{\bar{\sigma}}} \tag{35}$$

In Equations (34) and (35), the assumption is included that the induced magnetic field $\vec{B}_o^I$ is small compared to the exterior magnetic field $\vec{B}_o$, which is valid for low conductivity plasmas $\left(\left[\frac{B_o^I}{B_o}\right] \cong \left[\sigma v_o D_B\right] << 1\right)$. From Equation (35) it follows that $D_B \rightarrow 0$ for viscosity $\mu \rightarrow 0$ (μ now denotes the effective viscosity depending on the magnetic field in the plasma)[22] or electrical conductivity $\sigma \rightarrow \infty$, which is self-explanatory.

From Equation (35), it is recognized that the effect of the magnetic field on the instability considered can be estimated from the influence of the magnetic field on the boundary layer. Replacing D in Equation (33) by D_B gives the critical Reynolds number, Re_{cr}^B, for a plasma flow perpendicular to a magnetic field:

$$Re_{cr}^B = \left(\frac{\bar{v}_o \bar{\rho}_o}{\bar{B}_o} \sqrt{\frac{1}{\bar{\mu}\bar{\sigma}}}\right)_{cr} \cong 2500 \tag{36}$$

For illustration, compare the critical Reynolds numbers for a plasma flow with (Re_{cr}^B) and without (Re_{cr}) magnetic field. From Equations (33) and (36) follows:

$$\frac{Re_{cr}^B}{Re_{cr}} = \left(\frac{1}{D\,\bar{B}_o} \sqrt{\frac{\bar{\mu}}{\bar{\sigma}}}\right)_{cr} = \frac{1}{M_{cr}} \tag{36a}$$

where the Hartmann number[24] $M = D\,\bar{B}_o \sqrt{\frac{\bar{\sigma}}{\bar{\mu}}}$ has been introduced. It is obvious that a magnetic field has a stabilizing effect for large Hartmann numbers $M_{cr} \gg 1$ ($Re_{cr}^B \ll Re_{cr}$). In this case, the thickness, D_B, of the magneto-viscous boundary layer is small (gradient of the velocity profile only near the wall) compared to the thickness of the boundary layer of the corresponding nonmagnetoactive plasma flow. For small magnetic fields, $B_o \rightarrow 0$, the presumption upon which Equation (34) is based is no longer valid. Hence, in this region, the analysis presented does not apply.

A detailed analysis of new kinds of magnetoactive plasma flow instabilities, associated with the inhomogeneities of the plasma fields, is presented in the following subsection. There, viscous effects are neglected.

Convective Instability of Plasma Flow Across a Magnetic Field*

In analogy to general convective processes, instabilities associated with the inhomogeneities of the plasma are termed convective. Well known are the gravitational convective instability[24] (growth rate $\omega \sim g$; $\vec{g}$ = gravitational acceleration) and the magnetic convective instability[25] (growth rate $\omega \sim B/R$; R = radius of curvature of the magnetic field $\vec{B}$). In the first case, the instability is due to a transposition of the perturbed plasma by the gravitational field, and, in the second case, the instability is due to a transposition of the perturbed plasma by the tension of the magnetic field lines, which tend to contract towards its center of curvature. As a general feature, the growth rates of convective instabilities are proportional to the gradients of the equilibrium fields.

In various experimental devices—e.g., plasmadynamic accelerators[26] and energy converters[27] the plasma is in a state of inhomogeneous motion. Under this condition, an additional force density, $\vec{f} = \rho \vec{v} \cdot \nabla \vec{v}$, acts on the plasma due to the inertia of the mean mass flow. This force density is proportional to the gradient of the mean mass velocity, $\vec{v}$, and, therefore, of the convective type. In the presence of an exterior magnetic field, the mean flow induces an electric field which, together with exterior electric fields, gives rise to electron and ion streams in the plasma—the difference of the stream velocities being proportional to the curl of the self-magnetic field. The convective instabilities conditioned by the inertia force of the mean mass flow and by the induced particle streams were investigated as follows.

INSTABILITY OF THE MEAN PLASMA FLOW

Equilibrium State

The equilibrium configuration to be considered consists of a laminar, nonviscous plasma flow, moving with a nonuniform velocity, $\vec{v}_0$, parallel to the x-axis. (x, y, z are cartesian coordinates.) Perpendicular to the flow and parallel to the y-axis, a constant magnetic field, $\vec{B}_{0\perp}$, is applied. In the planes $z = \pm L$, the flow is bounded by electrodes, which are connected by an exterior circuit containing (1) a load, R, or (2) an electric power supply, P. By means of this circuit, a constant electric field $\vec{E}_0$ is impressed to the plasma.

The modifications (1) and (2) can, for example, be imagined to be associated with plasma flow production by (1) thermal expansion ("$\vec{v} \times \vec{B}$—converter") and (2) magnetic acceleration ("$\vec{j} \times \vec{B}$ accelerator").

*The material covered in this subsection was presented as a paper by H. E. Wilhelm at the VIth International Conference on Ionization Phenomena in Gases, Paris, 1963.

According to Ohm's law, a current density is developed in the z-direction of the plasma, which can be expressed in terms of the conductivity, σ, the electric field, $\vec{E}_o^I = \vec{v}_o \times \vec{B}_o$, induced by the flow across the total magnetic field, $\vec{B}_o = \vec{B}_{o\perp} + \vec{B}_o^I$, and the exterior electric field, $\vec{E}_o$ (Hall and electron pressure gradient $\vec{E}$-fields being neglected). The self-magnetic field, $\vec{B}_o^I$, of this current is given by

$$\nabla \times \vec{B}_o^I = \mu_o \sigma \left[\vec{E}_o + \vec{v}_o \times (\vec{B}_{o\perp} + \vec{B}_o^I) \right] \tag{37}$$

with $\nabla \cdot \vec{B}_o^I = 0$. In the absence of viscosity, the velocity field is a function of x alone, $\vec{v}_o = \vec{v}_o(x)$. From Equation (37) and $\nabla \cdot \vec{B}_o^I = 0$, it follows that the self-magnetic field is a function of x, $\vec{B}_o^I = \vec{B}_o^I(x)$, and is parallel to the exterior magnetic field $\vec{B}_{o\perp}$. From the equation of momentum balance,

$$\rho_o \vec{v}_o \cdot \nabla \vec{v}_o = - \nabla p_o + \frac{1}{\mu_o} (\nabla \times \vec{B}_o^I) \times (\vec{B}_{o\perp} + \vec{B}_o^I) \tag{38}$$

it follows that all force densities are parallel to the flow direction.

Summarizing, the general solution of the equilibrium state reads:

$$\rho_o = \rho_o(x), \quad p_o = p_o(x), \quad \vec{v}_o = \vec{v}_o(x), \quad \vec{B}_o^I = \vec{B}_o^I(x), \tag{39}$$

$$\vec{E}_o = \text{constant}$$
$$\sigma = \text{constant}$$
$$\vec{B}_{o\perp} = \text{constant}$$

If the total electric field is positive, $\vec{E}_o + \vec{v}_o \times \vec{B}_o > 0$, the magnetic body force is negative, $\frac{1}{\mu_o}(\nabla \times \vec{B}_o^I) \times \vec{B}_o < 0$—i.e., there exist solutions with decreasing velocity field, $\partial v_o / \partial x < 0$. If the total electric field is negative, $\vec{E}_o + \vec{v}_o \times \vec{B}_o < 0$, the magnetic body force is positive, $\frac{1}{\mu_o}(\nabla \times \vec{B}_o^I) \times \vec{B}_o > 0$—i.e., there exist solutions with increasing velocity field, $\partial v_o / \partial x > 0$. The last discussion refers to the condition of Figure 27—case 1 (upper sign), case 2 (lower sign).

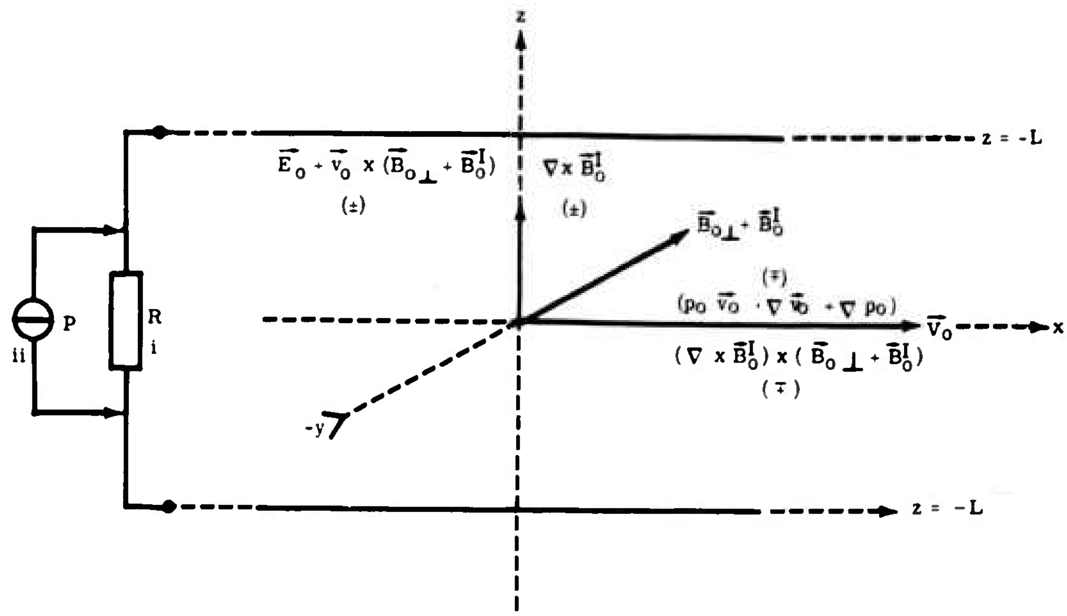

Figure 27. Nonuniform Plasma Flow Configuration

Perturbation State

In the perturbed state of the plasma every physical variable $q(\vec{r}, t)$ is composed by its equilibrium value $q_o(\vec{r})$ and a small perturbation $\tilde{q}(\vec{r}, t) << q_o(\vec{r})$. The perturbations are Fourier analyzed in the usual way:

$$\tilde{q}(\vec{r}, t) = \int_n \hat{q}_n \exp\left[i K_n(\vec{r}) + \omega_n t\right] \tag{40}$$

($\int_n$ stand for integration of the continuous and summation of the discrete components.) The spatial phase, $K_n(\vec{r})$, and the wave vector, $\vec{k}_n(\vec{r})$, of the elementary perturbations, n, are related by:

$$K_n(\vec{r}) = \int_o^{\vec{r}} \vec{k}_n(\vec{r}) \cdot d\vec{r}, \qquad \vec{k}_n(\vec{r}) = \nabla K_n(\vec{r}) \tag{41}$$

For a plasma not too strongly inhomogeneous with respect to the spatial dimension of the perturbation, Equation (40) may be rewritten in the "quasiclassical" form[28]

$$\tilde{q}(\vec{r}, t) = \int_n \hat{q}_n \exp\left[i \vec{k}_n \cdot \vec{r} + \omega_n t\right] \tag{42}$$

Another conclusion which can be made for a perturbation of small spatial extension ($\bar{\lambda} = 2\pi / |\bar{k}| \to 0$) is that in Equation (40) the amplitude $\hat{q}_{|k| \to 0}$ of the elementary long wavelength ($\lambda \to \infty$) perturbations is small compared to the amplitude $\hat{q}_{|k| \to \infty}$ of the elementary short wavelength ($\lambda \to 0$) perturbations. For this reason, the following inequality can be derived between the spatial derivatives "∇" of equilibrium fields, $q_o(\vec{r})$, and perturbations, $\tilde{q}_n(\vec{r}, t)$:

$$0\left[\tilde{q}_n (\nabla q_o)\right] \sim \epsilon 0\left[q_o (\nabla \tilde{q}_n)\right], \quad \epsilon << 1 \tag{43}$$

where $0[x]$ = order of magnitude of x.

For study of a macroscopic instability, the macroscopic approach is used. Dissipation and space charges are neglected throughout.[29] The field equations are the linearized equation of momentum conservation:

$$\begin{aligned} \rho_o\left[\frac{\partial}{\partial t} + \vec{v}_o \cdot \nabla\right] \vec{\tilde{v}} + \rho_o \vec{\tilde{v}} \cdot \nabla \vec{v}_o + \tilde{\rho} \vec{v}_o \cdot \nabla \vec{v}_o \\ = - \nabla\left(\tilde{p} + \frac{\vec{B}_o \cdot \vec{\tilde{B}}}{\mu_o}\right) + \frac{1}{\mu_o} \vec{B}_o \cdot \nabla \vec{\tilde{B}} + \frac{1}{\mu_o} \vec{\tilde{B}} \cdot \nabla \vec{B}_o \end{aligned} \tag{44}$$

and the linearized equations of conservation of mass, energy, and magnetic flux density:

$$\left[\frac{\partial}{\partial t} + \vec{v}_o \cdot \nabla\right] \tilde{\rho} = - (\vec{\tilde{v}} \cdot \nabla \rho_o + \rho_o \nabla \cdot \vec{\tilde{v}}) \tag{45}$$

$$\left[\frac{\partial}{\partial t} + \vec{v}_o \cdot \nabla\right] \tilde{p} = - (\vec{\tilde{v}} \cdot \nabla p_o + \gamma p_o \nabla \cdot \vec{\tilde{v}}) \tag{46}$$

$$\left[\frac{\partial}{\partial t} + \vec{v}_o \cdot \nabla\right] \vec{\tilde{B}} = - (\vec{\tilde{v}} \cdot \nabla \vec{B}_o + \vec{B}_o \nabla \cdot \vec{\tilde{v}} - \vec{B}_o \cdot \nabla \vec{\tilde{v}}) \tag{47}$$

In deriving Equations (45), (46), and (47), the unimportant terms $\sim \epsilon$,

$$\begin{aligned} \left|\tilde{\rho} \nabla \cdot \vec{v}_o\right| << \left|\rho_o \nabla \cdot \vec{\tilde{v}}\right|, \quad \left|\gamma \tilde{p} \nabla \cdot \vec{v}_o\right| << \left|\gamma p_o \nabla \cdot \vec{\tilde{v}}\right|, \\ \left|\vec{\tilde{B}} \nabla \cdot \vec{v}_o - \vec{\tilde{B}} \cdot \nabla \vec{v}_o\right| << \left|\vec{B}_o \nabla \cdot \vec{\tilde{v}} - \vec{B}_o \cdot \nabla \vec{\tilde{v}}\right| \end{aligned} \tag{48}$$

have been suppressed. Elimination of $\tilde{\rho}$, $\tilde{p}$, and $\tilde{\vec{B}}$ from Equation (44) by means of Equations (45), (46), and (47) gives the characteristic equation for the velocity perturbation $\tilde{\vec{v}}$:

$$\begin{aligned}
&\rho_o \left[\frac{\partial}{\partial t} + \vec{v}_o \cdot \nabla\right]^2 \tilde{\vec{v}} + \rho_o \left[\frac{\partial}{\partial t} + \vec{v}_o \cdot \nabla\right] \tilde{\vec{v}} \cdot \nabla \vec{v}_o - (\tilde{\vec{v}} \cdot \nabla \rho_o + \rho_o \nabla \cdot \tilde{\vec{v}}) \vec{v}_o \cdot \nabla \vec{v}_o \\
&\quad = \nabla \left[(\tilde{\vec{v}} \cdot \nabla p_o + \gamma p_o \nabla \cdot \tilde{\vec{v}}) + (\tilde{\vec{v}} \cdot \nabla \vec{B}_o + \vec{B}_o \nabla \cdot \tilde{\vec{v}} - \vec{B}_o \cdot \nabla \tilde{\vec{v}}) \cdot \frac{\vec{B}_o}{\mu_o} \right] - \\
&\qquad \frac{1}{\mu_o} \vec{B}_o \cdot \nabla (-\vec{B}_o \cdot \nabla \tilde{\vec{v}} + \vec{B}_o \nabla \cdot \tilde{\vec{v}}) - \\
&\qquad \frac{1}{\mu_o} (\tilde{\vec{v}} \cdot \nabla \vec{B}_o + \vec{B}_o \nabla \cdot \tilde{\vec{v}}) \cdot \nabla \vec{B}_o
\end{aligned} \tag{49}$$

The last magnetic convective expression vanishes as the $\vec{B}_o$-lines are straight-lined.

The general solution of Equation (49) is rather complicated. It is suitable to specify instabilities propagating in the three distinguished directions of the system.

Perturbations Propagating Parallel to the Flow

For $\vec{k} = \vec{k}_x$, it follows from the components of Equation (49) by consideration of the equilibrium condition, Equation (38): $\tilde{v}_y = 0$, $\tilde{v}_z = 0$, and

$$\begin{aligned}
&\left\{ \rho_o \left[\frac{\partial}{\partial t} + v_o \nabla_x\right]^2 + \rho_o \frac{\partial v_o}{\partial x}\left[\frac{\partial}{\partial t} + v_o \nabla_x\right] - v_o \frac{\partial v_o}{\partial x} \frac{\partial \rho_o}{\partial x} \right\} \tilde{v}_x \\
&\quad = \left(\gamma p_o + \frac{B_o^2}{\mu_o} \right) \nabla_x^{\,2} \tilde{v}_x .
\end{aligned} \tag{50}$$

From Equation (50), the dispersion equation is derived as condition for a nontrivial solution:

$$\omega + i k_x v_o = - \frac{1}{2} \frac{\partial v_o}{\partial x} \left\{ 1 \pm \sqrt{1 + 4 \left[\frac{\partial \ln \rho_o}{\partial \ln v_o} - k_x^2 \frac{C_s^{\,2} + C_B^{\,2}}{(\partial v_o / \partial x)^2} \right]} \right\} \tag{51}$$

$C_M = \left[C_s^2 + C_B^2\right]^{1/2}$, where $C_s^2 = \gamma p_o / \rho_o$ and $C_B^2 = B_o^2 / \mu_o \rho_o$, is the wave velocity for magneto-acoustic perturbations propagating perpendicular to $\vec{B}_o$.

The conditions for instability (Re $\omega > 0$) are obtained as:

I. $\frac{\partial v_o}{\partial x} < 0$ (52)

II. $\frac{\partial v_o}{\partial x} > 0$ and $\frac{\partial \ln \rho_o}{\partial \ln v_o} > 0.$ (53)

Against the perturbations regarded, according to Equation (52), a decreasing flow field is always unstable; according to Equation (53), an increasing flow field is unstable only when the condition $\partial \ln \rho_o / \partial \ln v_o > 0$ is satisfied. In the last case only long wavelength instabilities, for which $k_x^2 < \frac{\partial \ln \rho_o}{\partial \ln v_o} \cdot \frac{(\partial v_o / \partial x)^2}{C_s^2 + C_B^2}$, are excited.

Perturbations Propagating Parallel to the Magnetic Field

For $\vec{k} = \vec{k}_y$, it follows from the components of Equation (49) by consideration of the equilibrium condition, Equation (38):

$$\left[\rho_o \frac{\partial^2}{\partial t^2} - \nabla_y^2 \frac{B_o^2}{\mu_o}\right]\tilde{v}_z = 0\text{* and}$$

$$\left[\rho_o \frac{\partial^2}{\partial t^2} + \rho_o \frac{\partial v_o}{\partial x} \frac{\partial}{\partial t} - v_o \frac{\partial v_o}{\partial x} \frac{\partial \rho_o}{\partial x} - \nabla_y^2 \frac{B_o^2}{\mu_o}\right]\tilde{v}_x = \rho_o v_o \frac{\partial v_o}{\partial x} \nabla_y \tilde{v}_y \tag{54}$$

$$\left[\rho_o \frac{\partial^2}{\partial t^2} - \nabla_y^2 \gamma p_o\right]\tilde{v}_y = -\rho_o v_o \frac{\partial v_o}{\partial x} \nabla_y \tilde{v}_x \tag{55}$$

The determinant of Equations (54) and (55) set to zero leads to the dispersion equation:

$$\left[\omega^2 + k_y^2 C_s^2\right]\left(\omega^2 + \omega \frac{\partial v_o}{\partial x} - v_o^2 \frac{\partial \ln v_o}{\partial x} \cdot \frac{\partial \ln \rho_o}{\partial x} + k_y^2 C_B^2\right) = + k_y^2 \cdot \left(v_o^2 \cdot \frac{\partial \ln v_o}{\partial x}\right)^2 \tag{56}$$

---

*Solution: $\omega = \pm i k_y C_B$ (Alfvén-wave propagating parallel to $\vec{B}_o$).

The convective solutions of Equation (56) read, in the limiting case of:

- Short wavelengths

$$\lim_{|k_y| \to \infty} \omega = -\frac{1}{2}\frac{\partial v_o}{\partial x} \pm i\left[k_y C_B\right]_{k_y = \infty} \tag{57}$$

- Long wavelengths

$$\lim_{|k_y| \to 0} \omega = -\frac{1}{2}\frac{\partial v_o}{\partial x}\left\{1 \pm \sqrt{1 + 4\,\frac{\partial \ln \rho_o}{\partial \ln v_o}}\right\} \tag{58}$$

By applying the Routh-Hurwitz criterion to the polynomial of Equation (56), the same instability conditions are obtained as for perturbations propagating parallel to the flow.

<u>Perturbations Propagating Parallel to the Current</u>

For $\vec{k} = \vec{k}_z$, it follows from the components of Equation (49) by consideration of the equilibrium condition, Equation (38): $\tilde{v}_y = 0$ and

$$\left[\rho_o \frac{\partial^2}{\partial t^2} + \rho_o \frac{\partial v_o}{\partial x}\frac{\partial}{\partial t} - v_o \frac{\partial v_o}{\partial x}\frac{\partial \rho_o}{\partial x}\right]\tilde{v}_x = \rho_o v_o \frac{\partial v_o}{\partial x} \nabla_z \tilde{v}_z \tag{59}$$

$$\left[\rho_o \frac{\partial^2}{\partial t^2} - \nabla_z^2\left(\gamma p_o + \frac{B_o^2}{\mu_o}\right)\right]\tilde{v}_z = -\rho_o v_o \frac{\partial v_o}{\partial x} \nabla_z \tilde{v}_x \tag{60}$$

The determinant of Equations (59) and (60) set to zero leads to the dispersion equation:

$$\left[\omega^2 + k_z^2 (C_s^2 + C_B^2)\right]\left(\omega^2 + \omega\frac{\partial v_o}{\partial x} - v_o^2 \frac{\partial \ln v_o}{\partial x}\frac{\partial \ln \rho_o}{\partial x}\right) = +k_z^2 \cdot \left(v_o^2 \frac{\partial \ln v_o}{\partial x}\right)^2 \tag{61}$$

The convective solutions of Equation (61) read in the limiting case of:

- Short wavelengths

$$\lim_{|k_z| \to \infty} \omega = -\frac{1}{2}\frac{\partial v_o}{\partial x}\left\{1 \pm \sqrt{1 + 4\left[\frac{\partial \ln \rho_o}{\partial \ln v_o} + \frac{v_o^2}{C_s^2 + C_B^2}\right]}\right\} \tag{62}$$

- Long wavelengths

$$\lim_{|k_z| \to 0} \omega = -\frac{1}{2}\frac{\partial v_o}{\partial x}\left\{1 \pm \sqrt{1 + 4\,\frac{\partial \ln \rho_o}{\partial \ln v_o}}\right\} \tag{63}$$

By applying the Routh-Hurwitz criterion to the polynomial of Equation (61), the same instability conditions are obtained as for perturbations propagating parallel to the flow.

The convective instability considered is conditioned by the inertia forces of the flow and vanishes when the latter becomes uniform. It is due to fluctuations of the pressure, density, magnetic, and velocity fields. Remarkable is the fact that a flow slowing down always becomes convectively unstable.

CONVECTIVE INSTABILITY OF THE PARTICLE STREAMS

Equilibrium State

In this section special regard is given to a convective process connected with the electron and ion streams, which could not be comprehended by the previously discussed one-fluid approach. In order to study the effect in pure form, the inertia forces of the mean mass flow are eliminated by appropriate modification of the plasma model (Figure 27). Suppose the channel is bounded by additional nonconducting walls perpendicular to the flow, and that the current is produced by means of the exterior power supply. Then, in the equilibrium state, the mean mass velocity, $\vec{v}_o$, is zero, and the magnetic body force is balanced by the pressure gradient alone:

$$0 = -\nabla p_o + \frac{1}{\mu_o}(\nabla \times \vec{B}_o^I) \times (\vec{B}_{o\perp} + \vec{B}_o^I) \tag{64}$$

The difference between the ion and electron drift velocities in the quasineutral plasma,

$$\sum_{s=e,i} n_{os}\, e_s = 0 \tag{65}$$

(e, i = index for the electron and ion component, respectively) is given from Maxwell's equation by:

$$\vec{v}_{\perp i} - \vec{v}_{\perp c} = \frac{\nabla \times \vec{B}_o^I}{\mu_o\, n_{oi}\, e_i} \tag{66}$$

The drift velocities are constant. The total momentum of the streams vanishes:

$$\sum_{s=e,i} n_{os}\, m_s\, \vec{v}_{\perp s} = 0 \tag{67}$$

Finally, the condition that all forces acting on the plasma components s = e, i are in equilibrium reads:

$$\begin{aligned} 0 = -\nabla p_{os} + n_{os}\, e_s \left[\vec{E}_o + \vec{v}_{\perp s} \times (\vec{B}_{o\perp} + \vec{B}_o^I)\right] - \\ \sum_{r=e,i} n_{os}\, n_{or}\, f_{sr}\, (\vec{v}_{\perp s} - \vec{V}_{\perp r}) \end{aligned} \tag{68}$$

where f_{sr} is the friction coefficient of the s-component ($f_{ei} = f_{ie}$).

Perturbation State

In the nondissipative two-fluid approximation the following linearized field equations describing the perturbed state are obtained (s = e, i).

Equations of Momentum, Mass, and Energy Density Convervation:

$$\begin{aligned} n_{os}\, m_s \left[\frac{\partial}{\partial t} + \vec{v}_{\perp s} \cdot \nabla\right] \tilde{\vec{v}}_s = -\nabla \tilde{p}_s + \tilde{n}_s\, e_s \left[\vec{E}_o + \vec{v}_{\perp s} \times \vec{B}_o\right] + \\ n_{os}\, e_s \left[\tilde{\vec{E}} + \tilde{\vec{v}}_s \times \vec{B}_o + \vec{v}_{\perp s} \times \tilde{\vec{B}}\right] \end{aligned} \tag{69}$$

$$\left[\frac{\partial}{\partial t} + \vec{v}_{\perp s} \cdot \nabla\right] \tilde{n}_s = -(\tilde{\vec{v}}_s \cdot \nabla n_{so} + n_{os} \nabla \cdot \tilde{\vec{v}}_s) \tag{70}$$

$$\left[\frac{\partial}{\partial t} + \vec{v}_{\perp s} \cdot \nabla\right] \tilde{p}_s = -(\tilde{\vec{v}}_s \cdot \nabla p_{so} + \gamma_s\, p_{so} \nabla \cdot \tilde{\vec{v}}_s) \tag{71}$$

Maxwell's Equations:

$$\nabla \times \tilde{\vec{B}} = \mu_o \sum_{s=e,i} (\tilde{n}_s\, e_s\, \vec{v}_{\perp s} + n_{os}\, e_s\, \tilde{\vec{v}}_s) \tag{72}$$

$$\nabla \times \tilde{\vec{E}} = -\frac{\partial \tilde{\vec{B}}}{\partial t} \tag{73}$$

$$\nabla \cdot \tilde{\vec{B}} = 0 \tag{74}$$

$$\nabla \cdot \tilde{\vec{E}} = \epsilon_o^{-1} \sum_{s=e,i} \tilde{n}_s \, e_s \tag{75}$$

To obtain the convective solution ($\omega \sim \nabla q_o$) of Equations (69) through (75), any equation terms being relatively small of order ϵ [(Equation (43)] are neglected.

Multiplication of Equation (69) by ($\nabla \cdot$) gives, after neglecting terms $\sim \epsilon^2$ and $\sim \epsilon$ ($\vec{v}_{\perp s} \sim \epsilon^1$, $\vec{E}_o \sim \epsilon^1$)

$$- \nabla \tilde{p}_s + n_{os} \, e_s \left[\vec{E} + \tilde{\vec{v}}_s \times \vec{B}_o \right] \cong 0 \tag{76}$$

In the same approximation

$$\nabla \times \tilde{\vec{B}} \cong \mu_o \sum_{s=e,i} n_{os} \, e_s \, \tilde{\vec{v}}_s \tag{77}$$

is obtained from Equation (72).

From Equations (77) and (76) (s = e, i) results

$$- \nabla (\tilde{p}_e + \tilde{p}_i) \times \vec{B}_o + \frac{B_o^2}{\mu_o} \nabla \times \tilde{\vec{B}} - \frac{1}{\mu_o} (\vec{B}_o \cdot \nabla \times \tilde{\vec{B}}) \, \vec{B}_o \cong 0 \tag{78}$$

By means of Equations (76) and (78), it can be shown from Equation (75) that the plasma behaves neutral against perturbations with wavelengths $\lambda \gg d$, where $d = \sqrt{\epsilon_o \, kT_o / n_{oe} e_e^2}$ is the Debye shielding distance:[30]

$$\sum_{s=e,i} \tilde{n}_s \, e_s \cong 0 \tag{79}$$

Summation of Equations (69) (s = e, i) and multiplication by $\nabla \times$ gives, because of Equations (79) and (72), terms $\sim \epsilon^2$ being neglected:

$$\sum_{s=e,i} n_{os} \, m_s \left[\frac{\partial}{\partial t} + \vec{v}_{\perp s} \cdot \nabla \right] \nabla \times \tilde{\vec{v}}_s$$

$$\cong \frac{1}{\mu_o} (\vec{B}_o \cdot \nabla) \, \nabla \times \tilde{\vec{B}} + \frac{1}{\mu_o} \nabla \times (\tilde{\vec{B}} \cdot \nabla \, \vec{B}_o) + \frac{1}{\mu_o} \nabla (\vec{B}_o \cdot \nabla) \times \tilde{\vec{B}} \tag{80}$$

With exception of $(\vec{B}_o \cdot \nabla)\nabla \times \vec{\tilde{B}} \sim \epsilon^0$, the remaining terms in Equation (80) are $\sim \epsilon^1$. In applying the ϵ-approximation further, Equation (80) predicts that the convective solution is associated with perturbations propagating perpendicular to $\vec{B}_o$. Now, multiplying Equation (80) by $\nabla \times$ gives

$$\sum_{s=e,i} n_{os}\, m_s \left[\frac{\partial}{\partial t} + \vec{v}_{\perp s} \cdot \nabla\right] \vec{\tilde{v}}_s \cong \frac{1}{\mu_o} \vec{\tilde{B}} \cdot \nabla \vec{B}_o \tag{81}$$

In deriving Equation (81) it has been considered that $\vec{k} \perp \vec{B}_o$, and $\nabla \cdot \vec{\tilde{v}}_s \cong 0$, the latter following from Equation (70) or (71):

$$\left[\frac{\partial}{\partial t} + \vec{v}_{\perp s} \cdot \nabla\right] \tilde{p}_s + \vec{\tilde{v}}_s \cdot \nabla p_{so} = -\gamma_s\, p_{so}\, \nabla \cdot \vec{\tilde{v}}_s \cong 0 \tag{82}$$

Eliminating from Equation (81) $\vec{\tilde{v}}_e$ by means of Equation (77), then $\nabla \times \vec{\tilde{B}}$ by means of Equation (78) gives $(\tilde{p} = \tilde{p}_i + \tilde{p}_e)$

$$\begin{aligned}\left\{\sum_{s=e,i} n_{os}\, m_s \left[\frac{\partial}{\partial t} + \vec{v}_{\perp s} \cdot \nabla\right]\right\} \vec{\tilde{v}}_i \cong \frac{1}{\mu_o} \vec{\tilde{B}} \cdot \nabla \vec{B}_o + \\ \frac{n_{oe}\, m_e}{\mu_o\, n_{oi}\, e_i} \left(\frac{B_o^2}{\mu_o}\right)^{-1} \left[\frac{\partial}{\partial t} + \vec{v}_{\perp e} \cdot \nabla\right] \cdot \left[\nabla \tilde{p} \times \vec{B}_o + \frac{1}{\mu_o} (\vec{B}_o \cdot \nabla \times \vec{\tilde{B}})\, \vec{B}_o\right]\end{aligned} \tag{83}$$

and, further, after multiplication with ∇p_o, $(\nabla p_o \perp \vec{B}_o,\ \nabla p_o \perp \vec{\tilde{B}} \cdot \nabla \vec{B}_o)$ and by consideration of Equations (64) and (66),

$$\begin{aligned}\left\{\left[\frac{\partial}{\partial t} + \vec{v}_{\perp i} \cdot \nabla\right] + \frac{n_{oe}\, m_e}{n_{oi}\, m_i}\left[\frac{\partial}{\partial t} + \vec{v}_{\perp e} \cdot \nabla\right]\right. \vec{\tilde{v}}_i \cdot \nabla p_o \\ \cong -\frac{n_{oe}\, m_e}{n_{oi}\, m_i} \left[\left(\vec{v}_{\perp i} - \vec{v}_{\perp e}\right) \cdot \nabla\right] \left[\frac{\partial}{\partial t} + \vec{v}_{\perp e} \cdot \nabla\right] \tilde{p}\end{aligned} \tag{84}$$

Equation (84) becomes, with Equation (82), setting there s = i, a characteristics equation for the ion pressure perturbation $\tilde{p}_i$

$$\begin{aligned}\left[\frac{\partial}{\partial t} + \vec{v}_{\perp i} \cdot \nabla\right] \left\{\left[\frac{\partial}{\partial t} + \vec{v}_{\perp i} \cdot \nabla\right] + \frac{n_{oe}\, m_e}{n_{oi}\, m_i} \left[\frac{\partial}{\partial t} + \vec{v}_{\perp e} \cdot \nabla\right]\right\} \tilde{p}_i \\ \cong \frac{n_{oe}\, m_e}{n_{oi}\, m_i} \left[(\vec{v}_{\perp i} - \vec{v}_{\perp e}) \cdot \nabla\right] \left[\frac{\partial}{\partial t} + \vec{v}_{\perp e} \cdot \nabla\right] \tilde{p}_i\end{aligned} \tag{85}$$

From Equation (85) one derives the dispersion equation:

$$\omega^2 \left(1 + \frac{n_{oe}\, m_e}{n_{oi}\, m_i}\right) + i\, 2\, \omega\, \vec{k} \cdot \left(\vec{v}_{\perp i} + \frac{n_{oe}\, m_e}{n_{oi}\, m_i} \vec{v}_{\perp e}\right) - (\vec{k} \cdot \vec{v}_{\perp i})^2 - \frac{n_{oe}\, m_e}{n_{oi}\, m_i} (\vec{k} \cdot \vec{v}_{\perp e})^2 = 0 \tag{86}$$

Taking into account the relation in Equation (67), this expression reduces to:

$$\omega = \pm \sqrt{\frac{n_{oe}\, m_e}{n_{oi}\, m_i}}\, \vec{k} \cdot \vec{v}_{\perp e} \tag{87}$$

According to Equation (87), the particle streams are unstable. The instability is caused by the inertia forces of the perturbed electron and ion streams, which are in interaction with each other through the magnetic field. Both instabilities propagating in an opposite to the electron drift direction are excited. The effect vanishes for $\frac{m_e}{m_i} \rightarrow 0$.

CONCLUSION

Even beyond the critical Reynolds number above which the ordinary viscous flow instability sets in, magnetoactive plasma flows can become unstable due to convective processes. As a result of these instabilities, the directed kinetic energy of the plasma flow is partially transformed into irregular kinetic and potential energy of nonequilibrium fluctuations. From the large-scale fluctuations, this kinetic energy is transferred by nonlinear interactions to the small-scale fluctuations and by the latter into heat (the dissipation mechanisms in the plasma are proportional to the square of the wave number).

With respect to experimentation, the problem becomes that of determining the onset and existence of turbulence in the plasma flow. This can be done, for example, by measuring the intensity variation of electromagnetic waves scattered by the turbulence elements. Another method which can be proposed is to add strongly radiating test atoms to the plasma at one side of the channel. Assume that the transverse diffusion time of the test atoms is large with respect to the time interval within which the test atoms are carried by the longitudinal mass flow through the channel. Then, in laminar plasma flow the test radiation centers cannot be observed at the other side of the channel. In the case of turbulent plasma flow, however, transverse mass motions also take place. In the latter case, part of the test radiation centers will therefore reach the other side of the channel. Their concentration can then be determined there by measuring the intensity of the characteristic spectral lines of the test atoms.

In the state of developed instability, the plasma shows anomalous transport properties. It is of particular interest---if we extend the results to partially ionized gases---how the coefficients of recombination, ionization, and the ionization potential are changed by the nonequilibrium fluctuations. The investigation of the latter effects, which are presumably changing the ionization degree, will be investigated later.

V. REFERENCES

1. Finkelnberg, W. and Maecker, H. in Handbuch der Physik (Fluegge), Vol 22.

2. Euler, I. in Ann. Phys. 14, 145 (1954).

3. Inglis, D. R. and Teller, E. in Astrophys. J. 90, 439 (1939).

4. Mohler, F. L. in Astrophys. J. 90, 429 (1939).

5. Griem, H. R., Kolb, A. C., and Shen, K. Y. Naval Research Laboratory Report 5455 (1960).

6. Agnew, L. and Summers, C. "Experimental Cesium Line Shapes." Advanced Energy Conversion. Vol 3. Great Britain, Pergamon Press, 1963, pp 79-87.

7. Griem, H. Plasma Spectroscopy. McGraw Hill (to be published in 1964).

8. Maecker, H. and Peters, Th. in Z. Phys. 139, 448 (1954).

9. Schneider, R. T. and Mailaender, M. in Z. angew. Phys. 12, 521 (1960).

10. Schneider, R. T. in Proceedings of the Fifth International Conference on Ionization Phenomena in Gases, Munich (1961).

11. Schneider, R. T., Doctoral thesis, Stuttgart, Germany (1961).

12. Schneider, R. T. in Proceedings of the Third Symposium on Engineering Applications of Magnetohydrodynamics, Rochester, N. Y. (1962).

13. Schneider, R. T. Introduction to Short-Time Spectroscopic Techniques. Allison Division, GMC, EDR 2728 (1963).

14. Moore, C. E. Atomic Energy Levels, Circular of NBS 467, Volume II (May 1958).

15. Corliss, C. H. and Bozmann, W. R. Experimental Transition Probabilities for Spectral Lines of Seventy Elements. NBS Monograph 53 (July 1962).

16. Kvater, G. S. and Meister, T. G. Absolute Values of Transition Probabilities for Members of the Principal Series of Cesium. Leningrad Universitet, Vestnik, No. 9 (1952) pp 137-158.

17. Hoermann, H. in Zeitschr. f. Physik 97, 539 (1935).

18. Maecker, H. in Zeitschr. f. Physik 136 (1953) pp 119-136, and ibid. 139 (1954) pp 448-463.

19. Pearce, W. J. in Conference on Extremely High Temperature. Fischer and Mansur, ed. John Wiley and Sons, 1958, pp 123-124.

20. Tipton, D. L. and Schneider, R. T. Calculation and Measurement of the Radial Distribution of Line Broadening in a Cesium Plasma. In Second National Meeting of the Society of Applied Spectroscopy, San Diego, Oct. 1963.

21. Lamb, H. Hydrodynamics. Cambridge, At the University Press, 1958.

22. Herdan, R. and Liley, B. S. in Rev. Mod. Phys. 31 (1960) 732.

23. Cowling, T. G. Magnetohydrodynamics. New York, Interscience Publishers, Inc., 1957.

24. Landau, L. D. Mechanics of Continuous Media. Reading, Massachusetts, Addison-Wesley, 1958.

25. Wilhelm, H. E. in Z. f. Plasmaphysik. 3, 1 (1963).

26. Ludwig, G., Heil, M., Mueller, S., and Kaeppeler, H. J. Allison Research Memorandum No. 129, 1959.

27. Rosa, R. in Physics of Fluids. 4, 182 (1961).

28. Kadomtsev, B. B. in Soviet Physics. JETP 12, 517 (1961).

29. Bernstein, I. B., Frieman, E. A., Kruskal, M. D., and Kulsrud, R. M. in Proc. Roy. Soc. A244, 17 (1958).

30. Spitzer, L. Jr. Physics of Fully Ionized Gases. New York, Interscience Publishers, Inc.

DISTRIBUTION LIST

	No. copies
Director, Advanced Research Projects Agency The Pentagon Washington, D. C. 20301 Attn: Dr. John Huth	2
Office of Naval Research Power Branch (Code 429) Washington, D. C. 20360 Attn: John A. Satkowski	6
Commanding Officer Office of Naval Research Branch Office Box 39 Navy #100 Fleet Post Office New York, New York	1
Cognizant ONR Area Branch Office	1
U. S. Naval Research Laboratory Washington 25, D. C. Attn: Technical Information Division	6
Wright-Patterson Air Force Base Aeronautical Systems Division Ohio Attn: Don Warnock (ASRMFP-2)	1
Air Force Office of Scientific Research Washington 25, D. C. Attn: Dr. Milton M. Slawsky	1
U. S. Naval Ordnance Test Station Propulsion Applied Research Group China Lake, California Attn: Leroy J. Krzycki (Code 4506)	1
Rome Air Development Center Rome, New York Attn: Mr. Frank J. Mellura	1

	No. copies
U. S. Naval Ordnance Laboratory NA Division White Oak, Maryland Attn: Wallace Knutsen	1
Library	2
Defense Documentation Center Cameron Street Alexandria, Virginia 22314	20
U. S. Army Research & Development Laboratory Fort Belvoir, Virginia Attn: Frank Shields (ERD-EP)	1
NASA, Lewis Research Center 21,000 Brookpark Road Cleveland 35, Ohio Attn: Wolfgang Moeckel	1
Dr. B. Lubarsky	1
U. S. Atomic Energy Commission Division of Reactor Development Direct Energy Conversion Section, RD; AED Germantown, Maryland	1
Dr. T. Brogan AVCO - Everett Research Laboratory 2385 Revere Beach Parkway Everett, Massachusetts	1
Dr. J. Cole Department of Aeronautics California Institute of Technology Pasadena, California	1
Mr. Arthur Sherman General Electric - Valley Forge Valley Forge Space Technical Center Philadelphia 1, Pennsylvania	1

	No. copies
Dr. M. Talaat Martin Marietta Corporation Nuclear Division Baltimore 3, Maryland	1
Dr. W. D. Jackson Electrical Engineering Department Massachusetts Institute of Technology Cambridge 39, Massachusetts	1
Dr. Vernon H. Blackman MHD Research Incorporated 1535 Monrovia Street Newport Beach, California	1
Dr. B. C. Lindley Nuclear Research Centre C. A. Parsons & Co., Ltd. Fossway, Newcastle Upon Tyne 6 England	1
Dr. Robert Eustis Thermosciences Divsion Stanford University Standford, California	1
Mr. John Wright Central Electricity Research Laboratories Cleeve Road, Leatherhead, Surrey England	1
Dr. Richard Schamberg Rand Corporation 1700 S. Main Street Santa Monica, California	1
Dr. Sam Naiditch Unified Science Associates 826 Arroyo Parkway Pasadena, California	1

	No. copies
Dr. W. S. Emmerich Westinghouse Research Laboratories Beulah Road, Churchill Borough Pittsburgh 35, Pennsylvania	1
Dr. R. T. Schneider Allison Division General Motors Corporation Indianapolis, Indiana	1
Dr. D. G. Elliott Jet Propulsion Laboratory Pasadena, California	1

UNCLASSIFIED

UNCLASSIFIED